4-2021

A High-Throughput Approach to Characterizing ARV1 on the Regulation of Lipid Homeostasis Uncovers a Novel Interaction with Epidermal Growth Factor Receptor

Nicholas Anthony Wachowski

A HIGH-THROUGHPUT APPROACH TO CHARACTERIZING ARV1 ON THE REGULATION OF LIPID HOMEOSTASIS UNCOVERS A NOVEL INTERACTION WITH EPIDERMAL GROWTH FACTOR RECEPTOR

Nicholas Anthony Wachowski, B.S.

A Dissertation submitted to the Graduate School of Biomedical Sciences, Rowan University in partial fulfillment of the requirements for the M.S. Degree.

Stratford, New Jersey 08084

April 2021

Table of Contents

Acknowledgments

First and foremost, I want to thank everyone who helped me along the Master of Science in Molecular Pathology and Immunology program. The list of people that helped me in this difficult but rewarding program is rather extensive. Additionally, to all the people and organizations that invested their financial support, their time and expertise, I want to say thank you from the bottom of my heart, and I will forever be grateful for it.

To the director of Biomedical Sciences, Dr. Diane Worrad, and all the staff at Rowan University Graduate School of Biomedical Sciences (GSBS), thank you for allowing me and all the other students to have an opportunity to do research at this prestigious university. This is allowing the next generation of scientists to learn new skills and improve on their scientific skillsets to help others in need.

To the founder of Genesis Biotechnology Group (GBG), Dr. Eli Mordechai, along with all the members at GBG, thank you for allowing me to use your laboratories and for the resources you made available for me to do all this research. By allowing me to use your laboratories and the resources available to me, this allows myself and future scientists to learn new skills and to improve skills already known which will allow treatments for people who need it. Furthermore, I want to thank specifically the scientists at Oncoveda and the Institute of Metabolic Disorders (IMD) for all the help and support over the past few years. Everyone at IMD and Oncoveda were extremely supportive and happily helped me whenever I needed it. Specifically, at IMD, I want to thank Raymond Franks, thank you for all your help through these

years and keeping me motivated. You are a true friend! Also, I want to thank Joshua Wayne, for all the technical help whether it was help working with the fluorescent microscope, qRT-PCR machine, to ordering supplies. Joshua was always there to assist me. Everyone at IMD who include Jessie Lee Cunningham, Dr. Karla Frietze, Dr. Christopher Cultrara, Joshua Wayne, Alyssa Brown, Divi Das, Raymond Franks, Weidong Liu, and Dr. Joseph Nickels will all be lifetime long friends and I am extremely grateful to had all of them during this program.

To the members of my thesis advisory committee, Dr. Salvatore Caradonna, MSMPI Program Chair, Dr. Scott Gygax, Program Director of Biotechnology at Thomas Jefferson University, and Dr. Joseph Nickels, Coordinator of the Rowan-GBG MSMPI Program. Thank you for all your consistent support and motivation over the past few years. I am very grateful to have all your apart of my thesis advisory committee. Thank you.

To my mentors, Dr. Karla Frietze, Jessie Lee Cunningham, and Dr. Joseph Nickels, thank you for teaching me everything I know today. Jessie Lee Cunningham taught me every scientific technique I know today which include to name a few: immunoblotting, mammalian cell culture, genotyping, qRT-PCR, keeping my laboratory notebook up-to-date, and so many other techniques and skills. Seriously, thank you Jessie Lee, you made me the scientist I am today and will be forever grateful for that. I will buy you all the silver canned Monsters you want. To Dr. Karla Frietze, thank you so much with your expertise and constantly being there for me. Whether it was a quick question or teaching me a whole pathway in detail, you were

always there for me during this process. Thank you so much Karla. Go team RIG! To Dr. Nickels, thank you for allowing me to conduct my research in your lab. You were always there for me, whether it was a quick meeting in your office to discuss anything whether it was science related or not. You kept pushing me to strive for greatness and for that I thank you. Furthermore, you really made our lab feel like family. Thank you Joe.

To all my family, friends and to my girlfriend, Gabriella Scott, thank you for all your patience and support during this difficult program. I had to sacrifice a lot of my time and energy to complete this program and every single one of you understood that and supported me during the whole process. Without all your support and motivation, I would not have been able to finish this program. Thank you.

I dedicate my degree to my parents, Joseph, and Phyllis, and to my late-grandmother, Palma. My parents supported me every single second. Whether it was having meals prepared for me whenever I got home, to allow me to stay at home during this program, to your continuous support and motivation. Thank you, mom, and dad. I could not have done it without the both of you. To Palma, you introduced me to the science field when I was a child. You were the one that made me so interested in this field and showed me the importance of helping others. It was devastating to see you suffer everyday with the crippling effects of multiple sclerosis, since then I knew for the rest of my life, I would dedicate myself to the research field to help others. I am so fortunate to find and complete this program to allow me to further improve my research skills and to put me in a better position to help others.

This one is for you mom-mom, I know you are so happy for me up in heaven where you are walking around not needing a wheelchair.

Abstract

Acyl-CoA cholesterol acyl transferase related enzyme-2 required for viability 1 (ARV1) was first recognized in *Saccharomyces cerevisiae* in a study done in 2000 by Tinkelenberg et al. In yeast, the deletion of ARV1 results in numerous defects including abnormal sterol trafficking [1], the reduction of sphingolipid metabolism [2], synthesis of glycosylphosphatidylinositol (GPI) anchor [3], ER stress [4], and hypersensitivity of fatty acids leading to lipoapoptosis [5]. Arv1 germline deletion in mice displayed a lean phenotype with increased energy [6]. In humans, ARV1 mutations lead to epileptic encephalopathy [7].

Non-alcoholic fatty liver disease (NAFLD) consists of simple steatosis to non-alcoholic steatohepatitis (NASH), fibrosis, cirrhosis, and hepatocellular carcinoma [8]. NAFLD is the most common liver disease worldwide affecting 25% of the global population and 33% of the population in the United States [8]. NAFLD is on the rise due to irresponsible dietary and sedentary lifestyles. Currently, there is not a pharmacological treatment for NAFLD.

The specific aims include the generation of ARV1 over expression and ARV1 knockout in HepG2 cells, to investigate gene expression profiles in each respective ARV1 cell line using Qiagen RT^2 Profiler arrays and to identify novel pathways to validate Arv1 function in HepG2 cells. We found ARV1 over expression cells to be lipotoxic in HepG2 cells. We showcased EGFR phosphorylation of Arv1. We observed two different EGFR inhibitors where both “rescued” toxicity in Arv1 over expression cells.

Introduction

I. Non-Alcoholic Fatty Liver Disease

Non-alcoholic fatty liver disease (NAFLD) consists of simple steatosis to non-alcoholic steatohepatitis (NASH), fibrosis, cirrhosis, and hepatocellular carcinoma [8]. NAFLD is the most common liver disease worldwide affecting 25% of the global population and 33% of the population in the United States [8]. NAFLD includes both non-alcoholic fatty liver (NAFL) and NASH. NAFL is identified by steatosis of the liver, involving greater than 5% of the parenchyma, where there is no sign of hepatocyte injury [9]. Whereas NASH is defined by inflammatory damage to hepatocytes. Furthermore, the prevalence of NAFLD is consistently increasing every year worldwide due to an increase in sedentary lifestyle and irresponsible dietary lifestyle [10]. Moreover, there has been steady rise of NAFLD in relation to metabolic syndrome and diabetes. NAFLD has been projected in the next 20 years to be the major cause of liver related morbidity, mortality, along with a leading cause for liver transplantation [10]. Currently, NAFLD is the second leading reason for a liver transplantation.

A. Risk Factors

A.1 Cardiovascular risk and type II diabetes

Metabolic syndrome is a mixture of cardiovascular risk factors that predispose a person to cardiovascular disease and type II diabetes [9]. Currently, the diagnostic criteria require having 3 of 5 of the following factors: high-density lipoprotein-

cholesterol of less than 40 mg/dL in men and less than 50 mg/dL in women, triglycerides greater than 150 mg/dL or higher, an increased waist circumference, hypertension (systolic blood pressure 130 mmHg or greater or diastolic blood pressure of 85 mmHg or greater), and hyperglycemia (fasting glucose of 100 g/dL or greater) [9]. The incidence of NAFLD has been increasing with the rising rate of metabolic syndrome. Furthermore, the incidence of NAFLD increases with each additional criterion met for metabolic syndrome. When non-diabetic patients are compared to type 2 diabetes mellitus (T2DM) patients, T2DM patients were shown to have liver fat contents that are increased by 80% [11]. In addition, it has been shown that TD2M patients with NAFLD can have normal functional tests, implying that the prevalence of NAFLD may be even higher than reported [11]. Unfortunately, TD2M patients have a 2-4-fold increase for fatty liver complications and an extremely high risk of developing NASH [12].

A.2 Race

In a study based in the United States, it was found that African Americans had a lower degree of steatosis compared to Caucasians. Also, this study found a higher degree of NAFLD in Asians and Hispanics [13]. African Americans demonstrated a lower chance of developing liver failure while the Hispanic population demonstrated a higher occurrence of steatohepatitis and cirrhosis [14].

A.3 Gender and age

The role of gender for development of NAFLD have been inconclusive where some studies show a higher prevalence in males, whereas others show a higher

prevalence in females. However, the prevalence of NAFLD increases with age, 20% of people under the age of 20, and greater than 40% in people over 60 years old [15]. In addition to the prevalence of NAFLD with increasing age, the incidence of NASH and cirrhosis increase over the age of 50 compared to younger age groups [10]. Obesity has been shown in adults, as well as children, to be a substantial risk factor for the development of NAFLD [16]. Fatty liver is the most common liver aberration in the age bracket of 2-19. Interestingly, adulthood and pediatric NAFLD show higher levels in LDL, cholesterol, systolic blood pressure and triglycerides [16]. Luckily, the HCC incidence in pediatric patients with NAFLD is believed to be extremely rare. Currently, only one reported case of a 7-year-old boy with HCC in concurrence with NAFLD has been documented [17].

A.4 Diet

Diet is believed to be an independent risk factor for developing NAFLD, specifically an HFD [10].Interestingly, it has been demonstrated by caloric restriction and controlling dietary macronutrients, specifically fats and carbohydrates, to reduce metabolic syndrome [18]. The Western pattern diet (WPD) has a very high association with the possibility of developing metabolic syndrome and succeeding NAFLD [14]. Additionally, there is an association with the person's sedentary behavior and fitness with the risk of developing NAFLD/NASH, where the severity of NAFLD worsens with the lower the patient's physical activity. Furthermore, part of treatment for NAFLD involves a balance diet and exercise to manage insulin resistance and obesity. There are several studies addressing the effect of a balanced

diet with weight reduction and the positive effects on NAFLD like reducing hepatic fatty infiltration, improving serum liver enzymes, decreased hepatic inflammation and decreasing levels of fibrosis [19].

B. Genetics

Multiple studies have found evidence indicating NAFLD has a heritability component by performing twin studies, interethnic differences and familial aggregation [10]. Additionally, by performing whole exome sequencing on obese Caucasian volunteers with NAFLD and found deleterious mutations in Melanocortin 3 receptor gene and Bardet-Biedl syndrome 1 gene [20]. In 2008, the first genome wide association study was published, investigating hepatic triacylglycerol (HTAG) accumulation and demonstrated a direct association with the PNPLA3 gene [21]. In a meta-analysis study with 9915 participants done by Singal et al., found PNPLA3 to be directly associated with fibrosis severity [22]. Additionally, nine more studies with 2937 participants, found PNPLA3 to be linked with an increased risk for the development of HCC in patients with cirrhosis [22]. Interestingly, genome-wide association studies indicated a locus on chromosome 19 that is connected to plasma triglyceride and NAFLD, but it was unknown which gene(s) function this was. Until a study done by Mahdessian et al., where they performed gene expression studies and expressive quantitative locus trait analysis of 206 human liver samples to identify the unknown gene(s). Their data suggests TM6SF2 and it to be a master regulator of liver fat metabolism, therefore, effecting hepatic lipid droplet content and triglyceride secretion [23]. Current research has approximately 7 categories of genes to be

associated with NAFLD, these categories being the following: (1) hepatic lipid export/oxidation in steatosis (PNPLA3, TM6SF2, PPAR-α, NR1I2, MTTP, PEMT, APOE and APOC3); (2) steatosis-hepatic lipid import/synthesis (FADS1, SLC27A5, and LPIN1); (3) glucose metabolism and insulin resistance (ENPP1/IRS1, SLC2A1, GOAT, GCKR, TCF7L2, and PPAR-γ); (4) steatohepatitis-endotoxin response (CD14 and TLR4); (5) steatohepatitis-oxidative stress (SOD2, HFE, GCLC/GCLM and ABCC2); (6) fibrosis (AGTR1 and KLF6); (7) cytokines (IL6 and TNF) [10].

C. Pathogenesis

NAFLD correlates with deposition of fat in the liver, more specifically, triglyceride accumulation and free fatty acids in the liver. Free fatty acids and triglyceride accumulation is attributed to obesity and insulin resistance [24]. However, the pathogenic factors of NAFLD are multi-factorial and complex with a variety of theories behind its pathogenesis. Commonly, a two-hit model of the development of NAFLD has been suggested with the first hit involving sedentary lifestyle, high fat diet, obesity, hepatic lipid accumulation, and insulin resistance [25]. Whereas the second hit, involves the activation of the inflammatory system with an association of fibrogenesis [10]. However, this two-hit model has lost its favorability due to this model being ‘too simplistic’ and not accounting for a multitude of other factors like genetic predisposition. Nevertheless, a major role in the development of steatosis/NASH is insulin resistance, resulting in de novo lipogenesis, which leads to the reduction of adipose tissue lipolysis then a significant increase in fatty acids in the liver [26]. The dysfunction of adipose tissue due to insulin resistance can lead to the

alteration in production and secretion of inflammatory cytokines and adipokines. Furthermore, the accumulation of triglycerides in the liver generates reactive oxygen species, endoplasmic reticulum stress alongside mitochondrial dysfunction [10]. In addition, a plethora of nutrients can overwhelm the endoplasmic reticulum resulting in activating the unfolded protein response (UPR), then initiating the development of insulin resistance through a variety of mechanisms including inflammation and c-Jun N terminal kinase activation [27]. Importantly, the dysfunction of adipose, which is seen in T2DM, obesity and NAFLD impairs glucose and lipid metabolism [27].

D. Histopathology

NAFLD displays a wide range of histologic manifestations ranging from mild steatosis, to aggressive forms showing portal and/or lobular inflammation, to the ballooning of hepatocytes, fibrosis, and cirrhosis [10]. The presence of less than 5% of steatosis is deemed clinically insignificant. However, if a patient has at least 5% steatosis then the steatosis is ranked. Steatosis is ranked by a three-tiered system: 5%-33% is mild, 34%-66% is moderate, and greater than 66% is deemed severe steatosis [28]. Unfortunately, conventional imaging (magnetic resonance imaging, computed tomography, or ultrasound) is not sensitive enough to detect hepatic steatosis if its less than 30%. Therefore, advanced imaging like magnetic resonance imaging-estimated proton density fat fraction, controlled attenuation parameter, and ^{1}H - magnetic resonance spectroscopy is required for assessment.

E. Staging and Grading in NAFLD/NASH

There are three histological scoring systems to determine the staging of NAFLD/NASH including NASH clinical research network's NAFLD activity score (NASH CRN-NAS), steatosis, activity, and fibrosis (SAF), and the Brunt staging system. The NAS system uses a scoring system to determine an activity grade of NASH (see table #1). This scoring system includes steatosis, hepatocellular ballooning, and inflammation, as well as a separate fibrosis grading system. A score ≥ 4 diagnoses the patient with NASH. Whereas a score < 3 demonstrates an absence of NASH. The SAF staging system focuses on steatosis, activity, and fibrosis.

Table #1. **NAFLD/NASH Scoring using NASH CRN-NAS System**. The NAS histological scoring system uses numerical scores to determine the activity grade of NAFLD/NASH. This system focuses on steatosis, lobular inflammation and hepatocyte ballooning. If the sum is ≥ 4 then NASH is diagnosed. Separately, fibrosis is diagnosed from stage 0-4.

Steatosis Grade (0-3)	
<5%	0
5%-33%	1
34%-66%	2
>66%	3
Lobular Inflammation (0-3)	
No foci	0
<2 foci per 200x field	1
2-4 foci per 200x field	2
>4 foci per 200x field	3
Hepatocyte Ballooning (0-2)	
None	0
Few Balloons	1
Many cells/prominent ballooning	2

Fibrosis Stage	
None	0
Perisinusoidal or periportal	1
Mild, zone 3, perisinusoidal	1A
Moderate, zone 3, perisinusoidal	1B
Portal/periportal	1C
Perisinusoidal and portal/periportal	2
Bridging fibrosis	3
Cirrhosis	4

F. Occurrence and Progression of NAFLD

The global prevalence of NAFLD is estimated to be about 25%; in the Middle East and South America the prevalence ranges from 31-32%, in Europe and Asia ranging from 24-27% and 14% in Africa [29]. NAFLD is encompassed by liver lesions that include simple steatosis, steatohepatitis, fibrosis, and cirrhosis. The main feature in majority of patients include steatosis, however these patients normally do not have a high risk of adverse outcomes of the liver. However, patients with NAFLD have a 20-30% of developing NASH [30]. Furthermore, NASH can lead to cirrhosis and even end stage liver disease [31]. The progression of NAFLD to cirrhosis is more frequent to middle-aged and elderly people [31]. Additionally, NAFLD progression is associated with HCC [32]. A rising cause of HCC in Western countries is NAFLD-related cirrhosis, making up 10-34% of the etiologies for HCC [31]. Furthermore, it has been shown that 13-49% of HCCs develop in patients with non-cirrhotic NASH, indicating NAFLD and NASH significantly contribute to the development of cirrhosis and HCC [33]. Figure # 1 displays the progression of NAFLD along with the percentage of the population at each stage of NAFLD.

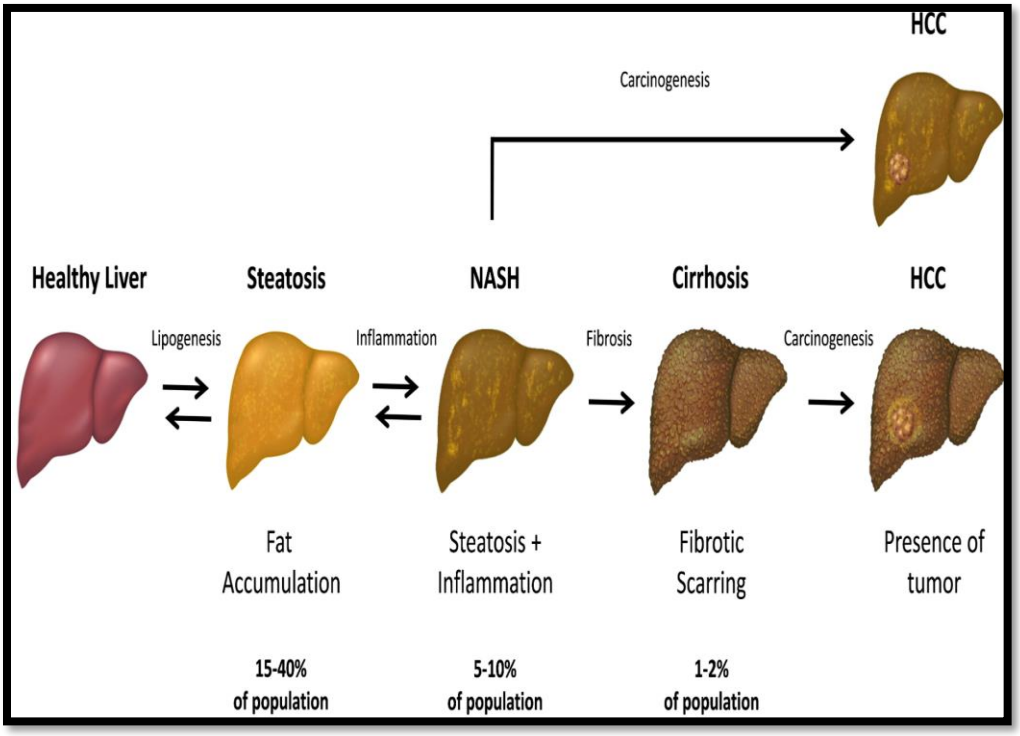

Figure # 1. **The Progression and stages of NAFLD**. The initial stage of NAFLD is steatosis, by the characterization of excessive fat accumulation in hepatic cells. Upon the development of inflammation, the liver steatosis may develop into NASH and potentially lead into liver cirrhosis. Both, NASH and cirrhosis patients have an increased risk of developing HCC. Importantly, steatosis and NASH are reversible, whereas cirrhotic tissue cannot revert to healthy tissue.

G. Diagnosis, Treatment and Screening

NAFLD, in most cases, is an incidental diagnosis where patients are asymptomatic, and steatosis of the liver is found due to imaging for another purpose [34]. However, in the absence of incidental finding, patients are often asymptomatic until the occurrence of liver decompensation. Fortunately, if the patient discloses certain factors like obesity, insulin resistance, or other factors associated with metabolic syndrome, the diagnosis can be reached much earlier than decompensation of the liver [34] Furthermore, a physical examination of the patient's BMI and visceral adiposity are useful clues to determine the presence of NAFLD. On the other hand, screening of patients who are at risk for the development of NAFLD is more challenging than originally expected due to liver function tests able to be in normal range even in the presence of NAFLD. The diagnosis of NAFLD is a four-pronged approach (see figure # 2).

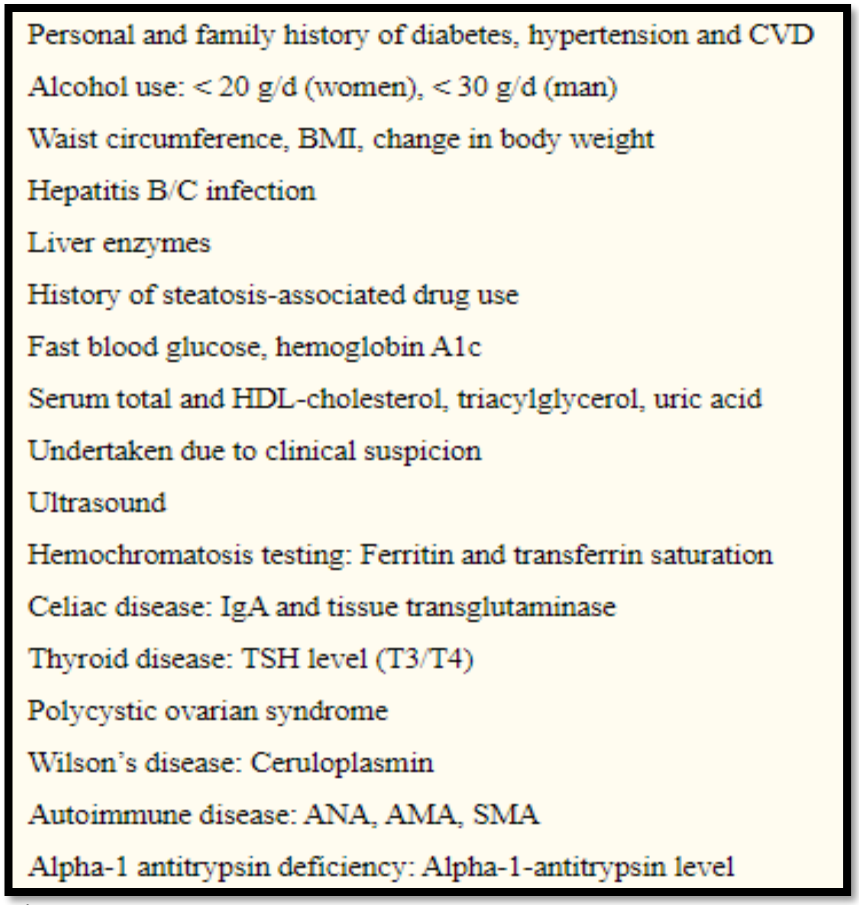

Figure # 2. **Key factors in the evaluation of a patient suspected with NAFLD**. This figure demonstrates the four-pronged approach. (1) Showing hepatic steatosis (via histology or imaging). (2) The consumption of alcohol is ruled out. (3) There are no rival etiologies. (4) No other causes for chronic liver damage can be found. Several key differential diagnoses that should be ruled out includes chronic hepatitis B and C, medication use, alcohol use, biliary disease, autoimmune hepatitis, parenteral nutrition, and malnutrition.

ANA: Anti-nuclear antibody; AMA: Anti-mitochondrial antibody; SMA: Anti-smooth antibody; CVD: Cardiovascular disease; BMI: Body mass index; HDL: High density lipoprotein; TSH: Thyroid stimulating hormone.

The most important treatment option for NAFLD includes a monitored diet and consistent exercise. In line with, is surgical interventions for the treatment of NAFLD. Additionally, medications are part of a treatment plan in battling NAFLD. There are 4 main pathways available for the treatment of NAFLD. First, targeting hepatic fat accumulation (elafibranor, pioglizone and saroglitazar), *de novo* lipogenesis inhibitors (aramchol), bile acid-farnesoid X receptor axis (obeticholic acid), incretins (liraglutide), and fibroblast growth factor FGF-21 analogues [35]. Second, immune modulators (amlexanox and cenicriviroc) and decrease of oxidative stress using medications that target TNF-α pathway (emricasan and pentoxifylline) [35]. Third, antifibrotics (simtuzumab) and lastly, anti-obesity medicine (orlistat). Therapies such as obeticholic acid, Orlistat, statins, Omega-3 have been studied indicating varied and limited outcomes [36]. Additionally, studies using chemokine receptors antagonists, fatty acid/bile acid conjugates, PPAR-α/δ agonists are currently being evaluated for their potential effect on treating NAFLD.

II. Hepatocellular Carcinoma

Hepatocellular carcinoma (HCC) is a primary cancer of the liver where it is derived from hepatocytes and occurs in more than 80% of liver cancer cases [37]. HCC accounts for the second highest cancer mortality rate worldwide [38]. Therefore, research has been targeting potential risk factors for hepatocarcinogenesis and more effective therapies. Even with recent advances in an improved early diagnosis and treatment of a short-term prognosis; long-term prognosis remains poor even after a curative treatment [39].More than 90% of HCCs develop due to chronic liver damage and inflammation caused by hepatitis B virus or hepatitis C virus [40]. Additionally, in developed countries, HCC is on the rise due to an increase prevalence of type 2 diabetes (T2DM) and obesity, which are two major risk factors for NAFLD [41]. Furthermore, the incidence of non-viral HCC is on a rapid increase, especially in the United States. It is observed that nearly all patients with non-viral HCC demonstrate obesity, show symptoms of metabolic syndrome and have non-alcoholic steatohepatitis [40]. The process by which obesity promotes hepatocarcinogenesis is still not completely understood. However, several tumor micro-environmental factors including elevated proinflammatory cytokines triggered by endoplasmic reticulum (ER) stress and oxidative stress, dysregulation of adipokines, altered gut microbiota and insulin resistance-mediated hyperinsulinism are considered to promote the development of HCC [40, 42].

III. ARV1

Acyl-CoA cholesterol acyl transferase (ACAT) related enzyme-2 required for viability 1 (ARV1) was first recognized in *Saccharomyces cerevisiae* in a study done in 2000 by Tinkelenberg et al. the research group was studying genes that could be involved in mediating sterol trafficking, therefore a screen for yeast mutants that were inviable in the absence of sterol esterification was performed. Mutations in the ARV1 gene, make cells dependent on sterol esterification for growth, temperature sensitive, nystatin-sensitive, and anaerobically inviable. Cells without ARV1 demonstrated altered sterol uptake along with trafficking sterol into the plasma membrane (PM)[1]. Furthermore, a database search of expressed sequence tags indicated a similarity of ARV1 in human, yeast, and other multicellular eukaryotes. Additionally, a full-length cDNA human ARV1 was sequenced and predicted a 271 amino acid protein. Interestingly, the search indicated a similarity amongst *Arabidopsis thaliana*, *Caenorhabditis elegans*, yeast, and humans, where a 61 amino acid NH2-terminal region which contains a zinc-binding motif along with a 33 amino acid block, this region is deemed as the Arv1 homology domain (AHD) [1]. A zinc-binding motif can serve a multitude of functions including charged lipid binding and the regulation of small molecule transport to name a few [1]. With the similarity of Arv1 AHD and the 6 transmembrane regions in yeast and human, the researchers tested to see if the functions in yeast and human were related. Their work indicated human Arv1 was able to rescue the growth defects in yeast with mutant Arv1. Further, reinforcing the working hypothesis of how important ARV1 is in sterol homeostasis, where there is a conserved component across different organisms.

Following the study done by Tinkelenberg et al., a study was done in 2002 by Swain et al., demonstrating Arv1 mutant in yeast have defects in sphingolipid metabolism [2]. Their study used [^{3}H] inositol and [^{3}H] dihydrosphingosine radiolabeling on mutant Arv1 yeast and found a decreased rate of biosynthesis as well as lower steady state levels of complex sphingolipids in the Arv1 mutant yeast [2]. Additionally, neutral lipid radiolabeling showcased the rate of biosynthesis of sterol ester were increased in the mutant yeast. Conversely, the mutant yeast indicated a decrease rate of biosynthesis of total fatty acid and fatty acid alcohols [2].

In 2010, Tong et al., used antisense oligonucleotides (ASOs) to knock-down murine livers and HepG2 cells indicating increased serum bile acids, activation of hepatic farnesoid X receptor (FXR) pathway, impaired anterograde transport of sterol from the ER to PM, and hypercholesterolemia [43]. Furthermore, this study suggests Arv1 to play an important role in bile acid homeostasis and regulation of cholesterol in hepatocytes [43].

In 2011, Shechtman et al., did a study on arv1 mutant yeast and on murine macrophages demonstrating with the loss or decrease of Arv1 resulting in the activation of the unfolded protein response (UPR). By using an electron microscope and a fluorescent microscope on Arv1 mutant yeast, their data suggests the accumulation of sterol, the expansion of subcellular membrane, and increased lipid droplet formation [4]. Additionally, by using a transcription profiler with the deletion of ARV1 in yeast indicated an activation of Hac1p along with an increase of expression of IRE1p, (IRE1p is a mediator of the UPR in yeast, whereas ATF6, PERK, and IRE1 in mammals). Furthermore, a decreased expression of Arv1 in

murine macrophages indicate the activation of the UPR. Specifically, an increase in activating transcription factor-4 (ATF4), C/EBP homologous protein (CHOP), and apoptosis [4]. Their study suggests the loss or decrease of Arv1 activates the UPR due to its role in lipid homeostasis. Importantly, the loss of Arv1 in different cells, all activate the UPR possibly due to its altered lipid metabolism resulting in an imbalance of the ER homeostasis. Furthermore, any mutations in ARV1 may influence diseases that play a role in lipids like obesity, type 2 diabetes, and atherosclerosis.

In 2014, a study done by Ruggles et al., found the most lipo-sensitive yeast strain was yeast with the deletion of ARV1. Additionally, in MIN6 pancreatic β-cells and HEK293 cells with decreased Arv1 expression displayed an increase in fatty acid sensitivity, decreased neutral lipid synthesis, and lipoapoptosis [5]. Interestingly, by over-expressing Arv1 by using an adenovirus in HEK293 cells and mouse livers, the group found increased lipid droplet number and increased triglyceride mass [5]. Additionally, in the over-expressing ARV1 cells, CD36 and DGAT1 were increased. Following up the finding of the increase of CD36 and DGAT1 in the over expression ARV1 cells. The group tested specific activators of RXR, PPARα, PPARγ, CAR, PXR, FXR, LXR on rodents and assessed the expression of ARV1. Their data suggests murine ARV1 expression is driven by PPARα [5]. Additionally, wild-type mice were treated with PPARα agonists, fenofibrate and GW7647, showing an increase in ARV1 expression. Overall, data from this study suggests murine ARV1 is a PPARα target, and Arv1 is likely a pivotal role in TAG homeostasis.

In 2015, a study done by Lagor et al., performed a germ line deletion of ARV1 in mice. The KO mice displayed decreased high density lipoprotein cholesterol and total cholesterol [44]. Additionally, the KO mice displayed a lean phenotype along with significant decrease of body weight and white adipose tissue (WAT) on regular chow. In line with, the decrease of WAT demonstrated higher adiponectin levels, improved glucose tolerance, increased rate of fatty acid oxidation, and increased energy expenditure [44].

In 2018, a study done by Gallo-Ebert et al., found Arv1 knock-out mice that were fed a high fat diet had lower blood cholesterol, lower triglyceride levels, resistant to diet induced obesity, and preserved insulin sensitivity and glucose tolerance [6]. Additionally, the group found an increase in PPARα in the knockout mice.

In summary, the ARV1 gene is located on 1q42.2, encoding a 271 amino acid protein. Importantly, the function of Arv1 in humans remains to be unknown. Arv1 is a transmembrane protein of the endoplasmic reticulum (ER) with a cytosolic N-terminal zinc binding motif. Next, comes the several transmembrane regions. Lastly, the C-terminal region facing the ER [7]. In yeast, the deletion of ARV1 results in numerous defects including abnormal sterol trafficking [1], the reduction of sphingolipid metabolism [2], synthesis of glycosylphosphatidylinositol (GPI) anchor [3], ER stress [4], and hypersensitivity of fatty acids leading to lipoapoptosis[5].In mice, a germline deletion in mice displayed a lean phenotype with increased energy.

Additionally, it has been observed by Palmer et al., a female individual had a Arv1 variant; this variant leads to an in-frame deletion of 40 amino acids. The loss of

these 40 amino acids results in the removal of over half the AHD, where the N-terminal of this has been shown to be required for function in yeast. This truncation led to the patient to have severe neurodegenerative problems [7]. Unfortunately, this patient only lived to be 12 months of age. The same research group tested on mice, tissue specific Arv1 deletion in the central nervous system. The mice experienced intense seizures and death [7].

If the human function is correlated to its role in yeast, then ARV1 may be a biomarker or targeted for treatment in the future for lipid-related diseases like NAFLD, type 2 diabetes, and atherosclerosis. However, Arv1 deficiency may be a syndrome of intellectual disability and/or developmental delay. Therefore, more research should be done to investigate its role on intellectual development.

Rationale

NAFLD is the most common liver disease worldwide affecting 25% of the global population and 33% of the population in the United States [8]. NAFLD consists of simple steatosis to non-alcoholic steatohepatitis (NASH), fibrosis, cirrhosis, and hepatocellular carcinoma [8]. Diet is believed to be an independent risk factor for developing NAFLD, specifically an HFD [10]. The most important treatment option for NAFLD includes a monitored diet and consistent exercise. Unfortunately, in most cases, NAFLD is an incidental diagnosis where patients are asymptomatic, and steatosis of the liver is found due to imaging for another purpose [34]. However, in the absence of incidental finding, patients are often asymptomatic until the occurrence of liver decompensation. Additionally, when a patient is symptomatic and the diagnosis is finally made, it can be already too late for reversal. Therefore, a biomarker and/or treatment for NAFLD is highly needed. Currently, there is no pharmacological treatment for NAFLD. Furthermore, NAFLD can progress to hepatocellular carcinoma. HCC is a primary cancer of the liver where it is derived from hepatocytes and occurs in more than 80% of liver cancer cases [37]. HCC accounts for the second highest cancer mortality rate worldwide [38]. Therefore, research has been targeting potential risk factors for hepatocarcinogenesis and more effective therapies. Even with recent advances in an improved early diagnosis and treatment of a short-term prognosis; long-term prognosis remains poor even after a curative treatment [39].

Acyl-CoA cholesterol acyl transferase (ACAT) related enzyme-2 required for viability 1 (ARV1) was first recognized in *Saccharomyces cerevisiae* in a study done

in 2000 by Tinkelenberg et al. The research group's data suggested Arv1 is involved in sterol uptake/transportation. Importantly, human Arv1 was able to "rescue" Arv1 mutant yeast allowing normal sterol uptake/transportation. Additional studies indicated the deletion of Arv1 in yeast and murine cells to show the reduction of sphingolipid metabolism [2], synthesis of glycosylphosphatidylinositol (GPI) anchor [3], ER stress [4], and hypersensitivity of fatty acids leading to lipoapoptosis [5].

Furthermore, germline deletion of ARV1 in mice demonstrated a lean phenotype with the addition of increase energy expenditure and improved glucose tolerance [44]. Therefore, if Arv1 has a role in lipid metabolism, it could suggest a change of Arv1 expression could be of use in patients with NAFLD.

Additionally, a neuronal deficiency of ARV1 causes autosomal recessive epileptic encephalopathy in mice and humans causing seizures and spontaneous death [7]. Therefore, more research is needed to understand how Arv1 can cause developmental delay/intellectual development.

Therefore, we want to generate ARV1 knock-out and ARV1 over-expressing cells in HepG2 to see any potential differences in amongst cell lines. Then, we want to want to take a broad and unbiased approach of looking at gene expression profiles amongst these cell lines by using Qiagen's RT^2 Profiler arrays. Lastly, to identify any potential changes in pathways amongst cell lines in HepG2 cells to validate the function of human Arv1.

Materials and Methods

I. Cell Culture

A. Wild Type Human Hepatocellular Carcinoma Cells

Human HepG2 cell line was acquired from American Type Culture Collection (ATCC) (ATCC® HB-8065™) was grown in a medium containing Dulbecco's modification of eagle medium (Corning, Cat. No. 10-013-CV) supplemented with 10% fetal bovine serum (Corning, Cat. No. 35-016-CV) and 1% penicillin-streptomycin (Corning, Cat. No. 30-002-CL). The cell lines were stored at 37℃ in 5% carbon dioxide (CO_2). All the cell lines were used from passages 8-13.

B. HepG2 Santa Cruz CRISPR Knockout/Homology Directed Repair of ARV1

CRISPR-Cas9 KO plasmid and Homology-Directed repair plasmid were obtained from Santa Cruz Biotechnology (Santa Cruz, Cat. No. sc-407460, sc-407460-HDR; respectively) (See Figure # 3). First, 800,000 HepG2 WT cells were counted using a cell counter (Corning CytoSmart, Cat. No. 6749). Simultaneously, the co-transfection reagents were prepared. Next, 2.5 µg of CRISPR ARV1 KO plasmid and 2.5 µg HDR plasmid were vortexed with 40 µL Enhancer from Qiagen Effectene transfection reagent kit (Qiagen, Cat. No. 301425) for 1 second. Next, incubated the mixture for 5 minutes at room temperature and briefly centrifuge. Then, added 25 µL Effectene transfection reagent to the DNA-Enhancer mixture and vortexed for 15 seconds. Next, incubated the sample for 15 minutes at room temperature to allow transfection complex formation. After the 15-minute incubation

time, 1 mL of antibiotic free growth media was added to the tube containing the transfection complexes and pipetted up and down several times. Separately, 2 mL growth medium (DMEM + 10% FBS) was added to a 60mm dish. The transfection complex was added dropwise to the 60mm dish and gently swirled. Next, the 800,00 cells were carefully added to the 60mm dish containing the growth medium/transfection complexes and was gently swirled. Cells were grown for 72 hours without antibiotic selection. Next, cells were grown under antibiotic selective pressure using puromycin at a concentration of 3 µg/ml for 2 weeks.

Cre vector reverse transfection was performed by using Cre plasma DNA (Santa Cruz, Cat. No.sc-418923), UltraCruz transfection reagent (Santa Cruz, Cat. No. sc-395739), plasmid transfection medium (Santa Cruz, Cat. No. sc-108062) and HepG2 KO/HDR cells. First, added 2.5 µl (1 µg/µl) of Cre vector DNA to 147.5 µl of UltraCruz transfection medium and pipetted up and down to ensure proper mixing. Incubated at room temperature for 5 minutes. Next, 15 µl of UltraCruz transfection reagent was added to 135 µl of plasmid transfection medium and pipetted up and down gently. Incubated at room temperature for 5 minutes. The 150 µl of DNA-transfection medium complex is drop-wise added to the 150 µl transfection reagent-transfection medium complex, totaling in 300 µl and was vortexed immediately. The HepG2 KO/HDR cells were split and counted using the cell counter (Corning CytoSmart, Cat. No. 6749). Next, 800,000 HepG2 KO/HDR were gently added to a 60 mm cell culture vessel with complete growth medium (no antibiotics). Simultaneously, the complexes were incubated for 30 minutes and the 300 µl was

drop-wise added to the HepG2 KO/HDR cells. Cells were grown for 72 hours then accessed using RNA extraction.

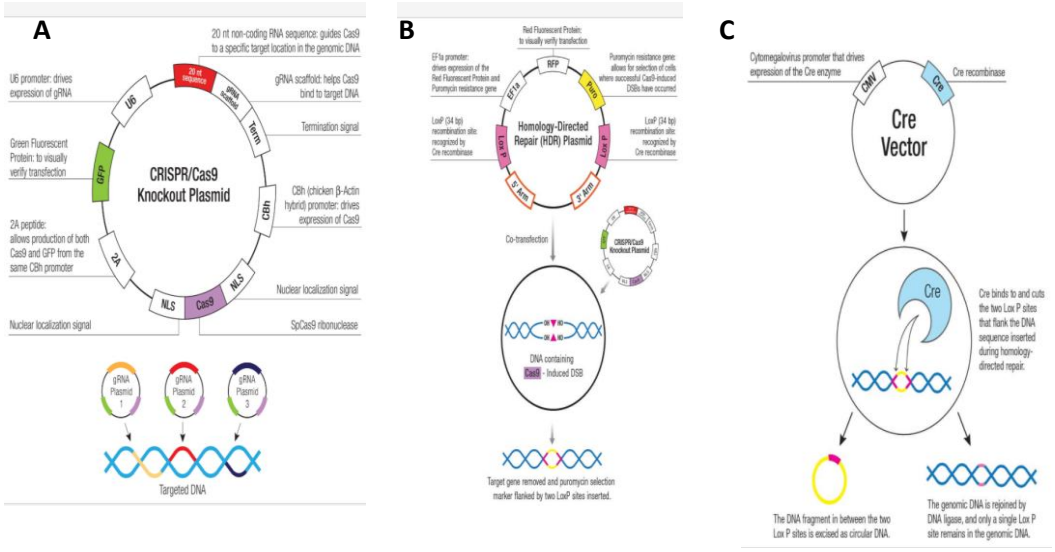

Figure # 3**. CRISPR/Cas9 Knockout and Homology Directed Repair**. Consists of three plasmids each encoding the Cas-9 nuclease and an Arv1-specific guide RNA (gRNA). The gRNA sequences direct the Cas-9 to induce a double stranded break in the genomic DNA [A]. Consists of 2-3 plasmids, each containing a homology directed-repair (HDR) template designed to specifically bind to the Cas-9 double stranded DNA break. Each plasmid inserts a red fluorescent protein (RFP) and a puromycin resistance gene [B]. The Cre vector expresses Cre recombinase to catalyze the site-specific DNA recombination between the two LoxP sites and to excise the genetic material [C] .

C. Transient Over-Expression of ARV1 in HepG2 Cells

HepG2 WT cells were reverse-transfected with 'JNB2166' pcDNA3.1 construct designed by former IMD employee Dr. Hsing-Yin Liu. By using Mirus TransIT-X2 system (Mirus, Cat. No. MIR 6004) in a 100 mm culture vessel with collagen coating (BioCoat, Cat. No. 356450) using 15.5 ml of complete growth medium with no antibiotics. First, the TransIT-X2 and ARV1 plasmid (See Figure #4) complexes were prepared. The TransIT-X2 was warmed to room temperature and was vortexed gently. Next, 1.5 ml of Opti-MEM I reduced-serum medium (Gibco, Cat. No. 31985062) was placed into a sterile tube. 15 µl of ARV1 plasmid at 1 µg/µl was added to the Opti-MEM and pipetted gently up and down. Next, added 45 µl of TransIT-X2 to the DNA mixture and pipetted gently up and down. At room temperature the complexes were incubated for 30 minutes. While the complexes were forming, 2 million HepG2 WT cells were split and counted using (Corning CytoSmart, Cat. No. 6749). After the 30-minute incubation period, both the HepG2 WT cells and TransIT-X2-ARV1 complexes were added dropwise to the 10 cm culture vessel with 15.5 ml complete growth media (no antibiotics) and was gently rocked to ensure even distribution. 72 hours later the cells were harvested for RNA extraction.

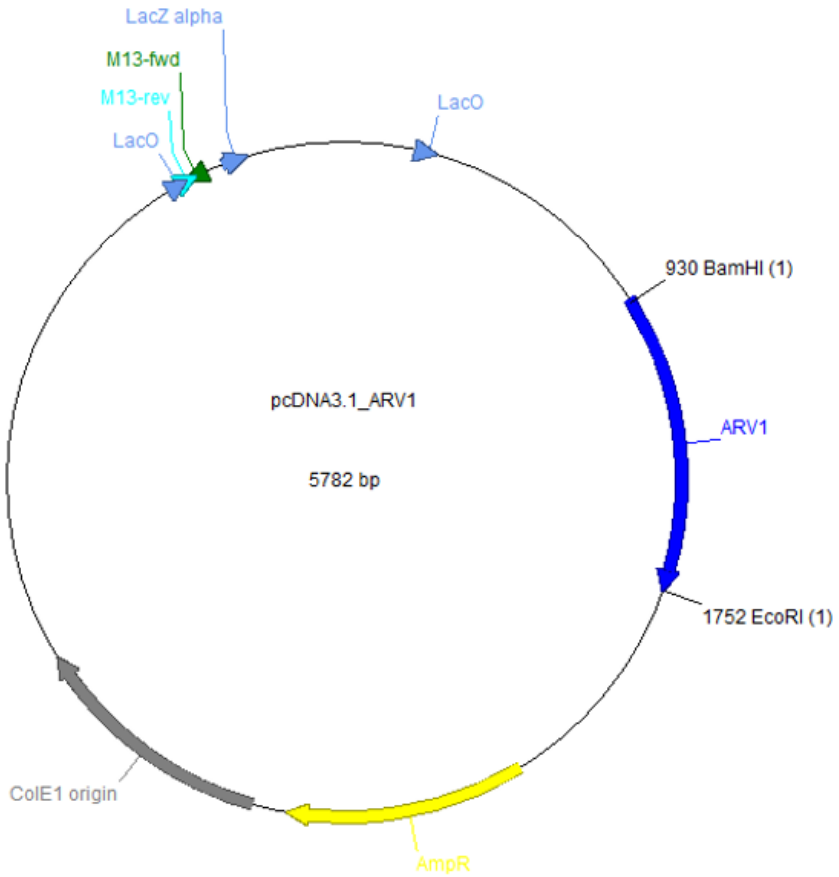

Figure # 4. **Plasmid Map of pcDNA3.1 Bearing Human ARV1 Sequence**. ARV1 was cloned in with restriction enzymes BamHI and EcoRI by Genscript, Map generated with ApE plasmid editor.

II. RNA Extraction

Mature RNA was isolated using miRNeasy Mini extraction kit (QIAGEN, Cat. No. 217004). HepG2 cells were directly lysed from a 10 cm cell culture dish using 700µL of QIAzol lysis reagent. Collected the lysate with a rubber policeman. The lysate was pipetted into a microcentrifuge tube and vortexed thoroughly until there were no visible clumps. The tube containing the homogenate was placed on the benchtop at room temperature for 5 minutes. Next, 140 µL of chloroform was added and the tube was shaken vigorously for at least 15 seconds. The tube containing the homogenate was placed on the benchtop at room temperature for 3 minutes to allow subsequent phase separation. Next, centrifuged for 15 minutes at 12,000 x g at 4°C. This centrifugation step allows the sample to separate into 3 phases: an upper, colorless aqueous phase containing RNA; a white interphase and lower pinkish red organic phase. Next, transferred the top phase only (approximately 350 µL) to a new collection tube. Added 1.5 volumes (approximately 525µL) of 100% ethanol to the new collection tube. Pipetted slowly up and down to make sure it was mixed thoroughly. Immediately, 700 µL of the sample was added to the RNeasy mini spin column in a 2mL collection tube. Centrifuged at 8000 x g for 15 seconds at room temperature and discarded the flow-through. The previous step was repeated until the remainder of the sample was used. Next, pipetted 350µL buffer RWT into the RNeasy mini spin column and centrifuged for 15 seconds at 8,000 x g. The flow-through was discarded. Added 10 µL DNase I stock to 70 µL Buffer RDD, mix by gently inverting the tube, the DNase kit (Qiagen, Cat. No. 79254) is separate from miRNeasy mini kit. Next, pipetted 80 µL of the DNase I incubation mix directly onto

the RNeasy membrane, failure to directly add to the membrane may cause the DNase digestion to be incomplete. Pipetted 350 µL buffer RWT into the RNeasy mini spin column and centrifuged for 15 seconds at 8000 x g. The flow-through was discarded. Pipetted 500 µL of buffer RPE to the RNeasy column and centrifuged for 2 minutes at 8,000 x g. The flow-through was discarded. Placed the RNeasy mini spin column into a new 2 mL collection tube and centrifuged at max speed for 1 minute to remove any residual buffer RPE. Transferred the RNeasy mini spin column to a new 1.5 mL collection tube. Pipetted 50 µL RNase-free water directly onto the membrane and allowed the column to sit on the benchtop for 5 minutes. Next, centrifuged for 1 minute at 8,000 x g to elute the RNA. The RNA concentration and quality were determined using a Nanodrop spectrophotometer (Thermo Scientific). First, the pedestal of the nanodrop was thoroughly cleaned with deionized water. Next, 2 µL of sample was loaded and gently closed, thus allowing the optical density to be measured at A260. All RNA samples produced A260/280 were between 1.8-2.10, thus allowing to continue with cDNA synthesis. All cell types (WT, KO, OE) RNA extraction was processed precisely the same mentioned in this section.

III. cDNA Synthesis

RNA was reverse transcribed using the RT^2 First Strand kit (Qiagen, Cat. No. 330404). First, all reagents from the kit were thawed and briefly spun down to bring the contents to the bottom of the tubes. Next, the genomic DNA elimination mix for each RNA sample was prepared; 32 µL of RNA at a concentration of 50 ng/µL totaling 1600 ng of RNA and thoroughly mixed with 8 µL buffer GE. Next, the 40 µL of genomic DNA mix was incubated at 42 ℃ for 5 minutes using a thermal cycler (2720 Thermal Cycler, Applied Biosystems). Immediately, this mixture was placed on ice. Next, the reverse-transcription mix was prepared; 16 µL 5x buffer BC3, 4 µL control P2, 8 µL RE3 reverse transcriptase mix and 12 µL RNase were gently mixed by pipetting up and down slowly. The reverse-transcription mix (40 µL) and genomic DNA elimination mix (40 µL) were combined by slowly pipetting up and down. The mix ran on the thermal cycler (2720 Thermal Cycler, Applied Biosystems) with the following steps: 42℃ for exactly 15 minutes then 95℃ for 5 minutes. Next, 364 µL RNase-free water was added to the mix. The cDNA concentration and quality were determined using a Nanodrop spectrophotometer (Thermo Scientific). First, the pedestal of the nanodrop was thoroughly cleaned with deionized water. Next, 2 µL of sample was loaded and gently closed, thus allowing the optical density to be measured at A260. All cDNA samples produced A260/280 were between 1.8-2.10, thus allowing to continue with real-time PCR. All cell types (WT, KO, OE) for cDNA synthesis were processed precisely the same mentioned in this section.

IV. Agarose Gel Electrophoresis of ARV1 cDNA

After the RNA for WT, KO and OE were extracted, an agarose gel was used to verify KO or OE using a 1% agarose gel using Tris/Borate/EDTA (TBE). First, 1 milligram of agarose was added to 100 ml of TBE buffer, and microwaved for 1 minute and 30 seconds, occasionally gently swirling. Then let the mixture to incubate at room temperature until it cooled slightly but was still warm. Next, added 8 µl of EtBr very carefully to the mixture and swirled the mixture, then poured into gel docking station to solidify. Next, was cDNA synthesis using qScript cDNA Supermix (QuantaBio, Catalog #95048). In a PCR tube, the following was added: 4 µl qScript cDNA Supermix, 8 µl RNA template (50 ng/µl) and 8 µl DNase-free water. This mixture ran on a thermal cycler () following the qScript protocol (see Figure # 5). After cDNA synthesis, the following mixture was prepared in a PCR tube: 2 µl forward primer (10 µg/µl), 2 µl reverse primer (10 µg/µl), 12.5 µl 2x master mix Phusion Hot Start Flex (New England Biolabs, Cat. No. M0536S), 4 µl cDNA (25 ng/µl) and 4.5 µl RNase-free water. This mixture was then placed in a thermal cycler on a custom cycling condition. Next, 25 µl of PCR reaction was mixed with 5 µl loading dye. The 30 µl mixture was pipetted onto the previously made agarose gel and ran on 140v for 1 hour. The gel was imaged on the auto-detect feature on the Amersham 600 using fluorescence.

A.

cDNA Synthesis	Temperature	Duration	Cycle(s)
	25°C	5 minutes	1
	42°C	30 minutes	1
	85°C	5 minutes	1
	4°C	Hold	1

B.

Arv1 PCR	Temperature	Duration	Cycle(s)
	95	3 minutes	1
	95	15 seconds	35
	65.5	15 seconds	
	72	15 seconds	
	72	3 minutes	1
	4	Hold	1

C.

Forward Primer	5'-ATG GGC AAC GGC GGG CG -3'
Reverse Primer	5'-TCA GAA GTC CTG AGA TTT AAA G -3'

Figure # 5. **Custom PCR Cycling Conditions and Primer Design**. Outlines the precise steps for generating cDNA using qScript cDNA Supermix [A]. Provides the cycling steps for Arv1 PCR [B]. The forward and reverse primers that were used for this reaction to look at the RNA level of Arv1 [C].

V. Qiagen RT^2 PCR Array

The desired cDNA was used on the real-time RT^2 Profiler PCR Array (Qiagen, Cat. No. PAHS-087Z). First, briefly centrifuged RT^2 SYBR Green qPCR master mix (Qiagen, Cat. No. 330500) to bring the contents down to the bottom. Next, the PCR components mix were prepared in a 5 mL loading reservoir: 2.6 mL SYBR Green qPCR master mix, 408 µL cDNA synthesis reaction, 2.192 mL RNase-free water. Next, 10 µL of PCR components mix was dispensed into each well in a 384 well plate using a single channel electronic repeater pipette (LabNet International, Cat. No. P3600L-200). The total amount of cDNA was 300 ng per well. After 10 µL was dispensed into all 384 wells then the plate was tightly sealed with optical adhesive film. Next, the plate was centrifuged for 1 minute at 1000 x g at room temperature. The plate was ran on Bio-Rad CFX384 Real-Time PCR system using a custom cycling program (see Table # 2).

Table # 2**. RT^2 PCR cycling conditions.** The custom temperature, duration, and cycles used.

Temperature	Duration	Cycle(s)	Note
50℃	10 minutes	1	
95℃	5 minutes	1	
95℃	10 seconds	39	
58℃	1 minute		
95℃	1 minute	1	Melt Curve
55℃	30 seconds	1	Melt Curve: Increment 0.5 ℃ for 5 seconds then plate read
95℃	50 seconds	1	

VI. PCR Array Plate Setup

A. PCR Array: Human Fatty Liver

Table # 3. RT^2 Profiler PCR Array: Fatty Liver List

Position	UniGene	GenBank	Symbol	Description
A01	Hs.429294	NM_005502	ABCA1	ATP-binding cassette, sub-family A (ABC1), member 1
A02	Hs.160556	NM_198834	ACACA	Acetyl-CoA carboxylase alpha
A03	Hs.471277	NM_001608	ACADL	Acyl-CoA dehydrogenase, long chain
A04	Hs.387567	NM_001096	ACLY	ATP citrate lyase
A05	Hs.464137	NM_004035	ACOX1	Acyl-CoA oxidase 1, palmitoyl
A06	Hs.11638	NM_016234	ACSL5	Acyl-CoA synthetase long-chain family member 5
A07	Hs.706754	NM_005622	ACSM3	Acyl-CoA synthetase medium-chain family member 3
A08	Hs.5298	NM_015999	ADIPOR1	Adiponectin receptor 1
A09	Hs.371642	NM_024551	ADIPOR2	Adiponectin receptor 2
A10	Hs.525622	NM_005163	AKT1	V-akt murine thymoma viral oncogene homolog 1
A11	Hs.633003	NM_000039	APOA1	Apolipoprotein A-I
A12	Hs.120759	NM_000384	APOB	Apolipoprotein B (including Ag(x) antigen)
B01	Hs.73849	NM_000040	APOC3	Apolipoprotein C-III
B02	Hs.654439	NM_000041	APOE	Apolipoprotein E
B03	Hs.271135	NM_005174	ATP5C1	ATP synthase, H+ transporting, mitochondrial F1 complex, gamma polypeptide 1
B04	Hs.141125	NM_004346	CASP3	Caspase 3, apoptosis-related cysteine peptidase
B05	Hs.120949	NM_000072	CD36	CD36 molecule (thrombospondin receptor)
B06	Hs.517106	NM_005194	CEBPB	CCAAT/enhancer binding protein (C/EBP), beta
B07	Hs.518249	NM_003418	CNBP	CCHC-type zinc finger, nucleic acid binding protein
B08	Hs.503043	NM_001876	CPT1A	Carnitine palmitoyltransferase 1A (liver)
B09	Hs.705379	NM_000098	CPT2	Carnitine palmitoyltransferase 2
B10	Hs.12907	NM_000773	CYP2E1	Cytochrome P450, family 2, subfamily E, polypeptide 1
B11	Hs.1644	NM_000780	CYP7A1	Cytochrome P450, family 7, subfamily A, polypeptide 1
B12	Hs.334305	NM_032564	DGAT2	Diacylglycerol O-acyltransferase 2
C01	Hs.380135	NM_001443	FABP1	Fatty acid binding protein 1, liver
C02	Hs.657242	NM_004102	FABP3	Fatty acid binding protein 3, muscle and heart (mammary-derived growth inhibitor)
C03	Hs.408061	NM_001444	FABP5	Fatty acid binding protein 5 (psoriasis-associated)
C04	Hs.244139	NM_000043	FAS	Fas (TNF receptor superfamily, member 6)
C05	Hs.83190	NM_004104	FASN	Fatty acid synthase
C06	Hs.155651	NM_021784	FOXA2	Forkhead box A2
C07	Hs.370666	NM_002015	FOXO1	Forkhead box O1
C08	Hs.212293	NM_000151	G6PC	Glucose-6-phosphatase, catalytic subunit
C09	Hs.461047	NM_000402	G6PD	Glucose-6-phosphate dehydrogenase
C10	Hs.1270	NM_000162	GCK	Glucokinase (hexokinase 4)
C11	Hs.1466	NM_000167	GK	Glycerol kinase
C12	Hs.445733	NM_002093	GSK3B	Glycogen synthase kinase 3 beta
D01	Hs.643495	NM_000859	HMGCR	3-hydroxy-3-methylglutaryl-CoA reductase
D02	Hs.116462	NM_178849	HNF4A	Hepatocyte nuclear factor 4, alpha
D03	Hs.856	NM_000619	IFNG	Interferon, gamma
D04	Hs.160562	NM_000618	IGF1	Insulin-like growth factor 1 (somatomedin C)
D05	Hs.642938	NM_000596	IGFBP1	Insulin-like growth factor binding protein 1
D06	Hs.193717	NM_000572	IL10	Interleukin 10
D07	Hs.126256	NM_000576	IL1B	Interleukin 1, beta

Table # 3. **RT^2 Profiler PCR Array: Fatty Liver List Continued.**

Position	UniGene	GenBank	Symbol	Description
D08	Hs.654458	NM_000600	IL6	Interleukin 6 (interferon, beta 2)
D09	Hs.465744	NM_000208	INSR	Insulin receptor
D10	Hs.471508	NM_005544	IRS1	Insulin receptor substrate 1
D11	Hs.213289	NM_000527	LDLR	Low density lipoprotein receptor
D12	Hs.705413	NM_002303	LEPR	Leptin receptor
E01	Hs.180878	NM_000237	LPL	Lipoprotein lipase
E02	Hs.431850	NM_002745	MAPK1	Mitogen-activated protein kinase 1
E03	Hs.138211	NM_002750	MAPK8	Mitogen-activated protein kinase 8
E04	Hs.647055	NM_032951	MLXIPL	MLX interacting protein-like
E05	Hs.338207	NM_004958	MTOR	Mechanistic target of rapamycin (serine/threonine kinase)
E06	Hs.493668	NM_182739	NDUFB6	NADH dehydrogenase (ubiquinone) 1 beta subcomplex, 6, 17kDa
E07	Hs.654408	NM_003998	NFKB1	Nuclear factor of kappa light polypeptide gene enhancer in B-cells 1
E08	Hs.432976	NM_007121	NR1H2	Nuclear receptor subfamily 1, group H, member 2
E09	Hs.438863	NM_005693	NR1H3	Nuclear receptor subfamily 1, group H, member 3
E10	Hs.282735	NM_005123	NR1H4	Nuclear receptor subfamily 1, group H, member 4
E11	Hs.75812	NM_004563	PCK2	Phosphoenolpyruvate carboxykinase 2 (mitochondrial)
E12	Hs.8364	NM_002612	PDK4	Pyruvate dehydrogenase kinase, isozyme 4
F01	Hs.553498	NM_006218	PIK3CA	Phosphoinositide-3-kinase, catalytic, alpha polypeptide
F02	Hs.132225	NM_181504	PIK3R1	Phosphoinositide-3-kinase, regulatory subunit 1 (alpha)
F03	Hs.95990	NM_000298	PKLR	Pyruvate kinase, liver and RBC
F04	Hs.654800	NM_025225	PNPLA3	Patatin-like phospholipase domain containing 3
F05	Hs.437403	NM_021129	PPA1	Pyrophosphatase (inorganic) 1
F06	Hs.103110	NM_005036	PPARA	Peroxisome proliferator-activated receptor alpha
F07	Hs.162646	NM_015869	PPARG	Peroxisome proliferator-activated receptor gamma
F08	Hs.527078	NM_013261	PPARGC1A	Peroxisome proliferator-activated receptor gamma, coactivator 1 alpha
F09	Hs.43322	NM_006251	PRKAA1	Protein kinase, AMP-activated, alpha 1 catalytic subunit
F10	Hs.417549	NM_002827	PTPN1	Protein tyrosine phosphatase, non-receptor type 1
F11	Hs.50223	NM_006744	RBP4	Retinol binding protein 4, plasma
F12	Hs.590886	NM_002957	RXRA	Retinoid X receptor, alpha
G01	Hs.558396	NM_005063	SCD	Arylacetamide deacetylase
G02	Hs.414795	NM_000602	SERPINE1	Serpin peptidase inhibitor, clade E (nexin, plasminogen activator inhibitor type 1), member 1
G03	Hs.292177	NM_012254	SLC27A5	Solute carrier family 27 (fatty acid transporter), member 5
G04	Hs.473721	NM_006516	SLC2A1	Solute carrier family 2 (facilitated glucose transporter), member 1
G05	Hs.167584	NM_000340	SLC2A2	Solute carrier family 2 (facilitated glucose transporter), member 2
G06	Hs.380691	NM_001042	SLC2A4	Solute carrier family 2 (facilitated glucose transporter), member 4
G07	Hs.527973	NM_003955	SOCS3	Suppressor of cytokine signaling 3
G08	Hs.592123	NM_004176	SREBF1	Sterol regulatory element binding transcription factor 1
G09	Hs.443258	NM_004599	SREBF2	Sterol regulatory element binding transcription factor 2
G10	Hs.463059	NM_003150	STAT3	Signal transducer and activator of transcription 3 (acute-phase response factor)
G11	Hs.241570	NM_000594	TNF	Tumor necrosis factor
G12	Hs.437638	NM_005080	XBP1	X-box binding protein 1
H01	Hs.520640	NM_001101	ACTB	Actin, beta
H02	Hs.534255	NM_004048	B2M	Beta-2-microglobulin
H03	Hs.592355	NM_002046	GAPDH	Glyceraldehyde-3-phosphate dehydrogenase
H04	Hs.412707	NM_000194	HPRT1	Hypoxanthine phosphoribosyltransferase 1
H05	Hs.546285	NM_001002	RPLP0	Ribosomal protein, large, P0
H06	N/A	SA_00105	HGDC	Human Genomic DNA Contamination
H07	N/A	SA_00104	RTC	Reverse Transcription Control
H08	N/A	SA_00104	RTC	Reverse Transcription Control
H09	N/A	SA_00104	RTC	Reverse Transcription Control
H10	N/A	SA_00103	PPC	Positive PCR Control
H11	N/A	SA_00103	PPC	Positive PCR Control
H12	N/A	SA_00103	PPC	Positive PCR Control

B. PCR Array: Human Liver Cancer

Table # 4. **RT^2 Profiler PCR Array: Liver Cancer Gene List**

Position	UniGene	GenBank	Symbol	Description
A01	Hs.404914	NM_003183	ADAM17	ADAM metallopeptidase domain 17
A02	Hs.525622	NM_005163	AKT1	V-akt murine thymoma viral oncogene homolog 1
A03	Hs.583870	NM_001147	ANGPT2	Angiopoietin 2
A04	Hs.624291	NM_004324	BAX	BCL2-associated X protein
A05	Hs.150749	NM_000633	BCL2	B-cell CLL/lymphoma 2
A06	Hs.516966	NM_138578	BCL2L1	BCL2-like 1
A07	Hs.591054	NM_001196	BID	BH3 interacting domain death agonist
A08	Hs.696238	NM_001166	BIRC2	Baculoviral IAP repeat containing 2
A09	Hs.728893	NM_001168	BIRC5	Baculoviral IAP repeat containing 5
A10	Hs.599762	NM_001228	CASP8	Caspase 8, apoptosis-related cysteine peptidase
A11	Hs.514821	NM_002985	CCL5	Chemokine (C-C motif) ligand 5
A12	Hs.523852	NM_053056	CCND1	Cyclin D1
B01	Hs.376071	NM_001759	CCND2	Cyclin D2
B02	Hs.461086	NM_004360	CDH1	Cadherin 1, type 1, E-cadherin (epithelial)
B03	Hs.654386	NM_001257	CDH13	Cadherin 13, H-cadherin (heart)
B04	Hs.370771	NM_000389	CDKN1A	Cyclin-dependent kinase inhibitor 1A (p21, Cip1)
B05	Hs.238990	NM_004064	CDKN1B	Cyclin-dependent kinase inhibitor 1B (p27, Kip1)
B06	Hs.512599	NM_000077	CDKN2A	Cyclin-dependent kinase inhibitor 2A (melanoma, p16, inhibits CDK4)
B07	Hs.390736	NM_003879	CFLAR	CASP8 and FADD-like apoptosis regulator
B08	Hs.476018	NM_001904	CTNNB1	Catenin (cadherin-associated protein), beta 1, 88kDa
B09	Hs.593413	NM_003467	CXCR4	Chemokine (C-X-C motif) receptor 4
B10	Hs.522378	NM_138709	DAB2IP	DAB2 interacting protein
B11	Hs.134296	NM_006094	DLC1	Deleted in liver cancer 1
B12	Hs.654393	NM_005225	E2F1	E2F transcription factor 1
C01	Hs.419815	NM_001963	EGF	Epidermal growth factor
C02	Hs.488293	NM_005228	EGFR	Epidermal growth factor receptor
C03	Hs.517517	NM_001429	EP300	E1A binding protein p300
C04	Hs.86131	NM_003824	FADD	Fas (TNFRSF6)-associated via death domain
C05	Hs.244139	NM_000043	FAS	Fas (TNF receptor superfamily, member 6)
C06	Hs.715588	NM_002012	FHIT	Fragile histidine triad gene
C07	Hs.654360	NM_002019	FLT1	Fms-related tyrosine kinase 1 (vascular endothelial growth factor/vascular permeability factor receptor)
C08	Hs.173859	NM_003507	FZD7	Frizzled family receptor 7
C09	Hs.110571	NM_015675	GADD45B	Growth arrest and DNA-damage-inducible, beta
C10	Hs.523836	NM_000852	GSTP1	Glutathione S-transferase pi 1
C11	Hs.396530	NM_000601	HGF	Hepatocyte growth factor (hepapoietin A; scatter factor)
C12	Hs.507991	NM_022475	HHIP	Hedgehog interacting protein
D01	Hs.37003	NM_005343	HRAS	V-Ha-ras Harvey rat sarcoma viral oncogene homolog
D02	Hs.523414	NM_000612	IGF2	Insulin-like growth factor 2 (somatomedin A)
D03	Hs.642938	NM_000596	IGFBP1	Insulin-like growth factor binding protein 1
D04	Hs.450230	NM_000598	IGFBP3	Insulin-like growth factor binding protein 3
D05	Hs.471508	NM_005544	IRS1	Insulin receptor substrate 1
D06	Hs.643813	NM_002211	ITGB1	Integrin, beta 1 (fibronectin receptor, beta polypeptide, antigen CD29 includes MDF2, MSK12)
D07	Hs.479756	NM_002253	KDR	Kinase insert domain receptor (a type III receptor tyrosine kinase)

Table # 4. **RT^2 Profiler PCR Array: Liver Cancer Gene List Continued**

Position	UniGene	GenBank	Symbol	Description
D08	Hs.555947	NM_016269	LEF1	Lymphoid enhancer-binding factor 1
D09	Hs.632486	NM_021960	MCL1	Myeloid cell leukemia sequence 1 (BCL2-related)
D10	Hs.132966	NM_000245	MET	Met proto-oncogene (hepatocyte growth factor receptor)
D11	Hs.597656	NM_000251	MSH2	MutS homolog 2, colon cancer, nonpolyposis type 1 (E. coli)
D12	Hs.280987	NM_002439	MSH3	MutS homolog 3 (E. coli)
E01	Hs.377155	NM_178812	MTDH	Metadherin
E02	Hs.202453	NM_002467	MYC	V-myc myelocytomatosis viral oncogene homolog (avian)
E03	Hs.654408	NM_003998	NFKB1	Nuclear factor of kappa light polypeptide gene enhancer in B-cells 1
E04	Hs.486502	NM_002524	NRAS	Neuroblastoma RAS viral (v-ras) oncogene homolog
E05	Hs.4817	NM_002545	OPCML	Opioid binding protein/cell adhesion molecule-like
E06	Hs.74615	NM_006206	PDGFRA	Platelet-derived growth factor receptor, alpha polypeptide
E07	Hs.465849	NM_006221	PIN1	Peptidylprolyl cis/trans isomerase, NIMA-interacting 1
E08	Hs.500466	NM_000314	PTEN	Phosphatase and tensin homolog
E09	Hs.196384	NM_000963	PTGS2	Prostaglandin-endoperoxide synthase 2 (prostaglandin G/H synthase and cyclooxygenase)
E10	Hs.395482	NM_005607	PTK2	PTK2 protein tyrosine kinase 2
E11	Hs.499094	NM_013258	PYCARD	PYD and CARD domain containing
E12	Hs.413812	NM_006908	RAC1	Ras-related C3 botulinum toxin substrate 1 (rho family, small GTP binding protein Rac1)
F01	Hs.476270	NM_007182	RASSF1	Ras association (RalGDS/AF-6) domain family member 1
F02	Hs.408528	NM_000321	RB1	Retinoblastoma 1
F03	Hs.655654	NM_005045	RELN	Reelin
F04	Hs.247077	NM_001664	RHOA	Ras homolog gene family, member A
F05	Hs.170019	NM_004350	RUNX3	Runt-related transcription factor 3
F06	Hs.481022	NM_003013	SFRP2	Secreted frizzled-related protein 2
F07	Hs.75862	NM_005359	SMAD4	SMAD family member 4
F08	Hs.465087	NM_005904	SMAD7	SMAD family member 7
F09	Hs.50640	NM_003745	SOCS1	Suppressor of cytokine signaling 1
F10	Hs.527973	NM_003955	SOCS3	Suppressor of cytokine signaling 3
F11	Hs.463059	NM_003150	STAT3	Signal transducer and activator of transcription 3 (acute-phase response factor)
F12	Hs.644653	NM_003199	TCF4	Transcription factor 4
G01	Hs.492203	NM_198253	TERT	Telomerase reverse transcriptase
G02	Hs.170009	NM_003236	TGFA	Transforming growth factor, alpha
G03	Hs.645227	NM_000660	TGFB1	Transforming growth factor, beta 1
G04	Hs.604277	NM_003242	TGFBR2	Transforming growth factor, beta receptor II (70/80kDa)
G05	Hs.174312	NM_138554	TLR4	Toll-like receptor 4
G06	Hs.521456	NM_003842	TNFRSF10B	Tumor necrosis factor receptor superfamily, member 10b
G07	Hs.478275	NM_003810	TNFSF10	Tumor necrosis factor (ligand) superfamily, member 10
G08	Hs.654481	NM_000546	TP53	Tumor protein p53
G09	Hs.73793	NM_003376	VEGFA	Vascular endothelial growth factor A
G10	Hs.591980	NM_000378	WT1	Wilms tumor 1
G11	Hs.356076	NM_001167	XIAP	X-linked inhibitor of apoptosis
G12	Hs.503692	NM_006106	YAP1	Yes-associated protein 1
H01	Hs.520640	NM_001101	ACTB	Actin, beta
H02	Hs.534255	NM_004048	B2M	Beta-2-microglobulin
H03	Hs.592355	NM_002046	GAPDH	Glyceraldehyde-3-phosphate dehydrogenase
H04	Hs.412707	NM_000194	HPRT1	Hypoxanthine phosphoribosyltransferase 1
H05	Hs.546285	NM_001002	RPLP0	Ribosomal protein, large, P0
H06	N/A	SA_00105	HGDC	Human Genomic DNA Contamination
H07	N/A	SA_00104	RTC	Reverse Transcription Control
H08	N/A	SA_00104	RTC	Reverse Transcription Control
H09	N/A	SA_00104	RTC	Reverse Transcription Control
H10	N/A	SA_00103	PPC	Positive PCR Control
H11	N/A	SA_00103	PPC	Positive PCR Control
H12	N/A	SA_00103	PPC	Positive PCR Control

C. PCR Array: Human Inflammatory Cytokines and Receptors

Table # 5. **RT^2 Profiler PCR Array: Inflammatory Cytokines and Receptors**

Position	UniGene	GenBank	Symbol	Description
A01	Hs.591680	NM_004757	AIMP1	Aminoacyl tRNA synthetase complex-interacting multifunctional protein 1
A02	Hs.73853	NM_001200	BMP2	Bone morphogenetic protein 2
A03	Hs.494997	NM_001735	C5	Complement component 5
A04	Hs.72918	NM_002981	CCL1	Chemokine (C-C motif) ligand 1
A05	Hs.54460	NM_002986	CCL11	Chemokine (C-C motif) ligand 11
A06	Hs.414629	NM_005408	CCL13	Chemokine (C-C motif) ligand 13
A07	Hs.272493	NM_032965	CCL15	Chemokine (C-C motif) ligand 15
A08	Hs.10458	NM_004590	CCL16	Chemokine (C-C motif) ligand 16
A09	Hs.546294	NM_002987	CCL17	Chemokine (C-C motif) ligand 17
A10	Hs.303649	NM_002982	CCL2	Chemokine (C-C motif) ligand 2
A11	Hs.75498	NM_004591	CCL20	Chemokine (C-C motif) ligand 20
A12	Hs.534347	NM_002990	CCL22	Chemokine (C-C motif) ligand 22
B01	Hs.169191	NM_005064	CCL23	Chemokine (C-C motif) ligand 23
B02	Hs.247838	NM_002991	CCL24	Chemokine (C-C motif) ligand 24
B03	Hs.131342	NM_006072	CCL26	Chemokine (C-C motif) ligand 26
B04	Hs.514107	NM_002983	CCL3	Chemokine (C-C motif) ligand 3
B05	Hs.75703	NM_002984	CCL4	Chemokine (C-C motif) ligand 4
B06	Hs.514821	NM_002985	CCL5	Chemokine (C-C motif) ligand 5
B07	Hs.251526	NM_006273	CCL7	Chemokine (C-C motif) ligand 7
B08	Hs.271387	NM_005623	CCL8	Chemokine (C-C motif) ligand 8
B09	Hs.301921	NM_001295	CCR1	Chemokine (C-C motif) receptor 1
B10	Hs.511794	NM_001123396	CCR2	Chemokine (C-C motif) receptor 2
B11	Hs.506190	NM_001837	CCR3	Chemokine (C-C motif) receptor 3
B12	Hs.184926	NM_005508	CCR4	Chemokine (C-C motif) receptor 4
C01	Hs.450802	NM_000579	CCR5	Chemokine (C-C motif) receptor 5
C02	Hs.46468	NM_004367	CCR6	Chemokine (C-C motif) receptor 6
C03	Hs.113222	NM_005201	CCR8	Chemokine (C-C motif) receptor 8
C04	Hs.592244	NM_000074	CD40LG	CD40 ligand
C05	Hs.591402	NM_000757	CSF1	Colony stimulating factor 1 (macrophage)
C06	Hs.1349	NM_000758	CSF2	Colony stimulating factor 2 (granulocyte-macrophage)
C07	Hs.2233	NM_000759	CSF3	Colony stimulating factor 3 (granulocyte)
C08	Hs.531668	NM_002996	CX3CL1	Chemokine (C-X3-C motif) ligand 1
C09	Hs.78913	NM_001337	CX3CR1	Chemokine (C-X3-C motif) receptor 1
C10	Hs.789	NM_001511	CXCL1	Chemokine (C-X-C motif) ligand 1 (melanoma growth stimulating activity, alpha)
C11	Hs.632586	NM_001565	CXCL10	Chemokine (C-X-C motif) ligand 10
C12	Hs.632592	NM_005409	CXCL11	Chemokine (C-X-C motif) ligand 11
D01	Hs.522891	NM_000609	CXCL12	Chemokine (C-X-C motif) ligand 12
D02	Hs.100431	NM_006419	CXCL13	Chemokine (C-X-C motif) ligand 13
D03	Hs.590921	NM_002089	CXCL2	Chemokine (C-X-C motif) ligand 2
D04	Hs.89690	NM_002090	CXCL3	Chemokine (C-X-C motif) ligand 3
D05	Hs.89714	NM_002994	CXCL5	Chemokine (C-X-C motif) ligand 5
D06	Hs.164021	NM_002993	CXCL6	Chemokine (C-X-C motif) ligand 6 (granulocyte chemotactic protein 2)
D07	Hs.77367	NM_002416	CXCL9	Chemokine (C-X-C motif) ligand 9
D08	Hs.194778	NM_000634	CXCR1	Chemokine (C-X-C motif) receptor 1
D09	Hs.846	NM_001557	CXCR2	Chemokine (C-X-C motif) receptor 2

Table # 5. **RT^2 Profiler PCR Array: Inflammatory Cytokines and Receptors Continued**

Position	UniGene	GenBank	Symbol	Description
D10	Hs.2007	NM_000639	FASLG	Fas ligand (TNF superfamily, member 6)
D11	Hs.211575	NM_000605	IFNA2	Interferon, alpha 2
D12	Hs.856	NM_000619	IFNG	Interferon, gamma
E01	Hs.504035	NM_001558	IL10RA	Interleukin 10 receptor, alpha
E02	Hs.654593	NM_000628	IL10RB	Interleukin 10 receptor, beta
E03	Hs.845	NM_002188	IL13	Interleukin 13
E04	Hs.654378	NM_000585	IL15	Interleukin 15
E05	Hs.459095	NM_004513	IL16	Interleukin 16
E06	Hs.41724	NM_002190	IL17A	Interleukin 17A
E07	Hs.278911	NM_013278	IL17C	Interleukin 17C
E08	Hs.272295	NM_052872	IL17F	Interleukin 17F
E09	Hs.1722	NM_000575	IL1A	Interleukin 1, alpha
E10	Hs.126256	NM_000576	IL1B	Interleukin 1, beta
E11	Hs.701982	NM_000877	IL1R1	Interleukin 1 receptor, type I
E12	Hs.81134	NM_000577	IL1RN	Interleukin 1 receptor antagonist
F01	Hs.567559	NM_021803	IL21	Interleukin 21
F02	Hs.528111	NM_145659	IL27	Interleukin 27
F03	Hs.694	NM_000588	IL3	Interleukin 3 (colony-stimulating factor, multiple)
F04	Hs.348390	NM_033439	IL33	Interleukin 33
F05	Hs.2247	NM_000879	IL5	Interleukin 5 (colony-stimulating factor, eosinophil)
F06	Hs.68876	NM_000564	IL5RA	Interleukin 5 receptor, alpha
F07	Hs.591873	NM_000880	IL7	Interleukin 7
F08	Hs.624	NM_000584	IL8	Interleukin 8
F09	Hs.960	NM_000590	IL9	Interleukin 9
F10	Hs.406228	NM_002186	IL9R	Interleukin 9 receptor
F11	Hs.36	NM_000595	LTA	Lymphotoxin alpha (TNF superfamily, member 1)
F12	Hs.376208	NM_002341	LTB	Lymphotoxin beta (TNF superfamily, member 3)
G01	Hs.407995	NM_002415	MIF	Macrophage migration inhibitory factor (glycosylation-inhibiting factor)
G02	Hs.489615	NM_005746	NAMPT	Nicotinamide phosphoribosyltransferase
G03	Hs.248156	NM_020530	OSM	Oncostatin M
G04	Hs.313	NM_000582	SPP1	Secreted phosphoprotein 1
G05	Hs.241570	NM_000594	TNF	Tumor necrosis factor
G06	Hs.81791	NM_002546	TNFRSF11B	Tumor necrosis factor receptor superfamily, member 11b
G07	Hs.478275	NM_003810	TNFSF10	Tumor necrosis factor (ligand) superfamily, member 10
G08	Hs.333791	NM_003701	TNFSF11	Tumor necrosis factor (ligand) superfamily, member 11
G09	Hs.54673	NM_003808	TNFSF13	Tumor necrosis factor (ligand) superfamily, member 13
G10	Hs.525157	NM_006573	TNFSF13B	Tumor necrosis factor (ligand) superfamily, member 13b
G11	Hs.181097	NM_003326	TNFSF4	Tumor necrosis factor (ligand) superfamily, member 4
G12	Hs.73793	NM_003376	VEGFA	Vascular endothelial growth factor A
H01	Hs.520640	NM_001101	ACTB	Actin, beta
H02	Hs.534255	NM_004048	B2M	Beta-2-microglobulin
H03	Hs.592355	NM_002046	GAPDH	Glyceraldehyde-3-phosphate dehydrogenase
H04	Hs.412707	NM_000194	HPRT1	Hypoxanthine phosphoribosyltransferase 1
H05	Hs.546285	NM_001002	RPLP0	Ribosomal protein, large, P0
H06	N/A	SA_00105	HGDC	Human Genomic DNA Contamination
H07	N/A	SA_00104	RTC	Reverse Transcription Control
H08	N/A	SA_00104	RTC	Reverse Transcription Control
H09	N/A	SA_00104	RTC	Reverse Transcription Control
H10	N/A	SA_00103	PPC	Positive PCR Control
H11	N/A	SA_00103	PPC	Positive PCR Control
H12	N/A	SA_00103	PPC	Positive PCR Control

D. PCR Array: Human Antiviral Response

Table # 6. **RT^2 Profiler PCR Array Antiviral Response**

Position	UniGene	GenBank	Symbol	Description
A01	Hs.281898	NM_004833	AIM2	Absent in melanoma 2
A02	Hs.660143	NM_021822	APOBEC3G	Apolipoprotein B mRNA editing enzyme, catalytic polypeptide-like 3G
A03	Hs.486063	NM_004849	ATG5	ATG5 autophagy related 5 homolog (S. cerevisiae)
A04	Hs.708030	NM_022461	AZI2	5-azacytidine induced 2
A05	Hs.694071	NM_052813	CARD9	Caspase recruitment domain family, member 9
A06	Hs.2490	NM_033292	CASP1	Caspase 1, apoptosis-related cysteine peptidase (interleukin 1, beta, convertase)
A07	Hs.5353	NM_001230	CASP10	Caspase 10, apoptosis-related cysteine peptidase
A08	Hs.599762	NM_001228	CASP8	Caspase 8, apoptosis-related cysteine peptidase
A09	Hs.514107	NM_002983	CCL3	Chemokine (C-C motif) ligand 3
A10	Hs.514821	NM_002985	CCL5	Chemokine (C-C motif) ligand 5
A11	Hs.472860	NM_001250	CD40	CD40 molecule, TNF receptor superfamily member 5
A12	Hs.838	NM_005191	CD80	CD80 molecule
B01	Hs.171182	NM_006889	CD86	CD86 molecule
B02	Hs.198998	NM_001278	CHUK	Conserved helix-loop-helix ubiquitous kinase
B03	Hs.520898	NM_001908	CTSB	Cathepsin B
B04	Hs.716407	NM_001912	CTSL1	Cathepsin L1
B05	Hs.181301	NM_004079	CTSS	Cathepsin S
B06	Hs.632586	NM_001565	CXCL10	Chemokine (C-X-C motif) ligand 10
B07	Hs.632592	NM_005409	CXCL11	Chemokine (C-X-C motif) ligand 11
B08	Hs.77367	NM_002416	CXCL9	Chemokine (C-X-C motif) ligand 9
B09	Hs.578973	NM_015247	CYLD	Cylindromatosis (turban tumor syndrome)
B10	Hs.6278	NM_015533	DAK	Dihydroxyacetone kinase 2 homolog (S. cerevisiae)
B11	Hs.380774	NM_001356	DDX3X	DEAD (Asp-Glu-Ala-Asp) box polypeptide 3, X-linked
B12	Hs.190622	NM_014314	DDX58	DEAD (Asp-Glu-Ala-Asp) box polypeptide 58
C01	Hs.55918	NM_024119	DHX58	DEXH (Asp-Glu-X-His) box polypeptide 58
C02	Hs.86131	NM_003824	FADD	Fas (TNFRSF6)-associated via death domain
C03	Hs.728789	NM_005252	FOS	FBJ murine osteosarcoma viral oncogene homolog
C04	Hs.525600	NM_001017963	HSP90AA1	Heat shock protein 90kDa alpha (cytosolic), class A member 1
C05	Hs.163173	NM_022168	IFIH1	Interferon induced with helicase C domain 1
C06	Hs.37026	NM_024013	IFNA1	Interferon, alpha 1
C07	Hs.211575	NM_000605	IFNA2	Interferon, alpha 2
C08	Hs.529400	NM_000629	IFNAR1	Interferon (alpha, beta and omega) receptor 1
C09	Hs.93177	NM_002176	IFNB1	Interferon, beta 1, fibroblast
C10	Hs.597664	NM_001556	IKBKB	Inhibitor of kappa light polypeptide gene enhancer in B-cells, kinase beta
C11	Hs.673	NM_000882	IL12A	Interleukin 12A (natural killer cell stimulatory factor 1, cytotoxic lymphocyte maturation factor 1, p35)
C12	Hs.674	NM_002187	IL12B	Interleukin 12B (natural killer cell stimulatory factor 2, cytotoxic lymphocyte maturation factor 2, p40)
D01	Hs.654378	NM_000585	IL15	Interleukin 15
D02	Hs.83077	NM_001562	IL18	Interleukin 18 (interferon-gamma-inducing factor)
D03	Hs.126256	NM_000576	IL1B	Interleukin 1, beta
D04	Hs.654458	NM_000600	IL6	Interleukin 6 (interferon, beta 2)
D05	Hs.624	NM_000584	IL8	Interleukin 8
D06	Hs.522819	NM_001569	IRAK1	Interleukin-1 receptor-associated kinase 1
D07	Hs.75254	NM_001571	IRF3	Interferon regulatory factor 3

Table__: RT^2 Profiler PCR Array Antiviral Response Continued

Position	UniGene	GenBank	Symbol	Description
D08	Hs.521181	NM_001098629	IRF5	Interferon regulatory factor 5
D09	Hs.166120	NM_001572	IRF7	Interferon regulatory factor 7
D10	Hs.458485	NM_005101	ISG15	ISG15 ubiquitin-like modifier
D11	Hs.714791	NM_002228	JUN	Jun proto-oncogene
D12	Hs.145442	NM_002755	MAP2K1	Mitogen-activated protein kinase kinase 1
E01	Hs.514012	NM_002756	MAP2K3	Mitogen-activated protein kinase kinase 3
E02	Hs.657756	NM_005921	MAP3K1	Mitogen-activated protein kinase kinase kinase 1
E03	Hs.644143	NM_003188	MAP3K7	Mitogen-activated protein kinase kinase kinase 7
E04	Hs.431850	NM_002745	MAPK1	Mitogen-activated protein kinase 1
E05	Hs.485233	NM_001315	MAPK14	Mitogen-activated protein kinase 14
E06	Hs.861	NM_002746	MAPK3	Mitogen-activated protein kinase 3
E07	Hs.138211	NM_002750	MAPK8	Mitogen-activated protein kinase 8
E08	Hs.570362	NM_020746	MAVS	Mitochondrial antiviral signaling protein
E09	Hs.632221	NM_000243	MEFV	Mediterranean fever
E10	Hs.517307	NM_002462	MX1	Myxovirus (influenza virus) resistance 1, interferon-inducible protein p78 (mouse)
E11	Hs.82116	NM_002468	MYD88	Myeloid differentiation primary response gene (88)
E12	Hs.654408	NM_003998	NFKB1	Nuclear factor of kappa light polypeptide gene enhancer in B-cells 1
F01	Hs.81328	NM_020529	NFKBIA	Nuclear factor of kappa light polypeptide gene enhancer in B-cells inhibitor, alpha
F02	Hs.159483	NM_183395	NLRP3	NLR family, pyrin domain containing 3
F03	Hs.592072	NM_022162	NOD2	Nucleotide-binding oligomerization domain containing 2
F04	Hs.414332	NM_002535	OAS2	2'-5'-oligoadenylate synthetase 2, 69/71kDa
F05	Hs.465849	NM_006221	PIN1	Peptidylprolyl cis/trans isomerase, NIMA-interacting 1
F06	Hs.129758	NM_003978	PSTPIP1	Proline-serine-threonine phosphatase interacting protein 1
F07	Hs.499094	NM_013258	PYCARD	PYD and CARD domain containing
F08	Hs.58314	NM_152901	PYDC1	PYD (pyrin domain) containing 1
F09	Hs.502875	NM_021975	RELA	V-rel reticuloendotheliosis viral oncogene homolog A (avian)
F10	Hs.519842	NM_003804	RIPK1	Receptor (TNFRSF)-interacting serine-threonine kinase 1
F11	Hs.313	NM_000582	SPP1	Secreted phosphoprotein 1
F12	Hs.642990	NM_007315	STAT1	Signal transducer and activator of transcription 1, 91kDa
G01	Hs.281902	NM_006704	SUGT1	SGT1, suppressor of G2 allele of SKP1 (S. cerevisiae)
G02	Hs.505874	NM_013254	TBK1	TANK-binding kinase 1
G03	Hs.29344	NM_182919	TICAM1	Toll-like receptor adaptor molecule 1
G04	Hs.657724	NM_003265	TLR3	Toll-like receptor 3
G05	Hs.659215	NM_016562	TLR7	Toll-like receptor 7
G06	Hs.660543	NM_138636	TLR8	Toll-like receptor 8
G07	Hs.87968	NM_017442	TLR9	Toll-like receptor 9
G08	Hs.241570	NM_000594	TNF	Tumor necrosis factor
G09	Hs.460996	NM_003789	TRADD	TNFRSF1A-associated via death domain
G10	Hs.510528	NM_003300	TRAF3	TNF receptor-associated factor 3
G11	Hs.591983	NM_004620	TRAF6	TNF receptor-associated factor 6
G12	Hs.528952	NM_005082	TRIM25	Tripartite motif containing 25
H01	Hs.520640	NM_001101	ACTB	Actin, beta
H02	Hs.534255	NM_004048	B2M	Beta-2-microglobulin
H03	Hs.592355	NM_002046	GAPDH	Glyceraldehyde-3-phosphate dehydrogenase
H04	Hs.412707	NM_000194	HPRT1	Hypoxanthine phosphoribosyltransferase 1
H05	Hs.546285	NM_001002	RPLP0	Ribosomal protein, large, P0
H06	N/A	SA_00105	HGDC	Human Genomic DNA Contamination
H07	N/A	SA_00104	RTC	Reverse Transcription Control
H08	N/A	SA_00104	RTC	Reverse Transcription Control
H09	N/A	SA_00104	RTC	Reverse Transcription Control
H10	N/A	SA_00103	PPC	Positive PCR Control
H11	N/A	SA_00103	PPC	Positive PCR Control
H12	N/A	SA_00103	PPC	Positive PCR Control

VII. Statistical Analysis Qiagen qRT-PCR Arrays

C_T values were exported to an Excel file to create a table of C_T values. This table was then uploaded on to the Qiagen data analysis web portal at http://www.qiagen.com/geneglobe. Samples were assigned to control and test groups. C_T values were normalized to glyceraldehyde 3-phoshphate dehydrogenase (GAPDH) and hypoxanthine-guanine phosphoribosyl transferase1 (HPRT1) except "Inflammatory Cytokines and Receptors" plates; these plates were normalized to just HPRT1. The data analysis web portal calculates fold change/regulation using delta delta C_T method, where delta C_T is calculated between gene of interest (GOI) and an average of the reference gene(s) (GAPDH and HPRT1), followed by delta-delta C_T calculations (delta C_T (Test Group) – delta C_T (Control Group)). Fold change is then calculated using 2 ^ (-delta delta C_T) formula. The p-values are calculated based on the Student's t-test of the replicate 2^ (-Delta C_T) values for each gene in the control group and treatment groups, a p-value less than 0.05 with a fold-change ≥2 is indicated as significant. The p-value calculation used is based on parametric, unpaired, two-sample equal variance, two-tailed distribution. The C_T cut-off was set to 36. The criteria for the PCR array reproducibility: If the Average C_T Positive PCR Control (PPC) is 30 +/-2 and no two arrays have Average PPC C_T are > 2 away from one another then the sample and the group will be deemed 'Pass'. Criteria for the reverse transcription control (RTC): If delta C_T (AVG RTC – AVG PPC) < = 5, RT efficiency reports 'Pass'. Criteria for Genomic DNA Contamination (GDC): If C_T (GDC) >= 35, then the GDC QC reports 'Pass'. The statistics were performed by Qiagen Analysis Center. https://geneglobe.qiagen.com/us/analyze/.

VIII. Immunoblot

HepG2 WT, HepG2 KO and HepG2 OE cell lines were grown on collagen culture dishes (BioCoat, Cat. No. 356450) until approximately 80% confluency. Once confluency was reached, the media was removed, and the culture plates were gently washed with ice-cold phosphate buffered saline (PBS). Next, 300 µL of 8M urea lysis buffer (Urea: Thermo Fisher Scientific, Cat. No. BP169-500, protease inhibitor, protein phosphatase inhibitor) was added to each culture dish and was scraped with a cell lifter (Corning, Cat. No.3008). The lysate was added to a 1.5 mL microcentrifuge tube and placed in a rotator in 4 ℃ for 3 hours. The lysate was diluted with PBS to make 4M urea. The lysates were then placed back into the rotator in 4 ℃ overnight. The next day, the microcentrifuge tubes were placed in a microcentrifuge and spun at 10,000 rpm for 15 minutes. The supernatant was removed and placed into a new microcentrifuge tube. The protein concentrations were determined by the Bradford assay. Cell lysates were resuspended in 6x sample buffer and incubated at 95 ℃ for 7 minutes. All samples were subjected to 4-12% SDS-PAGE (GenScript, Cat. No. M00654) using Tris-MOPS-SDS running buffer (GenScript, Cat. No. M00138) ran at 140v for 45 minutes. Resolved proteins were transferred onto a nitrocellulose membrane using an Invitrogen iBlot. The immunoblot membranes were blocked for 1 hour with 5% non-fat milk (TBST) and washed once for ten minutes with TBST (Tris-buffered saline, 0.1% Tween 20). The membranes were incubated with primary antibody overnight at the specified dilution (See Table # 7) using BSA. Three washes with TBST, each wash being 30 minutes. Then, the appropriate secondary antibody (1:1000) was added and incubated for 1 hour using BSA. Three more washes with

TBST, each wash for 30 minutes. Each of the membranes were immersed in chemiluminescent agent horseradish-peroxidase HRP for 1-2 minutes then exposed for 1-3 minutes on the Amersham 600 on auto-expose settings.

Table # 7. **Immunoblot Antibodies.** The following antibodies were used to determine the level of protein. The manufacturer, catalog number and dilution are included for each antibody used.

Antibody	Manufacturer	Catalog Number	Dilution
Anti-Arv1	Origene	AP50263PU-N	1:5000
Anti-Beta-Actin	Santa Cruz	Sc-376421	1:1000
Anti-Cleaved-Casp1	Cell Signaling	4199S	1:1000
Anti-Casp1	Invitrogen	PA5-29342	1:1000
Anti-PPARα	Santa Cruz	Sc-398394	1:1000
Anti-EGFR	Cell Signaling	4267S	1:1000
Anti-phospho-EGFR	Cell Signaling	2234S	1:500
Anti-FABP1	Cell Signaling	13368S	1:500
Anti-ADAM17	Santa Cruz	Sc-390859	1:1000
Anti-PERK	Cell Signaling	5683S	1:1000
Anti-IRE1-α	Cell Signaling	3294S	1:1000
Anti-DDIT3	Cell Signaling	2895S	1:500
Anti-ATF6	Cell Signaling	65880T	1:1000
Anti-NLRP3	Cell Signaling	13158S	1:1000
Anti-PARP	Cell Signaling	9542s	1:1000
Anti-XBP-1s	Cell Signaling	12782s	1:500
Anti-p-PERK	Sigma	SAB5700521	1:500

IX. Lipid Stain Droplet

HepG2 wild-type and HepG2 ARV1 transient over-expressed cells were seeded at 700,000 cells per well of a 6-well collagen coated plate. The following treatments were used: HepG2 WT cells +/- 500µM palmitic acid for 2 hours and +/- EGFR inhibitor (10 µM) (PD168393 or Gefitinib), HepG2 ARV1 over-expression cells +/- 500µM palmitic acid for 2 hours and +/- EGFR inhibitor (PD168393 or Gefitinib). The HepG2 cells were treated with 0.3% DMSO/BSA as the control. Lipid stain was performed by using Biotium LipidSpot™ 610 (Biotium, Catalog #70069) and nuclear stain was performed by using Hoechst (Invitrogen, Catalog #H3570). See figure #_ for the timeline of this experiment. All images were manually set to the same specifications. For brightfield images: Exposure Target 120, Exposure Time 10 ms and Gain 1.00. Lipid stain in the red channel images: Exposure Target 120, Exposure time 400 ms and Gain 5.00. Nuclear stain in the blue channel images: Exposure Target 120, Exposure time 4.00 ms and Gain 5.00.

Experimental Results

I. Cell Line Morphology and Cell Line Confirmation

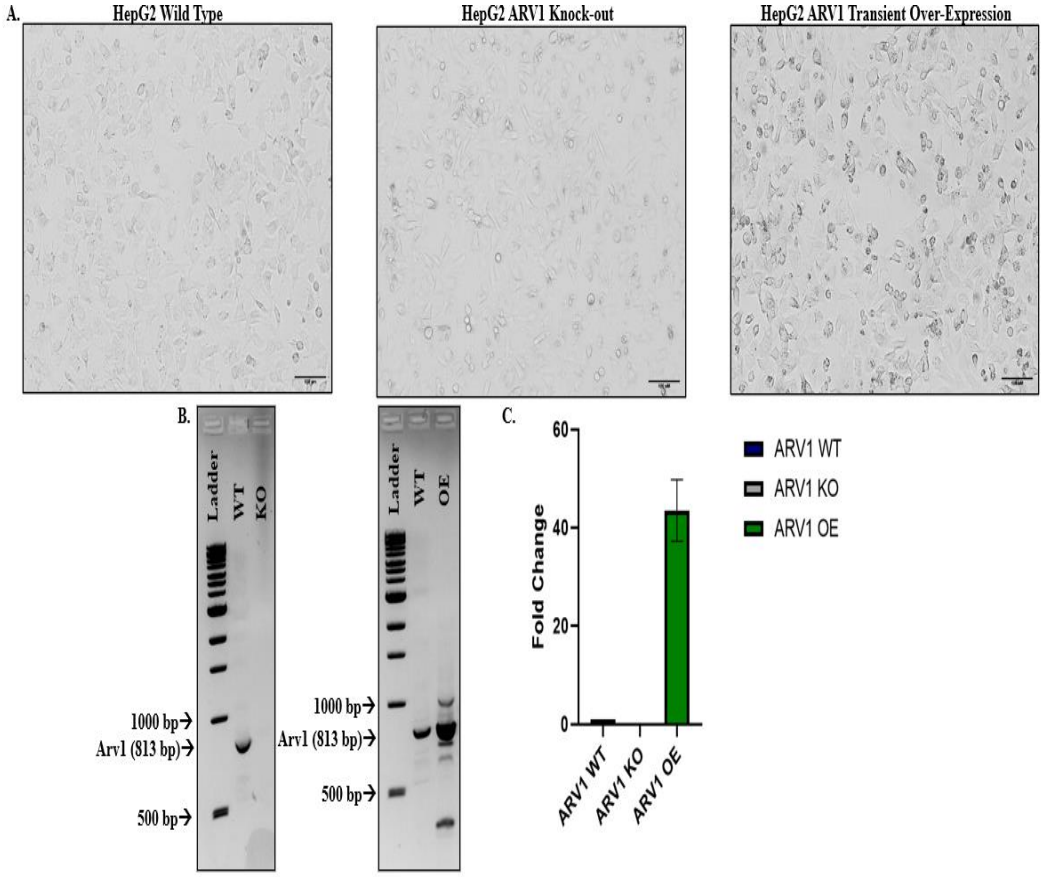

Figure # 6. **Cell Line Morphology and Cell Line Confirmation.** 10x magnification looking at HepG2 Wild type, ARV1 knock-out, and ARV1 over-expression cell lines using Nikon [**A**]. , the following mixture was prepared in a PCR tube: 2 µl forward primer (10 µg/µl) Arv1, 2 µl reverse primer (10 µg/µl) Arv1, 12.5 µl 2x master mix Phusion Hot Start Flex (New England Biolabs, Cat. No. M0536S), 4 µl cDNA (25 ng/µl) and 4.5 µl RNase-free water. This mixture was then placed in a thermal cycler on a custom cycling condition. Next, 25 µl of PCR reaction was mixed with 5 µl loading dye. The 30 µl mixture was pipetted onto the previously made agarose gel and ran on 140v for 1 hour. The gel was imaged on the auto-detect feature on the Amersham 600 using fluorescence. [**B**] 10 µL of HepG2 WT, HepG2 ARV1 KO, and HepG2 ARV1 OE cDNA was pipetted onto a 384-well plate on the Bio-Rad CFX 384 PCR machine along with a control gene (GAPDH) and Arv1 forward and reverse primer set. Two technical replicates with 3 biological replicates were used. Normalization was done by the traditional delta delta-Ct method using GAPDH as the control gene. The fold-change for each replicate and gene was copied into GraphPad Prism 5. The bar graph was generated using GraphPad Prism 5. The Mean and SEM are shown. [**C**].

Brightfield images of HepG2 WT, HepG2 ARV1 KO, and HepG2 ARV1 OE cells lines showed no initial distinctive differences in cell morphology nor differences in growth, however HepG2 ARV1 OE cells show gradual decline in cellular health 72 hours post transfection. cDNA of HepG2 WT, HepG2 ARV1 KO, and ARV1 OE were loaded onto a 1% agarose gel, UV imaging suggests the cell line is confirmed at the transcriptional level. Additionally, to quantitatively access gene expression of ARV1 in the OE line and KO line qRT-PCR was performed (see Figure # 6). qRT-PCR demonstrated a 40-fold increase of ARV1 gene expression in the OE cell line compared to the WT cells. The KO cell line did not generate a reaction at all even up to the full cycling program which was up to 40 cycles. This indicates the ARV1 KO at the transcriptional level is not present. To identify ARV1 expression on the protein level we performed immunoblots. To verify the accuracy of the antibody we used ARV1 KO mouse lysate as a control. The gold standard for an antibody is the ability for the band to disappear in the presence of the KO animal. However, no available antibodies on the market could be KO verified based on our mouse models. Although currently available antibodies may suggest trends in ARV1 expression without KO validation, I cannot confirm ARV1 protein expression in three cell lines. This data is consistent with previous ARV1 studies that also do not validate ARV1 protein expression. Additionally, many ARV1 studies only displayed Arv1 expression looking at PCR levels or by immunoblot by probing a tagged Arv1 [5, 7, 44].

II. RT^2 Human Fatty Liver Array

The human fatty liver array has the expression of 84 pathway related genes that are involved in the mechanisms of NAFLD and hepatic insulin resistance. The fatty liver array was chosen to see if there is an interaction whether direct or indirect with Arv1 and lipid dysregulation in the liver. The array includes various genes involved in the following pathways: insulin signaling, adipokine signaling, non-insulin dependent diabetes mellitus, carbohydrate metabolism, beta-oxidation, cholesterol metabolism and transport, oxidative phosphorylation, other lipid metabolism and transport, inflammatory response, and apoptosis. The complete list of genes in this array is shown in Table # 3. The array plate has 4 replicates of each gene. The WT HepG2, ARV1 KO, and ARV1 OE cell lines ran on separate plates. All genes that had a fold change of 2.0 or greater were chosen with p-values less than 0.05.

Using this array, a general down-regulation of genes in the ARV1 OE cell line compared to the ARV1 KO cell line, possibly due to an increase of overall lipid metabolism. Where the cell is trying to balance the lipid overload. Additionally, cholesterol oxidation/transport was downregulated in both cell lines, however more genes and the downregulation were increased in the OE cell line. Interestingly, G6PD and GSK3B were downregulated in the OE cell line, whereas they were increased to almost the same fold-change in the KO cell line. Furthermore, G6PD is involved in the first step of the pentose phosphate pathway, whereas GSK3B is a negative regulator of glucose homeostasis. Interestingly, in both KO and OE, FABP1 was downregulated, however in the OE it was downregulated further. FABP1 plays a

variety of roles including fatty acid transport, uptake, and metabolism. Furthermore. PPARα was decreased in the OE cell line. PPARα is a master regulator of lipid metabolism. This potentially suggests PPARα is downregulated due to the increase of overall lipid metabolism by ARV1. However, in the KO cell line, we would suspect PPARα to be increased. It is possible in the ARV1 KO cells, that an alternative lipid metabolism pathway is turned on and/or increased. Further research will need to be done to verify this (See Figure # 7).

A.

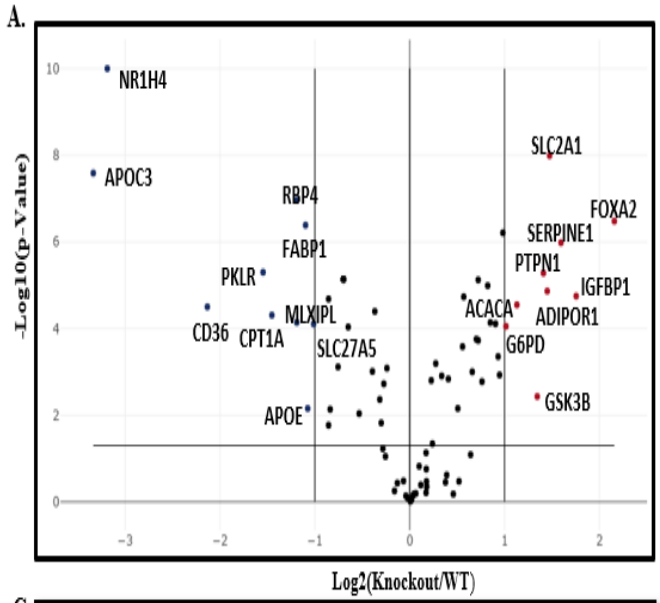

B.

Gene	Fold Change	Significance
FOXA2	4.46	***
IGFBP1	3.37	***
SERPINE1	3.02	***
SLC2A1	2.78	***
ADIPOR1	2.73	***
PTPN1	2.66	***
GSK3B	2.54	***
ACACA	2.19	***
G6PD	2.02	***
SLC27A5	-2.02	***
APOE	-2.11	***
FABP1	-2.14	***
MLXIPL	-2.28	***
RBP4	-2.29	***
CPT1A	-2.74	***
PKLR	-2.92	***
CD36	-4.39	***
NR1H4	-9.11	***
APOC3	-10.09	***

C.

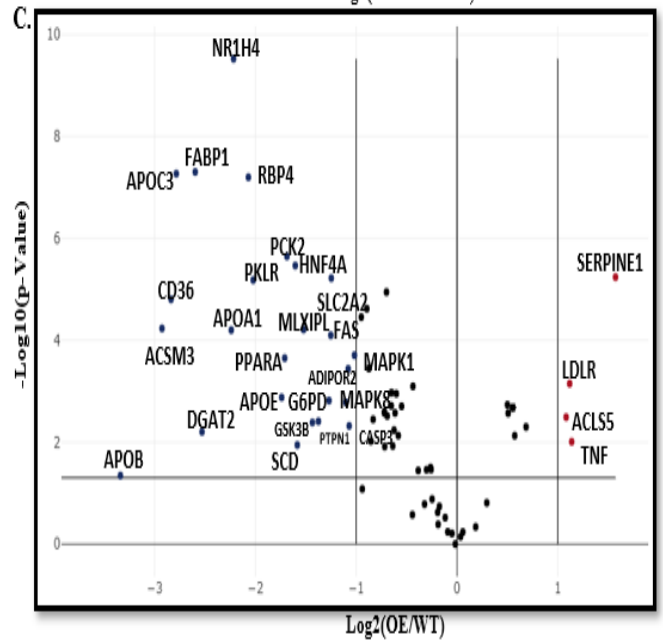

D.

Gene	Fold Change	Significance
SERPINE1	2.98	***
TNF	2.2	***
LDLR	2.17	***
ACSL5	2.12	***
MAPK1	-2.02	***
CASP3	-2.1	***
ADIPOR2	-2.11	***
MAPK8	-2.15	***
SLC2A2	-2.37	***
FAS	-2.38	***
G6PD	-2.41	***
PTPN1	-2.59	***
GSK3B	-2.7	***
MLXIPL	-2.87	***
SCD	-3	***
HNF4A	-3.04	***
PCK2	-3.22	***
PPARA	-3.27	***
APOE	-3.34	***
PKLR	-4.06	***
RBP4	-4.2	***
NR1H4	-4.65	***
APOA1	-4.72	***
DGAT2	-5.77	***
FABP1	-6.05	***
APOC3	-6.89	***
CD36	-7.15	***
ACSM3	-7.61	***
APOB	-10.12	*

Figure # 7 . **Fatty Liver Volcano Plots.** The X-axis is equal to the Log Squared of (Knockout gene/Wild Type gene). The Y-axis is the -Log10(p-Value). The more left or right a gene is the more of a fold-change. The higher the gene point, the more significant it is. Any points inside the two vertical lines are less than a 2-fold change. Any points lower than the horizontal line is above a 0.05 p-value., therefore deemed insignificant. This dataset is from the KO cell line from the fatty liver array [A]. States the significant gene names, fold-change and significance. Significance is defined as p-value ≤0.05 is *, p-value ≤ 0.01 is **, p-value ≤ is 0.001 is ***. All genes calculated as *** significance [B]. The X-axis is equal to the Log Squared of (Over expression gene/Wild Type gene). The Y-axis is the -Log10(p-Value). The more left or right a gene is the more of a fold-change. The higher the gene point, the more significant it is. Any points inside the two vertical lines are less than a 2-fold change. Any points lower than the horizontal line is above a 0.05 p-value., therefore deemed insignificant. This dataset is from the OE cell line from the fatty liver array [C]. States the significant gene names, fold-change and significance. Significance is defined as p-value ≤0.05 is *, p-value ≤ 0.01 is **, p-value ≤ is 0.001 is ***. All genes calculated as a *** significance except APOB with a * significance [D].

III. RT^2 Human Liver Cancer Array

The human liver cancer array consists of 84 pathway related genes involved in the progression of hepatocellular carcinoma and other forms of hepatocarcinogenesis. This array can provide insight into the mechanisms of hepatic oncogenesis with the alteration of ARV1. The pathways involved are commonly up-regulated genes in HCC, commonly down-regulated genes in HCC, signal transduction, epithelial-to-mesenchymal transition (EMT), cell cycle, apoptosis, immune and inflammatory responses, extracellular matrix (ECM) and cell adhesion molecules, angiogenesis, DNA damage and repair. The full list of genes in this array are in Table # 4. The array plate has 4 replicates of each gene. The WT HepG2, ARV1 KO, and ARV1 OE cell lines were processed on separate plates. All genes that had a fold change of 2.0 or greater were chosen with p-values less than 0.05.

Interestingly, the general regulation of genes in both KO and OE are upregulated. This array has multiple genes that are normally downregulated in hepatocellular carcinoma. The only gene that has been shown to be downregulated that is normally downregulated in this specific cancer is CDKN1A, CDKN1A is a regulator cell cycle progression at G1. Interestingly, CDKN1A is downregulated in the KO cell line but is regulated in the OE cell line. Additionally, CDKN1B is upregulated in the OE cell line, which is involved in inhibiting cell cycle progression in G1.

Furthermore, EGFR and ADAM17 are both upregulated in KO and OE cell lines. EGFR is a hallmark of cancer, where the ‘on’ switch is constantly on to allow abnormal growth and is found in a multitude of cancers. Additionally, ADAM17 is a

protease acting upon a variety of substrates including EGFR. ADAM17 is involved in a variety of pathways including pathophysiological and physiological such as development, regeneration, chronic inflammation, immunity and tumorigenesis [45]. Furthermore, it has been shown that an increase of ADAM17 leads to an increase of EGFR ligands which can increase tumor progression. Separately, GADD45β is upregulated drastically potentially indicating apoptosis in the OE cell line (see Figure # 8).

A.

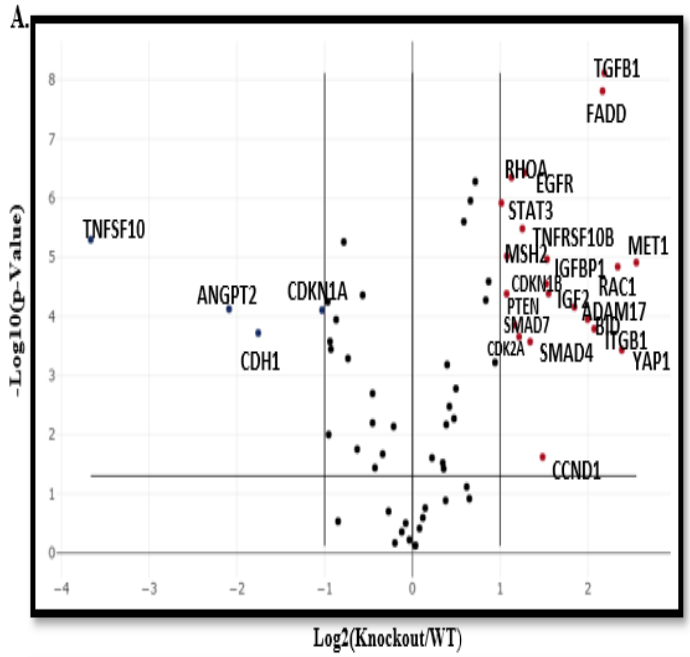

B.

Gene	Fold Change	Significance
MET	5.86	***
YAP1	5.23	***
RAC1	5.06	***
TGFB1	4.55	***
FADD	4.49	***
ITGB1	4.2	***
BID	3.99	***
ADAM17	3.6	***
IGF2	2.93	***
IGFBP1	2.9	***
CDKN1B	2.88	***
CCND1	2.8	*
SMAD4	2.53	***
EGFR	2.43	***
TNFRSF10B	2.38	***
CDKN2A	2.32	***
SMAD7	2.24	***
RHOA	2.19	***
MSH2	2.11	***
PTEN	2.1	***
STAT3	2.02	***
CDKN1A	-2.04	***
FZD7	-2.16	*
CDH1	-3.38	***
ANGPT2	-4.25	***
TNFSF10	-12.67	***

C.

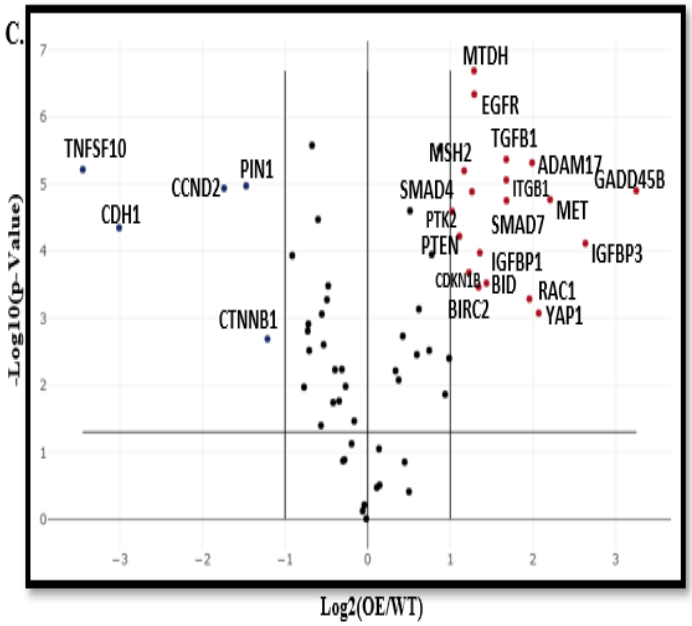

D.

Gene	Fold Change	Significance
GADD45B	9.51	***
IGFBP3	6.21	***
MET	4.62	***
YAP1	4.2	***
ADAM17	3.97	***
RAC1	3.88	***
ITGB1	3.2	***
SMAD7	3.2	***
TGFB1	3.2	***
BID	2.71	***
IGFBP1	2.56	***
BIRC2	2.54	***
EGFR	2.45	***
MTDH	2.44	***
SMAD4	2.4	***
CDKN1B	2.34	***
MSH2	2.25	***
PTEN	2.16	***
PTK2	2.03	***
CTNNB1	-2.32	***
PIN1	-2.77	***
CCND2	-3.33	***
CDH1	-8.04	***
TNFSF10	-10.91	***

Figure # 8.. **Liver Cancer Volcano Plots**. The X-axis is equal to the Log Squared of (Knockout gene/Wild Type gene). The Y-axis is the -Log10(p-Value). The more left or right a gene is the more of a fold-change. The higher the gene point, the more significant it is. Any points inside the two vertical lines are less than a 2-fold change. Any points lower than the horizontal line is above a 0.05 p-value., therefore deemed insignificant. This dataset is from the KO cell line from the liver cancer array [A]. States the significant gene names, fold-change and significance. Significance is defined as p-value ≤0.05 is *, p-value ≤ 0.01 is **, p-value ≤ is 0.001 is All genes calculated as *** significance except CCND1 and FZD7 both with * significance [B]. The X-axis is equal to the Log Squared of (Over expression gene/Wild Type gene). The Y-axis is the -Log10(p-Value). The more left or right a gene is the more of a fold-change. The higher the gene point, the more significant it is. Any points inside the two vertical lines are less than a 2-fold change. Any points lower than the horizontal line is above a 0.05 p-value., therefore deemed insignificant. This dataset is from the OE cell line from the liver cancer array [C]. States the significant gene names, fold-change and significance. Significance is defined as p-value ≤0.05 is *, p-value ≤ 0.01 is **, p-value ≤ is 0.001 is ***. All genes calculated as a *** significance [D].

IV. RT^2 Human Inflammatory Cytokines and Receptors Array

The human inflammatory cytokines and receptors array provides 84 key pathway related genes mediating in the inflammatory response. This array can potentially provide insight into the state of inflammation and the mechanisms behind the inflammation, further eliciting the potential role of ARV1. The key pathway related genes include various chemokines, chemokine receptors, interleukins, and interleukin receptors. The comprehensive table of genes are in Table # 5. The array plate has 4 replicates of each gene. The WT HepG2, ARV1 KO, and ARV1 OE cell lines were processed on separate plates. All genes that had a fold change of 2.0 or greater were chosen with p-values less than 0.05.

Unlike previous arrays, the human inflammatory cytokines array is the first to show the antagonistic relationship between overexpression and gene deletion of ARV1. We see a global change in upregulation of genes in the KO cell line, whereas more genes were downregulated in the OE cell line. This is our first evidence that ARV1 expression can directly influence inflammatory cytokines. However, in both cell lines CCR10 was upregulated. CCR10 is involved with transducing a signal to increase the level of intracellular calcium ion level. However, in both cell lines CCL15 and TLR4 were downregulated. CCL15 is a chemotactic factor for monocytes and T-cells and TLR4 is involved in the recognition of pathogens and the activation of the innate immune response. (see Figure # 9).

A.

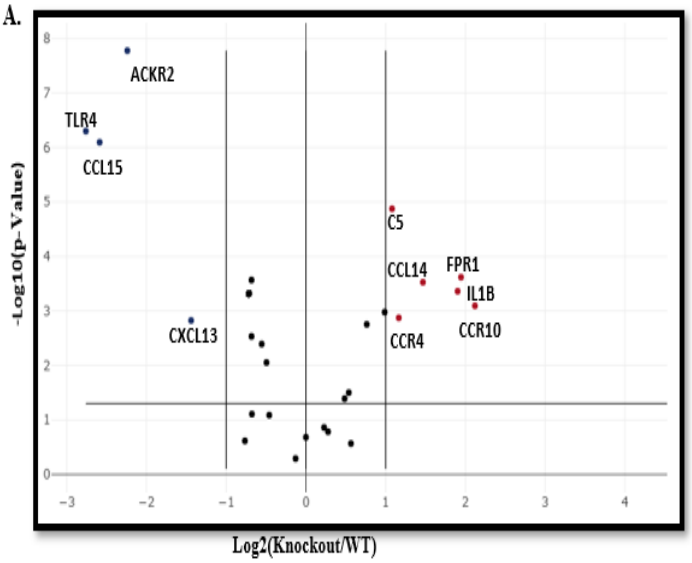

B.

Gene	Fold Change	Significance
CCR10	4.35	***
FPR1	3.85	***
IL1B	3.74	***
CCL14	2.77	***
CCR4	2.24	***
C5	2.11	***
CXCL13	-2.71	***
ACKR2	-4.72	***
CCL15	-6.01	***
TLR4	-6.77	***

C.

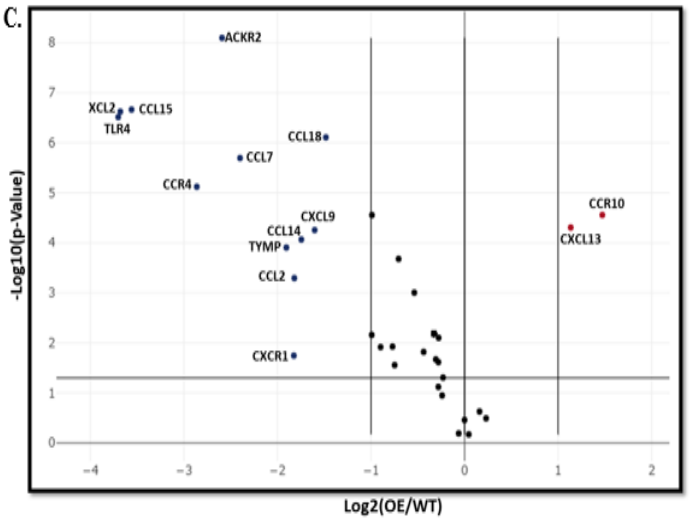

D.

Gene	Fold Change	Significance
CCR10	2.78	***
CXCL13	2.2	***
CCL18	-2.79	***
CXCL9	-3.04	***
CCL14	-3.35	***
CCL2	-3.53	***
CXCR1	-3.54	***
TYMP	-3.75	***
CCL7	-5.28	***
ACKR2	-6.03	***
CCR4	-7.27	***
CCL15	-11.79	***
XCL2	-12.82	***
TLR4	-13.02	***

Figure # 9 . **Inflammatory Cytokines and Receptors Volcano Plots**. . The X-axis is equal to the Log Squared of (Knockout gene/Wild Type gene). The Y-axis is the -Log10(p-Value). The more left or right a gene is the more of a fold-change. The higher the gene point, the more significant it is. Any points inside the two vertical lines are less than a 2-fold change. Any points lower than the horizontal line is above a 0.05 p-value., therefore deemed insignificant. This dataset is from the KO cell line from the cytokines array [A]. States the significant gene names, fold-change and significance. Significance is defined as p-value ≤0.05 is *, p-value ≤ 0.01 is **, p-value ≤ is 0.001 is ***. All genes calculated as *** significance[B]. The X-axis is equal to the Log Squared of (Over expression gene/Wild Type gene). The Y-axis is the -Log10(p-Value). The more left or right a gene is the more of a fold-change. The higher the gene point, the more significant it is. Any points inside the two vertical lines are less than a 2-fold change. Any points lower than the horizontal line is above a 0.05 p-value., therefore deemed insignificant. This dataset is from the OE cell line from the cytokines array [C]. States the significant gene names, fold-change and significance. Significance is defined as p-value ≤0.05 is *, p-value ≤ 0.01 is **, p-value ≤ is 0.001 is ***. All genes calculated as a *** significance [D]

V. RT^2 Human Antiviral Array

The human antiviral response array allows insight into the innate antiviral immune response by including the three different families of pattern recognition receptors (PRRs). The three families which activate the innate immunity include toll-like receptors (TLRs), RIG-1-like receptors and nod-like receptors (NLRs). These receptors activate downstream signaling activating the expression of inflammatory cytokines including alpha and beta interferons. Alpha and beta interferons mediate type-I interferon signaling. Type-I interferon signaling activates natural killer cells, dendritic cells, and the adaptive immune response This array allows the study of interactions in the innate immune response and to elicit the role of ARV1 potentially further. The comprehensive table of genes in this array are shown in Table # 6. The array plate has 4 replicates of each gene. The WT HepG2, ARV1 KO, and ARV1 OE cell lines were processed on separate plates. All genes that had a fold change of 2.0 or greater were chosen with p-values less than 0.05.

In both KO and OE cell lines, CASP1 was drastically downregulated. CASP1 is involved in the execution-phase of apoptosis. CASP1 is activated by its formation with an inflammasome complex, then CASP1 initiates a proinflammatory response through the cleavage and activation of IL-18, IL-1β. Interestingly, in the inflammatory cytokines and chemokines array, IL-1β in the KO cell line was upregulated, indicating a proinflammatory response. Whereas, in the antiviral array in the OE cell line IL-18 is upregulated. Additionally, TNF was upregulated in the OE cell line. TNF is a multifunctional proinflammatory cytokine with a variety of

processes including lipid metabolism, cell proliferation, cell differentiation, and apoptosis (see Figure # 10).

A.

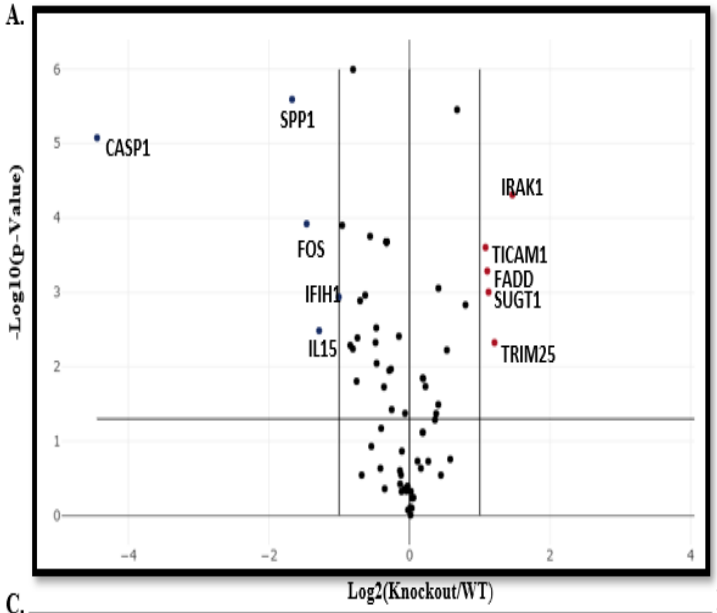

B.

Gene	Fold Change	Significance
IRAK1	2.76	***
TRIM25	2.31	**
SUGT1	2.18	***
FADD	2.15	***
TICAM1	2.12	***
IF1H	-2.01	***
IL15	-2.44	**
FOS	-2.76	***
SPP1	-3.18	***
CASP1	-27.78	***

C.

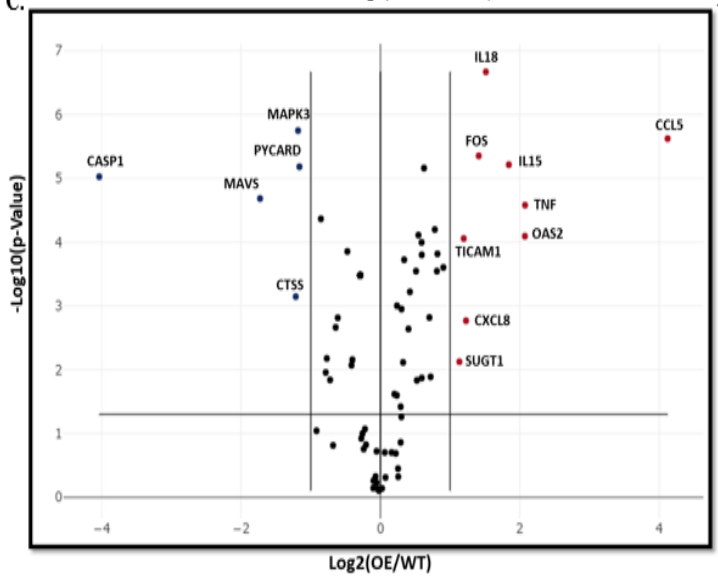

D.

Gene	Fold Change	Significance
CCL5	17.39	***
OAS2	4.21	***
TNF	4.21	***
IL15	3.59	***
IL18	2.85	***
FOS	2.66	***
CXCL8	2.34	***
TICAM1	2.29	***
SUGT1	2.19	***
PYCARD	-2.24	***
MAPK3	-2.27	***
CTSS	-2.32	***
MAVS	-3.31	***
CASP1	-16.39	***

Figure # 10. **Antiviral Volcano Plots**. The X-axis is equal to the Log Squared of (Knockout gene/Wild Type gene). The Y-axis is the -Log10(p-Value). The more left or right a gene is the more of a fold-change. The higher the gene point, the more significant it is. Any points inside the two vertical lines are less than a 2-fold change. Any points lower than the horizontal line is above a 0.05 p-value., therefore deemed insignificant. This dataset is from the KO cell line from the antiviral array [A]. States the significant gene names, fold-change and significance. Significance is defined as p-value ≤0.05 is *, p-value ≤ 0.01 is **, p-value ≤ is 0.001 is ***. All genes calculated as *** significance except TRIM25 and IL15 with a ** significance [B]. The X-axis is equal to the Log Squared of (Over expression gene/Wild Type gene). The Y-axis is the -Log10(p-Value). The more left or right a gene is the more of a fold-change. The higher the gene point, the more significant it is. Any points inside the two vertical lines are less than a 2-fold change. Any points lower than the horizontal line is above a 0.05 p-value., therefore deemed insignificant. This dataset is from the OE cell line from the antiviral array [C]. States the significant gene names, fold-change and significance. Significance is defined as p-value ≤0.05 is *, p-value ≤ 0.01 is **, p-value ≤ is 0.001 is ***. All genes calculated as a *** significance [D].

VI. Heat Map Generation from Qiagen PCR Arrays

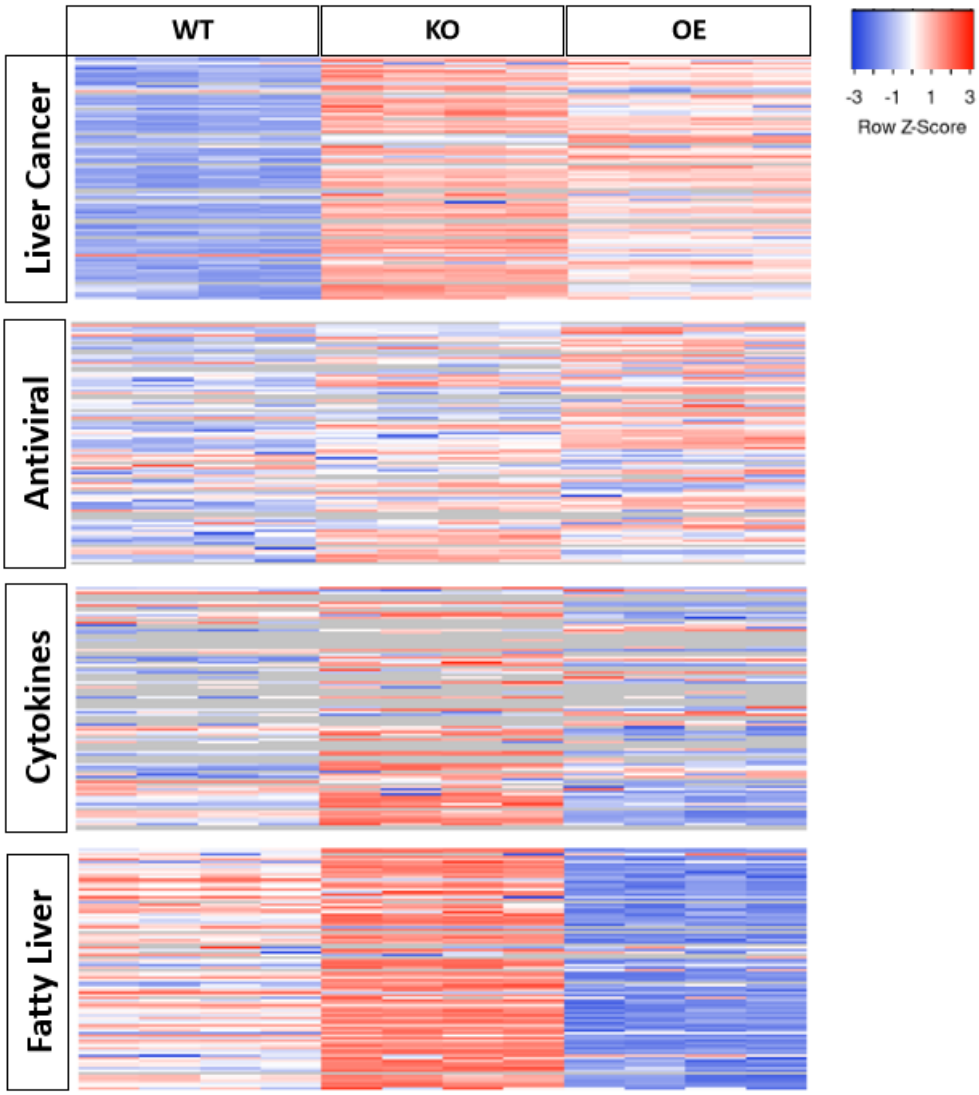

Figure # 11. **Heat Map of Raw Ct Scores from Qiagen's RT PCR Arrays.** A heat map was generated using raw Ct scores by using the Euclidean measurement method. Each row represents a replicate of a gene for that specified array. Each column represents a different gene (96 per array). The heat map was broken down into 4 main parts: Liver Cancer, Antiviral, Cytokines, and Fatty Liver. Red indicates a decrease in Ct score, blue indicates an increase in Ct score, white indicates no change and grey indicates a not applicable score.
The following website was used to generate this heatmap.
www.heatmapper.ca.

To elucidate the vast data from the Qiagen PCR arrays, we generated a heat map based on unnormalized raw Ct values to visualize any potential differences amongst WT, KO, and OE cell lines (see Figure # 11). This heat map allowed us to see a general overview of changes, albeit being unnormalized therefore more analysis using normalized values is needed. Based off the unnormalized values, the liver cancer array in the KO cell indicated many genes to be upregulated, whereas in the OE cell line to only be slightly elevated. The antiviral and cytokines arrays did not show much change amongst KO and OE cell lines. Interestingly, the fatty liver array indicated an upregulation of genes in the KO cell line and a downregulation of genes in the OE cell line. Reminder that this is based solely off unnormalized values, a normalized approach is needed to consider any claims.

VII. Data Analysis from Qiagen PCR Arrays using Enrichr

To further examine the data in an unbiased approach from the Qiagen RT^2 arrays we used an interactive and collaborative gene list enrichment analysis tool, Enrichr. This tool computes a list of gene-set libraries from previous studies done. This tool allows us to look at pathways that are significantly changed from an unbiased approach. After normalization to WT, we took the significant unregulated genes in the ARV1 KO and ARV1 OE cell lines and separated them into 4 categories: upregulated KO genes, downregulated KO genes, upregulated OE genes, and downregulated OE genes. We inputted each category separately into Enrichr where the program generated tables.

In figure # 12 A, demonstrates an association of the KO upregulated genes to be involved in hyperglycemia and cancer. In Figure #12 B, indicates PPAR signaling, proteins induced in NAFLD, and lipid metabolism phenotypes in the downregulated genes of the KO cell line

In Figure # 13 A, depicts of the upregulated OE genes to be involved mainly in cancer and fatty acid activation. In Figure # 13 B, illustrates the downregulated OE genes to be involved in lipid metabolism and proteins induced in NAFLD.

Interestingly, this unbiased approach suggests ARV1 is potentially involved in NAFLD and overall lipid metabolism, which agrees with previous research. Unfortunately, this analysis can only show us what pathways are involved in and not necessarily if that pathway is being upregulated or downregulated. For example, in Figure B. it indicates a significant change in PPAR signaling but we do not know if

this pathway is being upregulated or downregulated. However, this does allow us to see what changes are occurring at the transcription levels in the KO and OE cell lines.

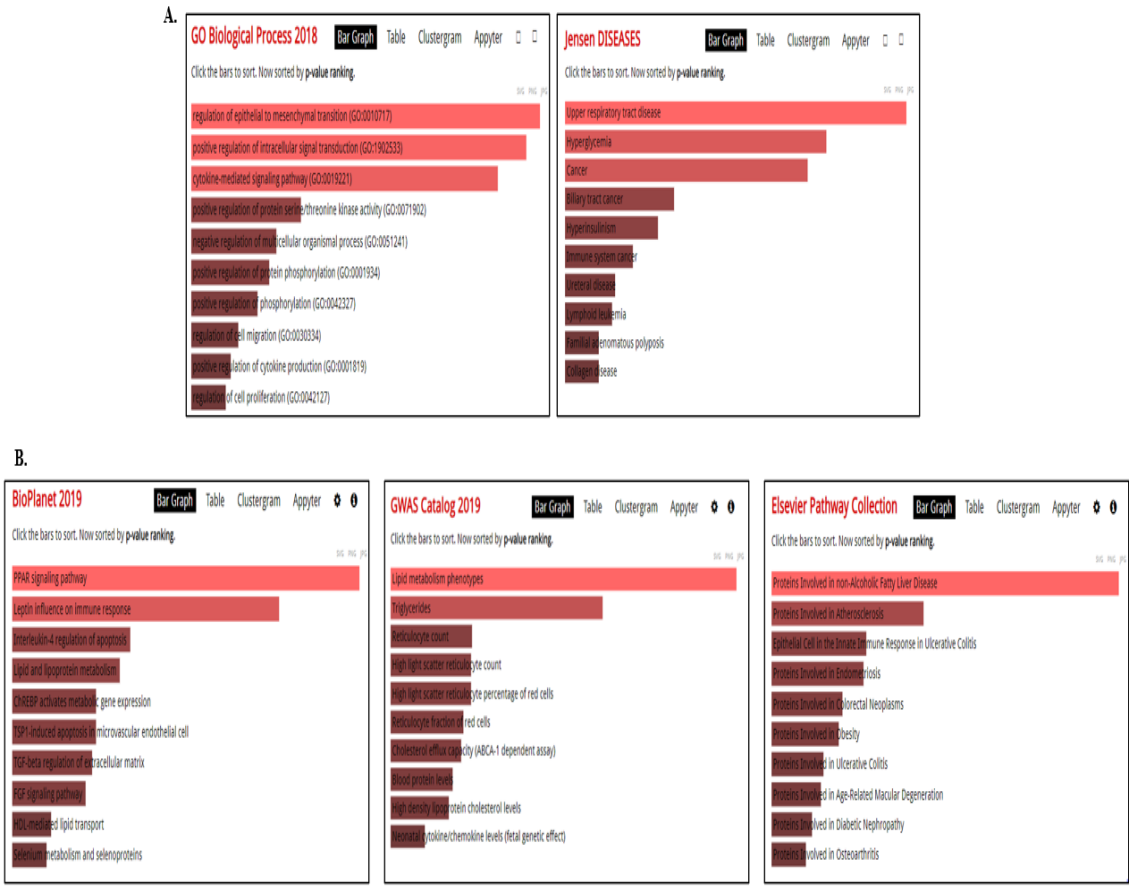

Figure #12. **Enrichr Analysis using Significant Upregulated and Downregulated Genes in ARV1 KO Cell Line**. The significantly upregulated genes based off RT2 Profiler arrays were inputted into the Enrichr database [**A**]. The significantly downregulated genes based of RT2 Profiler arrays were inputted into the Enrichr database [**B**].

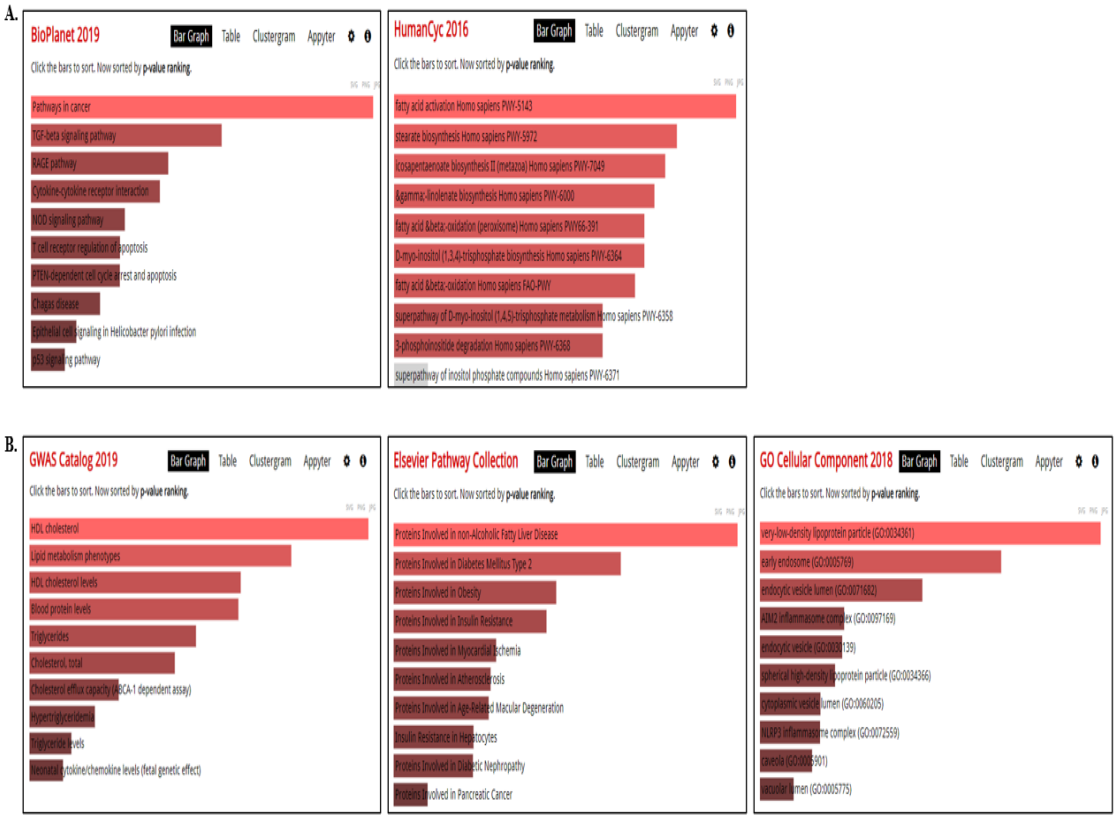

Figure # 13. **Enrichr Analysis using Significant Upregulated and Downregulated Genes in ARV1 OE Cell Line**. The significantly upregulated genes based off RT2 Profiler arrays were inputted into the Enrichr database [**A**]. The significantly downregulated genes based of RT2 Profiler arrays were inputted into the Enrichr database [**B**].

VIII. Immunoblot Analysis of RT-Profiler Gene Hits

We wanted to investigate the proteins of interest based off the RT^2 profiler arrays and previous work done on ARV1. Therefore, we performed immunoblots with untreated HepG2 WT, HepG2 ARV1 KO, and ARV1 OE lysates and probed for PERK, IRE1-α, ATF6, CHOP, phospho-PERK, Xbp1-s, EGFR, phospho-EGFR, ADAM17, PPARα, FABP1, Caspase 1, NLRP3 and APOB (see Figure # 14). We probed for PERK, IRE1-α, ATF6, CHOP, phospho-PERK, and Xbp1-s because previous research done by Shectman et al., showed in decreased ARV1 murine macrophages displayed an increase in ATF4 and CHOP in murine macrophages. Additionally, the study found in ARV1 mutant yeast to have an increase of IRE1-α.

We probed for PPARα and FABP1 because both genes are involved in metabolism. PPARα is a key regulator in lipid metabolism and was downregulated in the OE cell line on the arrays. FABP1 is involved in fatty acid metabolism/transport. FABP1 was downregulated in both OE and KO cell lines in the fatty liver array. Previous work done by Ruggles et al., suggested Arv1 being a target of PPARα.

We probed for NLRP3 and Caspase 1 because Caspase 1 was highly decreased in both cell lines in the array. We wanted to look at NLRP3 because current research is being done at IMD on this protein and wanted to see if the change of expression of ARV1 would influence NLRP3.

. Also, a significant increase in FABP1 in the ARV1 OE cell line was observed. Additionally, Caspase 1 was significantly decreased in both KO and OE cell lines. Specifically, in the UPR pathway for the proteins that we probed for only total-IRE1-α was significantly increased in the ARV1 OE cell lines. There was not

any detection for the following antibodies: Xbp1-s, p-EGFR, NLRP3, p-PERK, APOB and CHOP.

We probed for EGFR and ADAM17 because both genes were upregulated in both KO and OE cell lines and because a high expression of these proteins are normally indicative of a variety of cancers. Significant differences in cell lines looking at protein levels were observed including a 2+ fold increase of EGFR in both the ARV1 KO and ARV1 OE cell lines.

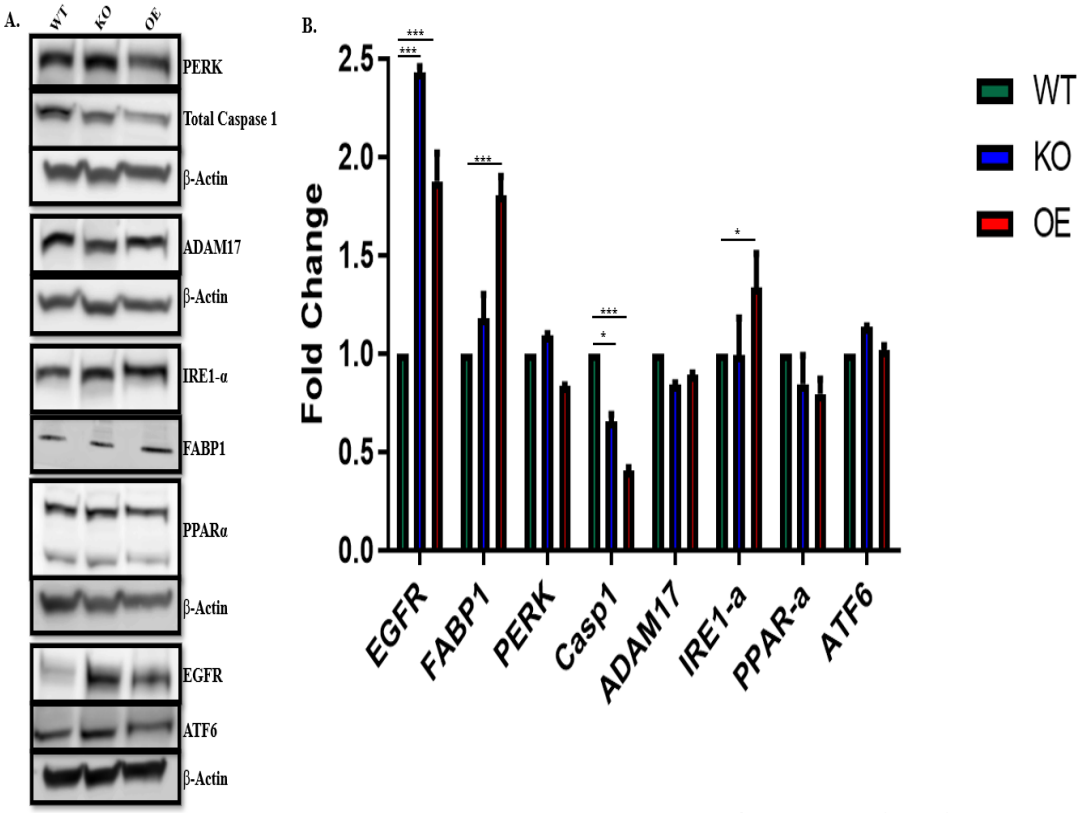

Figure # 14. **Immunoblot of Basal Levels of HepG2 ARV1 WT, ARV1 Knock-Out, and ARV1 Transient Over-Expression with Densitometry**. 25 µg of HepG2 WT, ARV1 KO, and ARV1 OE lysates were ran on a 4-12% SDS-PAGE using TRIS-MOPS-SDS running buffer on 140v for 45 minutes. The resolved proteins were transferred onto a nitrocellulose membrane for 10 minutes. The blots were then blocked, washed, primary antibody overnight, washes, secondary antibody, washed, quickly immersed into chemiluminescent reagent and then imaged on the Amersham 600 on auto-detect mode. Densitometry was calculated by using ImageJ [**A**]Normalization was done by using the Analysis function on ImageJ from the TIF files. The respective β-actin for each protein was used to normalize. The normalized values were copied into GraphPad Prism 5 where a 2-Way Anova test was performed and graphed on GraphPad PRISM 5. The following significance is represented by: $P < 0.05$ represented by *, $P < 0.01$ represented by **, $P < 0.001$ represented by ***. N of 3 [**B**].

The epidermal growth factor receptor (EGFR, also known as ErbB1 or HER-1) is a transmembrane receptor belonging to the receptor tyrosine kinases (RTK) family [46]. EGFR is composed of an extracellular domain followed by a transmembrane domain and an intracellular domain. The EGFR ligands bind to the extracellular domain, the EGFR ligands include epidermal growth factor (EGF), transforming growth factor α (TGF-α), amphiregulin (AR), betacellulin (BTC), epiregulin (EREG), epigen (EPGN) and heparin-binding EGF (HB-EGF) [47]. The intracellular domain contains the tyrosine kinase domain and the carboxy-terminal tail where the key tyrosine residues reside [48]. Furthermore, EGFR ligands are synthesized bound to the membrane as immature precursors and the ligand being proteolytically cleaved from the cell surface enables solubilization, diffusion and receptor binding [49].

The shedding of EGFR-ligands is primarily catalyzed by 'A disintegrin and metalloproteinase' (ADAM) family. Interestingly, among the different ADAM family members, tumor-necrosis factor α (TNF-α)-converting enzyme (TACE) also known as ADAM17 plays the main role in EGFR ligand cleavage [50]. Interestingly, ADAM17 displayed an upregulation in both ARV1 KO and ARV1 OE cell lines in the RT profiler arrays. This could suggest ADAM17 having an indirect role on Arv1, possibly through EGFR. Upon ligand binding and activation of the intrinsic kinase domain, a variety of proteins containing Src-homology 2 domains (SH2) such as SHC-transforming protein (SHC), growth factor receptor-bound protein 2 (Grb2), and phospholipase C γ (PLCγ) can bind to the phosphorylated tyrosine residues and activate the intricate downstream signaling cascades [48]. The main activated

pathways include Ras-Raf-MEK-ERK1/2 and the signal-transducer and activator of transcription (STAT) 3 and STAT5 pathways involved in differentiation and proliferation. Also, the phosphatidylinositol-3-kinase (PI3K)-Akt-mechanistic target of rapamycin (mTOR) pathway involved in survival.

Fas-mediated apoptosis play a major role in the development of hepatocyte apoptosis, contributing to a variety of liver diseases. Therefore, the development of therapies to inhibit hepatocyte apoptosis have been studied extensively. Interestingly, it has been found the activation EGFR signals hepatocytes to pro-survival.

Interestingly, loss of ADAM17 in hepatocytes increased Fas-induced apoptosis [51]. Suggesting ADAM17 is protective against Fas-induced apoptosis along with its function of shedding EGFR ligands. All this data suggests EGFR signaling system is hepatoprotective against Fas-mediated injury in experimental models of acute liver damage.

Liver fibrosis occurs in most types of chronic liver damage, where it is characterized by the deposition of excessive extracellular matrix proteins (ECM)[48]. The structural changes in the liver due to the excessive ECM can lead to cirrhosis, pre-neoplastic nodules and can lead to hepatocellular carcinoma [52]. Therefore, liver injury and cirrhosis have a strong connection to hepatocarcinogenesis. Furthermore, studies have been done to see the potential relationship between EGFR ligands and EGFR in fibrosis and cirrhosis. By studying the classical CCl_4 model for chronic toxic liver injury in mice, expression of HB-EGF, AR and TGF-α was increased [53].

In a NASH mouse model with an MCD diet alongside patient samples with NASH, it was found that AR was upregulated [54]. Whereas, TGF-α over-expression attenuated NASH after the feeding of mice with MCD diet [55]. Furthermore, administration of EGF had a hepatoprotective feature against alcohol-induced liver damage [53]. Importantly, this data suggests EGFR plays a major role in both acute and chronic liver diseases, where these diseases are pre-stages on the way to the development of hepatocellular carcinoma.

EGFR is over-expressed in human cirrhotic liver tissue and HCCs [56]. In 68% of HCC, EGFR is over-expressed alongside metastasis, aggressive tumors, and very poor patient survival [53]. Moreover, over-expression of EGFR ligands; EGF, TGF-α, AR, HB-EGF, also ADAM17 have been shown to be in human liver tumor cells and tissues [56]. Furthermore, a polymorphism of the EGF gene was associated with an increased risk of HCC in patients with liver cirrhosis [57]. Inhibiting EGFR with anti-EGFR antibodies like cetuximab and small inhibitor molecules like gefitinib or erlotinib have demonstrated promising results in HCC cell lines and animal studies. However, only moderate results have been observed in clinical studies.

A study by Choung et al., displayed the inhibition of EGFR on HFD mice to have a decrease of sterol responsive elementary binding protein 1 and 2 along with a decrease of phosphatidylinositol 3-kinase/protein kinase B signaling. This prevented HFD-induced hypercholesteremia and hepatic steatosis by the reduction of cholesterol synthesis, de novo lipogenesis and improving fatty acid oxidation [58].

Therefore, more research is needed to be done to improve cell-specific signaling pathways that are involved in liver diseases. Alongside, to develop better therapies targeting EGFR to potentially treat liver damage and diseases.

Furthermore, Dr. Karla Frietze had identified that ARV1 might be linked to EGFR through an independent study. We therefore formed a collaboration to further the possible implication into the role of EGFR in ARV1 function.

IX. Bioinformatic Analysis of Arv1

To identify possible modes of function and regulation in ARV1, the cytoplasmic n-terminal region was analyzed by software to find motif predictions (see Figure # 15). Bioinformatic analysis suggest ARV1 contains a conserved zinc finger motif and a conserved tyrosine residue that contains an EGFR consensus motif. Therefore, suggesting EGFR may phosphorylate Arv1 at the tyrosine 68 residue.

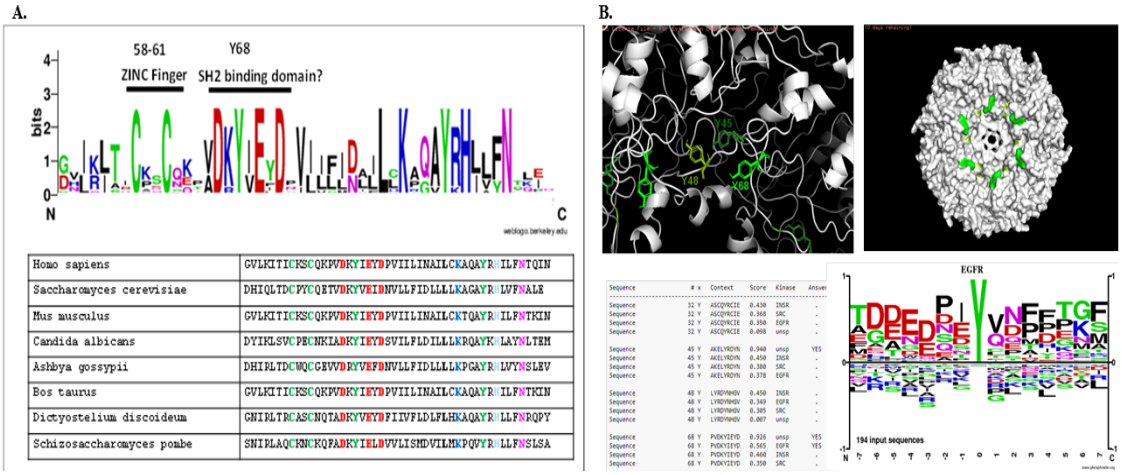

Figure # 15. **N-Terminal Region of Arv1 is Conserved Across Species and Arv1 Contains an EGFR Consensus Site**. Sequence alignment of human ARV1 aligned to verified peptide sequences of ARV1 shows a possible zinc finger motif on residues 58-61 and possible SH2 binding domain on Y68 [A]. Tyrosine residues are mapped in green on the predicted ARV1 hexamer. Using netphosK3.1, predicts that EGFR is the preferred kinases on tyrosine residue Y68 [B].
Work and Figures done by Dr. Karla Frietze.

X. In Vitro Kinase Assay

The in vitro kinase assay was used to determine whether EGFR can directly phosphorylate Arv1. The results indicate EGFR can phosphorylate ARV1. EGFR was able to phosphorylate both N60 ARV1 and N90 ARV1 but not the EGFR empty vector control, suggesting EGFR has the potential to phosphorylate other sites upstream of Y68 (See Figure # 16).

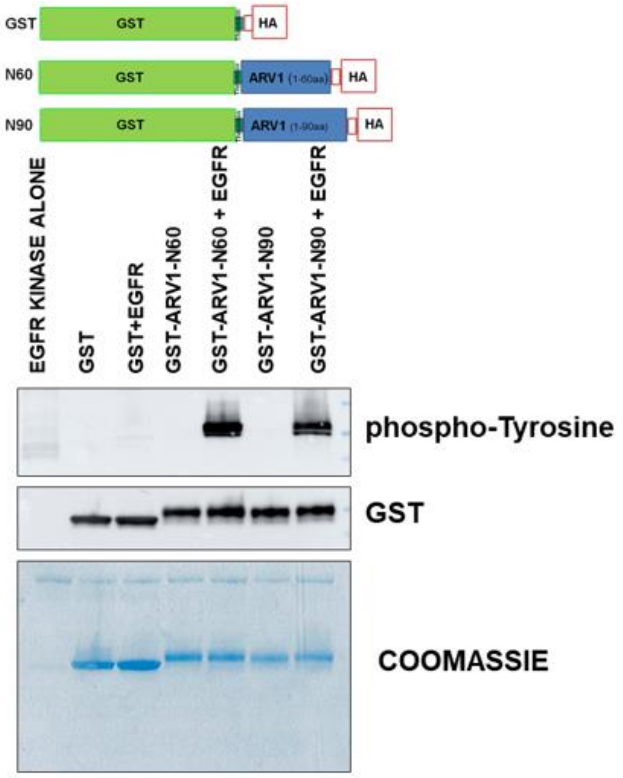

Figure # 16. **EGFR can Phosphorylate ARV1**. Glutathione S-transferase (GST) constructs bearing the N-terminus of ARV1. The first 60 amino acids and first 90 amino acids of ARV1 were used. Active EGFR kinase and the GST-ARV1 constructs were used as substrates. Following the in vitro kinase assay, the reactions were ran on an SDS-PAGE gel. Followed by probing of phospho-Tyrosine and GST as the control. **Work and Figures attributed to Dr. Karla Frietze from the Institute of Metabolic Disorders**.

XI. Lipid Staining and Imaging

We reasoned that if Arv1 was critical for lipid synthesis and/or export this may be important during cellular growth and cell division. EGFR is a necessary receptor for cellular growth, therefore if ARV1 was being regulated by EGFR we can hypothesize that EGFR up regulation may correlate with up regulation of ARV1 leading to lipid synthesis. We reasoned that if we treated OE cells with EGFR inhibitors we could rescue the cellular health. Specifically, we tested whether EGFR inhibitors could offer some protection to OE cells in the presence of high doses of palmitic acid. We used two different EGFR inhibitors, Gefitinib and PD168393. Gefitinib competes with the binding of ATP to the tyrosine kinase of EGFR. PD168393 is an irreversible inhibitor of EGFR, where this compound docks into the ATP binding pocket of the tyrosine kinase of EGFR. See Figure # 17 for lipid spot timeline.

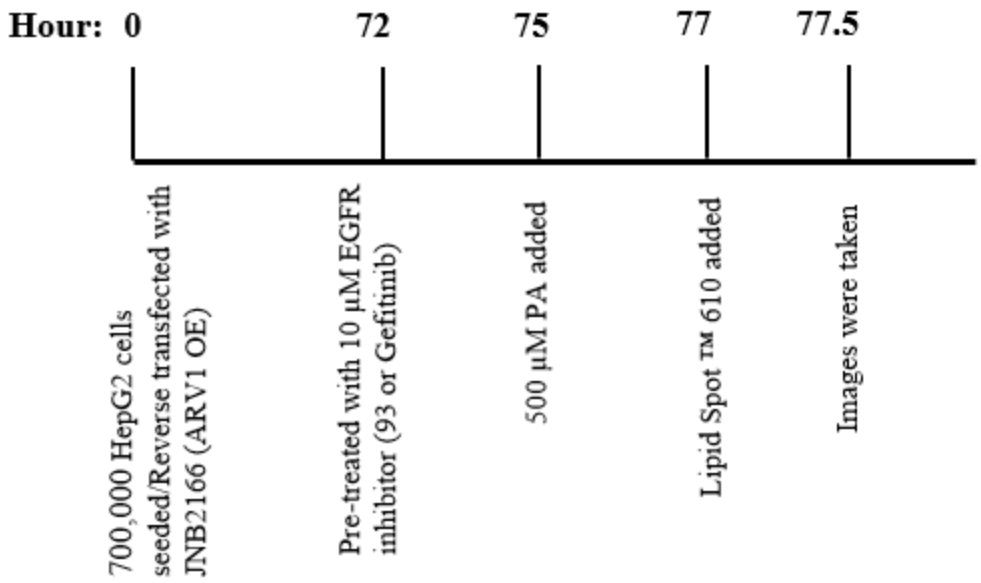

Figure # 17. Timeline for Lipid Stain. HepG2 WT cells/HepG2 WT cells were reverse-transfected with JNB2166 (ARV1 OE). 700,000 cells were seeded into each well (6-well collagen coated). 72 hours, EGFR inhibitor (PD168393 or Gefitinib) was added. 3 hours later, 500 µM PA was added. 2 hours later, Lipid Spot 610 was added. 30 minutes later, images were taken on Nikon Eclipse TE300 using AM Scope using manual settings.

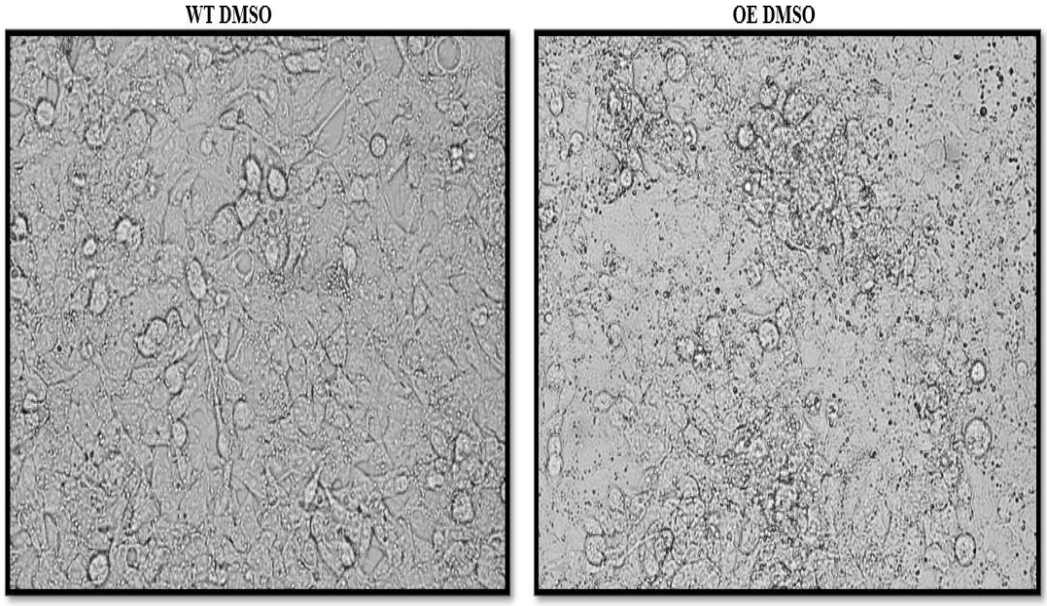

Figure # 18. **Brightfield Images at 20x Magnification Showing HepG2 WT and HepG2 ARV1 OE in DMSO**. The images were taken on 20x magnification on the Nikon Eclipse TE300 using AM Scope.

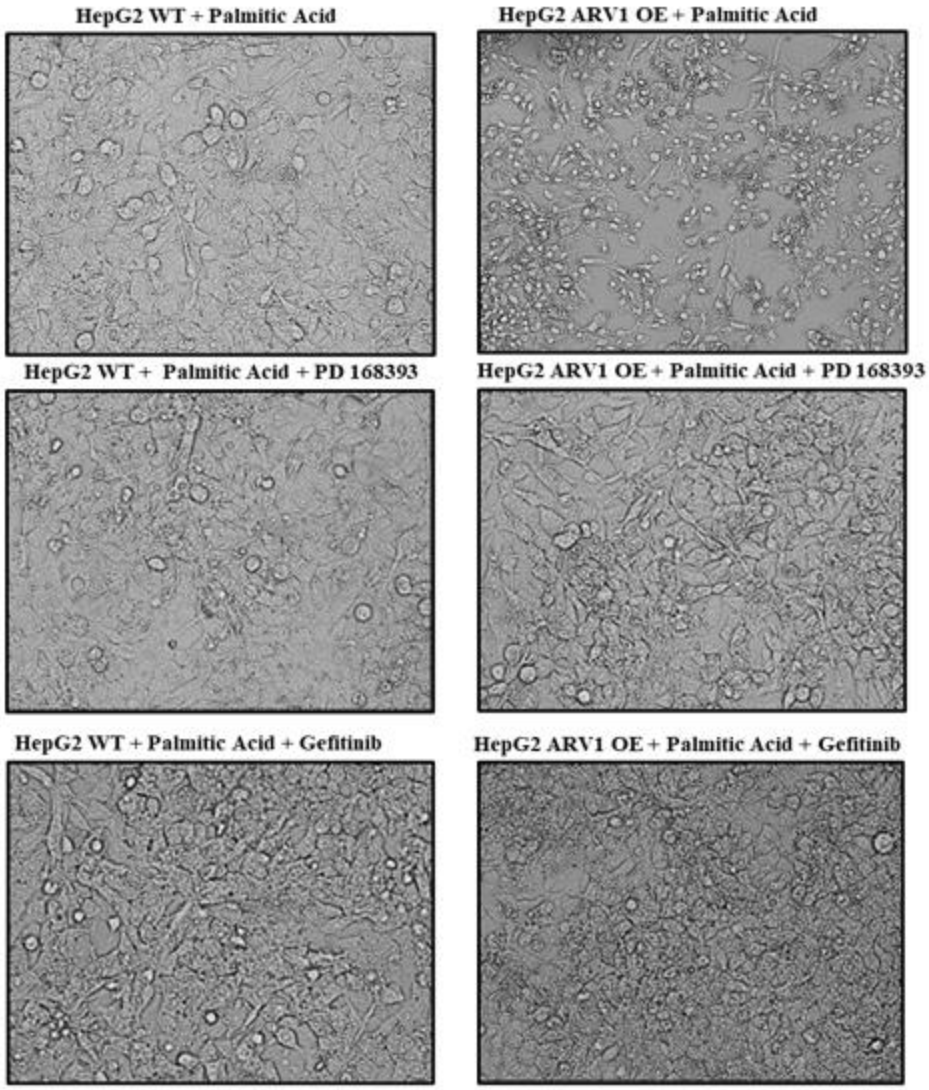

Figure # 19. **Brightfield Images at 20x Magnification**. The images were taken at 20x magnification on the Nikon Eclipse TE300 using AM Scope using manual settings. HepG2 Wild-type with 500 µM PA for 2 hours and HepG2 ARV1 over-expressing cells with PA +/- two different EGFR inhibitors 10 µM (PD168393 or Gefitinib) are shown.

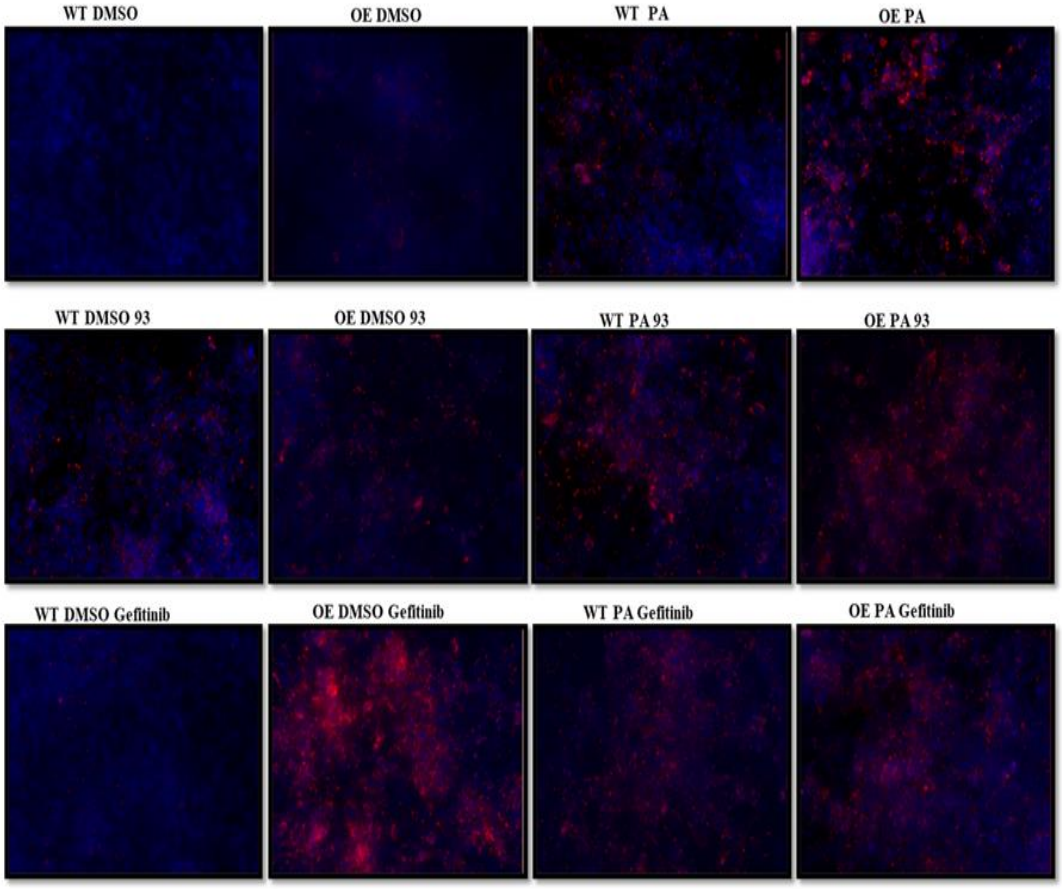

Figure # 20. **20x Magnification of Merge Images**. The blue channel (nuclear stain) and red channel (lipid stain) for each cell type/treatment were merged using ImageJ.

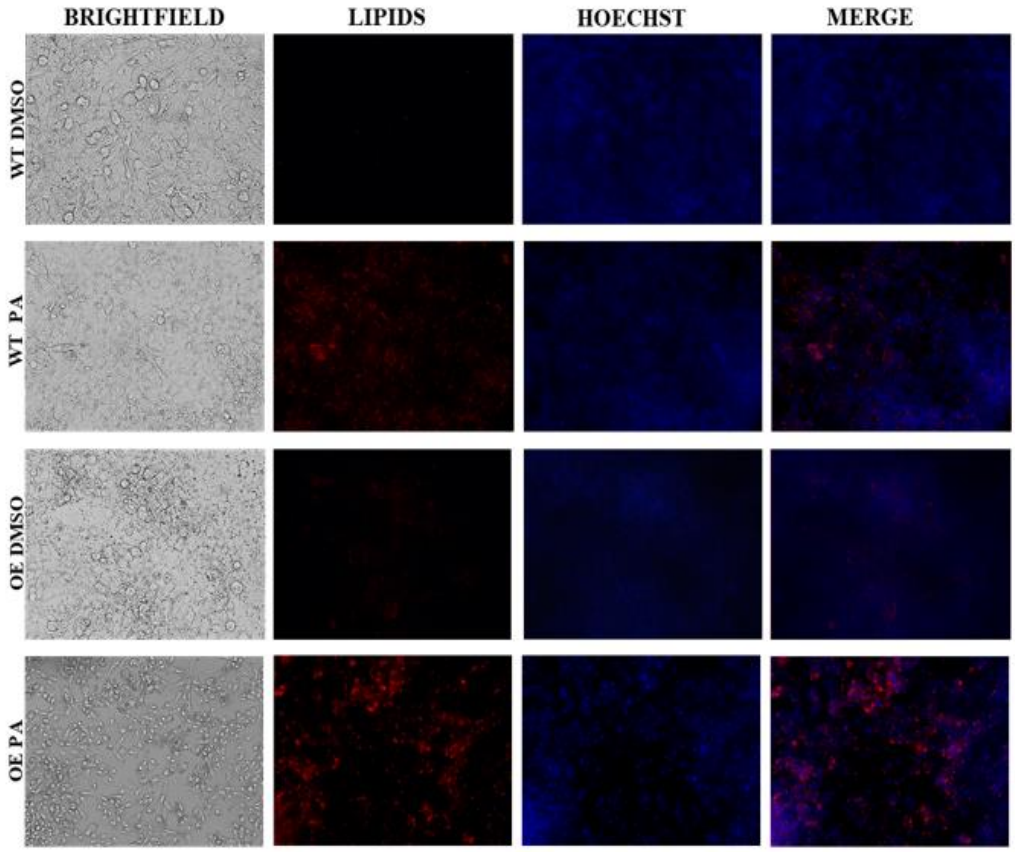

Figure # 21. **20x Magnification Lipid Stain for HepG2 WT +/- PA and HepG2 OE +/- PA**. Images were taken on the Nikon Eclipse TE300 using the AM Scope software using the 20x objective. The following manual settings were used for all cell types/treatments. For brightfield images: Exposure Target 120, Exposure Time 10 ms and Gain 1.00. The lipid stain in the Red channel images: Exposure Target 120, Exposure Time 400 ms and Gain 5.00. The nuclear stain in the blue channel images: Target 120, Exposure Time 4.00 ms and Gain 5.00.

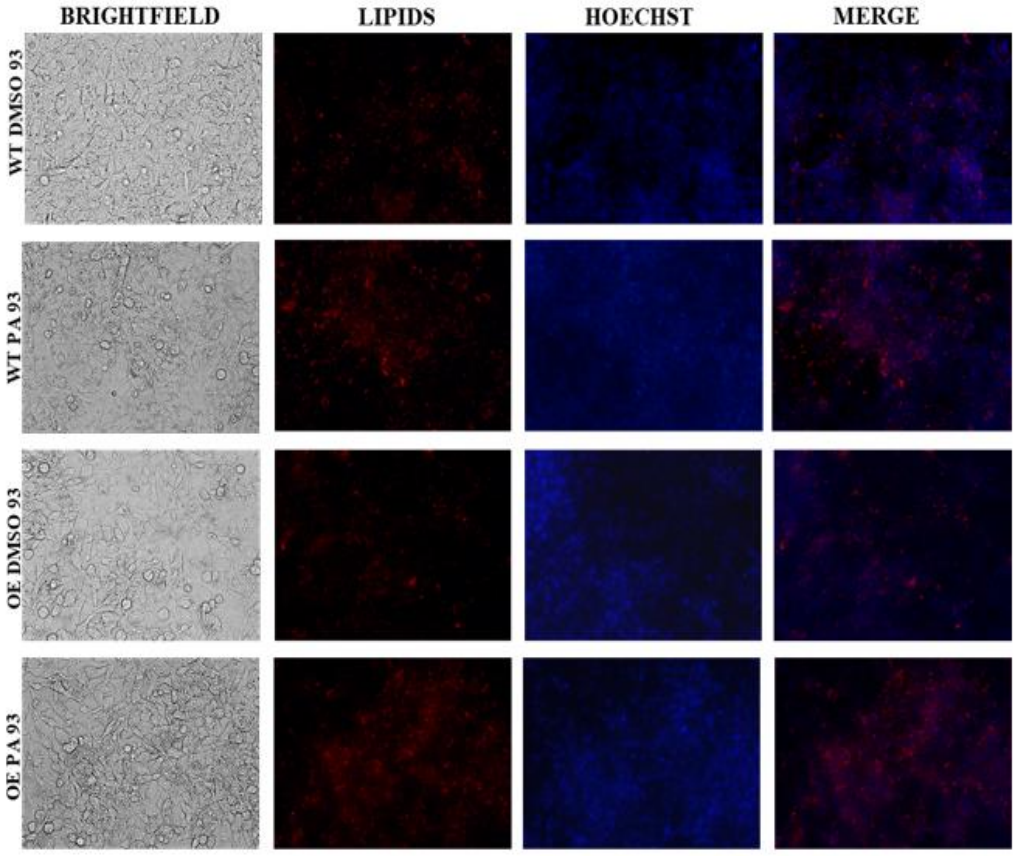

Figure # 22. **20x Magnification Lipid Stain for HepG2 WT + EGFR Inhibitor 93 +/- PA and HepG2 ARV1 OE + EGFR Inhibitor 93 +/- PA**. Images were taken on the Nikon Eclipse TE300 using the AM Scope software using the 20x objective. The following manual settings were used for all cell types/treatments. For brightfield images: Exposure Target 120, Exposure Time 10 ms and Gain 1.00. The lipid stain in the Red channel images: Exposure Target 120, Exposure Time 400 ms and Gain 5.00. The nuclear stain in the blue channel images: Target 120, Exposure Time 4.00 ms and Gain 5.00.

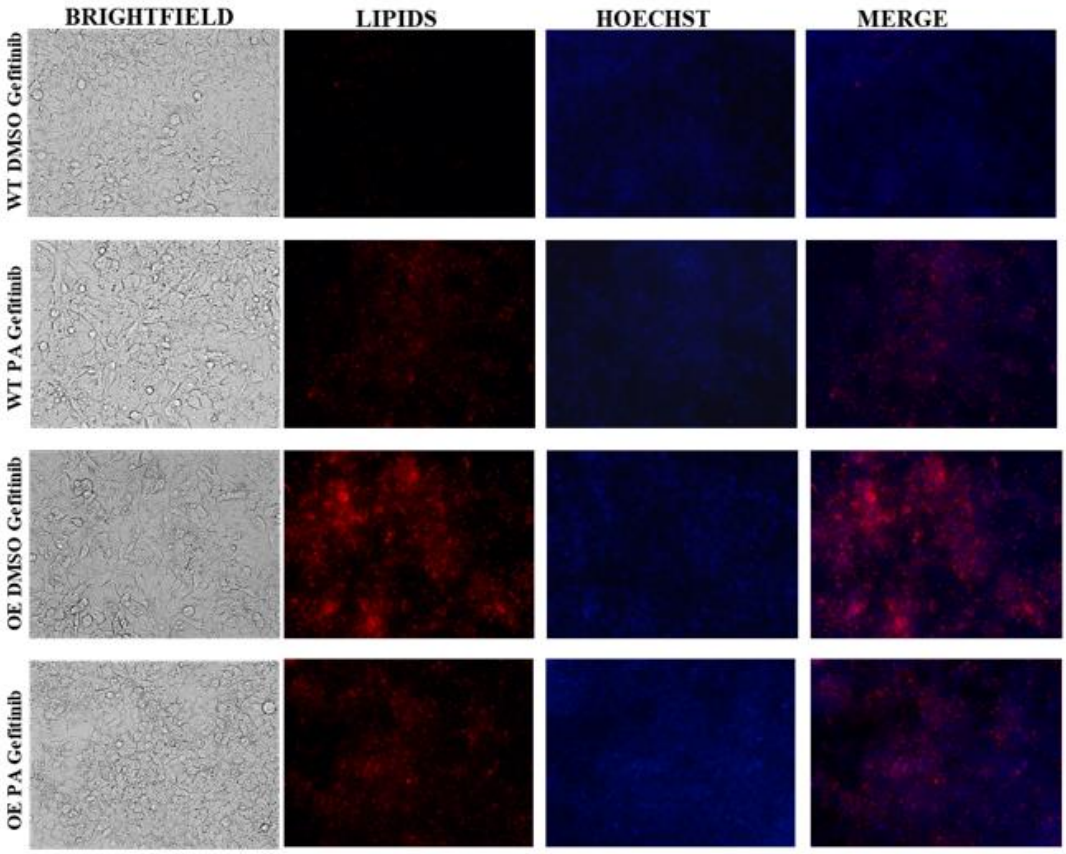

Figure # 23. **20x Magnification Lipid Stain for HepG2 WT + EGFR Inhibitor Gefitinib +/- PA and HepG2 ARV1 OE + Gefitinib +/- PA**. Images were taken on the Nikon Eclipse TE300 using the AM Scope software using the 20x objective. The following manual settings were used for all cell types/treatments. For brightfield images: Exposure Target 120, Exposure Time 10 ms and Gain 1.00. The lipid stain in the Red channel images: Exposure Target 120, Exposure Time 400 ms and Gain 5.00. The nuclear stain in the blue channel images: Target 120, Exposure Time 4.00 ms and Gain 5.00

In Figure # 18, displays side-by-side comparison of HepG2 WT and HepG2 ARV1 OE cells both only treated with DMSO. This displays pathology of pre-apoptotic/unhealthy cells in the OE cell line.

In Figure # 19, shows all the treatments in palmitic acid. The ARV1 OE cells clearly indicate less cells attached, indicating cell death. The WT with palmitic acid seems to be relatively healthy and growing. Interestingly, in both EGFR inhibitors, the cell viability is drastically increased.

In figures # 20-23, do not show too much difference. One thing of note is the increased lipid stain droplets in the OE with palmitic acid..

The main key difference amongst cell lines is the massive cell death of ARV1 OE cells in PA and the rescue of ARV1 OE cells in PA with either EGFR inhibitor.

Discussion

I. Summary and Findings

A. Cell Line Generation

ARV1 knock out and ARV1 transiently over expression were generated in HepG2 cells. We verified these cell lines by cDNA agarose gel and by qRT-PCR by using a ARV1 primer set. Unfortunately, we could not verify Arv1 WT, KO, or OE on the protein level by immunoblotting even using ARV1 KO mouse lysate. Additionally, this data is consistent with previous ARV1 studies that also do not validate ARV1 protein expression. Many ARV1 studies only displayed Arv1 expression looking at PCR levels or by immunoblot by probing a tagged Arv1 [5, 7, 44].

B. Qiagen RT2 Profiler Arrays

We purchased four qRT-PCR arrays from Qiagen to potentially identify the function of ARV1 in humans. The four arrays include fatty liver, liver cancer, antiviral response, and cytokines/chemokines. We found an overall decrease in lipid profile in the OE cell line in the fatty liver array. Possibly due to a compensatory mechanism in place where the cell ‘” senses” lipid overload in the OE cell and counteracts it with lowering overall lipid expression. Additionally, we found FABP1, and PPARα downregulated in the OE cell line.

In the liver cancer array, we found CDKN1A to be downregulated in the KO cell line, CDKN1A is a regulator cell cycle progression at G1, but is regulated in the

OE cell line. Additionally, CDKN1B is upregulated in the OE cell line, which is involved in inhibiting cell cycle progression in G1. This could suggest a halt in growth in the OE cell line.

Furthermore, EGFR and ADAM17 are both upregulated in KO and OE cell lines. EGFR is a hallmark of cancer, where the 'on' switch is constantly on to allow abnormal growth and is found overexpressed in a multitude of cancers. Additionally, ADAM17 is a protease acting upon a variety of substrates including EGFR. ADAM17 is involved in a variety of pathways including pathophysiological and physiological such as development, regeneration, chronic inflammation, immunity and tumorigenesis [45]. Furthermore, it has been shown that an increase of ADAM17 leads to an increase of EGFR ligands which can increase tumor progression. Separately, GADD45β is upregulated drastically potentially indicating apoptosis in the OE cell line.

The cytokines/chemokines and antiviral response arrays did not show much change. The only significant change that we noticed was CASP1 in both KO and OE cell lines, CASP1 was drastically downregulated. CASP1 is involved in the execution-phase of apoptosis. CASP1 is activated by its formation with an inflammasome complex, then CASP1 initiates a proinflammatory response through the cleavage and activation of IL-18, IL-1β.

C. Validation by Immunoblot

We wanted to look at the protein level of un-treated HepG2 WT, KO, and OE ARV1. We found a significant decrease of CASP1 in both KO and OE, of which more significance in the OE cell line. We found a significant increase in EGFR in

both KO and OE cell lines. We found a significant increase of IRE1α and FABP1 in the OE.

D. EGFR and Arv1 Interaction

We initially found an upregulation of both EGFR and ADAM17 in both KO and OE cell lines in the RT^2 arrays. Simultaneously, Dr. Karla Frietze had identified that ARV1 might be linked to EGFR through an independent study. We therefore formed a collaboration to further the possible implication into the role of EGFR in ARV1 function. Dr. Frietze and I wanted to identify possible modes of function and regulation in ARV1, the cytoplasmic n-terminal region was analyzed by software to find motif predictions. Bioinformatic analysis suggest ARV1 contains a conserved zinc finger motif and a conserved tyrosine residue that contains an EGFR consensus motif. Therefore, suggesting EGFR may phosphorylate Arv1 at the tyrosine 68 residue. Next, an in vitro kinase assay was performed. The first 60 and first 90 amino acids of Arv1 were used with GST as substrates and EGFR was used as the kinase. Our data suggests EGFR can phosphorylate both N60 and N90 Arv1, suggesting there may be multiple or upstream sites where EGFR can phosphorylate Arv1. Lastly, we performed a lipid stain and imaging experiment on HepG2 Arv1 WT and ARV1 OE cells +/- palmitic acid +/- EGFR inhibitors. Our data displayed the OE cell line even in just DMSO to be unhealthy/pre-apoptotic. Furthermore, OE + palmitic acid displayed massive cell death. Interestingly, OE + either EGFR inhibitor displayed improved cell viability.

In conclusion, the KO and OE cell lines displayed changes in overall lipid metabolism, whereas the OE had an even greater display of this. Additionally, we saw

an increase in EGFR in both KO and OE cell lines. Additionally, with the help of Dr. Karla Frietze, our data suggested EGFR can directly phosphorylate Arv1 on potentially tyrosine 68 residue or possibly more sites. Lastly, by lipid stain and imaging, our data showcases OE cells to be unhealthy in even DMSO and displaying massive cell death with the addition of palmitic acid. Interestingly, we were able to "rescue" the OE cells in palmitic acid with the addition of either EGFR inhibitor.

II. Open Questions and Future Directions

A. Open Questions

Our main question we have is at which tyrosine residue(s) is EGFR phosphorylating Arv1?

Does EGFR regulate Arv1? If so, what activates EGFR to regulate Arv1? Could it be ADAM17?

Specifically, why are the Arv1 OE cells lipotoxic to even just DMSO?

B. Future Directions

We have several experiments planned and in progress for the future direction of Arv1 and EGFR. We want to further define the mechanism of Arv1 and EGFR in regulating lipid synthesis/export. To do this, we want to make Arv1 point mutations on several key tyrosine residues and see if any of the point mutation(s) prevent lipid synthesis/export. We would repeat experiments with the point mutations to see any differences. Some of the experiments include in vitro kinase assay, lipid stain and immunoblots.

Another experiment we would do is using Qiagen's Profiler EGF/PDGF array with HepG2 WT and OE cells +/- palmitic acid +/- EGF inhibitors. This could allow us to narrow down any intermediate players involved and to potentially see if Arv1 is involved in other pathways. This could ultimately lead us to a whole pathway for Arv1.

Additionally, we want to use siRNA EGFR and to repeat all the previous experiments to see if there are any changes in lipid profile and/or toxicity.

Summary and Conclusions

Previous research suggested the deletion of ARV1 results in numerous defects including abnormal sterol trafficking [1], the reduction of sphingolipid metabolism [2], synthesis of glycosylphosphatidylinositol (GPI) anchor [3], ER stress [4], and hypersensitivity of fatty acids leading to lipoapoptosis [5]. Furthermore, germline deletion of ARV1 in mice demonstrated a lean phenotype with the addition of increase energy expenditure and improved glucose tolerance [44]. Additionally, a neuronal deficiency of ARV1 causes autosomal recessive epileptic encephalopathy [7]. Interestingly, the expression of human ARV1 can 'rescue' viability and growth defects in yeast when this gene is absent.

Therefore, we wanted to potentially elicit the function of ARV1 in humans, therefore, we used CRISPR/CAS-9 knock-out technology and a transient over-expression model of ARV1 in the hepatocellular carcinoma cell line, HepG2. We used the HepG2 cell line because we wanted to use a relevant cell line to both NAFLD and potentially Arv1.

First, we verified our cell lines by cDNA agarose gel and was hoping to verify ARV1 KO and ARV1 OE on the protein level by immunoblotting. Unfortunately, there is not a dependable Arv1 antibody on the market currently. Therefore, all our work was verified only at the transcriptional level. In line with, many other ARV1 studies only published at the transcriptional level and/or immunoblot by probing a tag protein on Arv1.

Next, we wanted to take a shotgun approach at eliciting the role of ARV1, so we ordered four qRT-PCR arrays from Qiagen. The plates were specifically designed to look at the following pathways: human fatty liver, human liver cancer, human antiviral response, and human inflammatory cytokines and receptors. The data from the fatty liver array suggested an overall downregulated trend in the OE cell line. Potentially indicating an overall lipid decrease possibly trying to compensate for the overexpression of ARV1. This agrees with previous studies indicating Arv1 being involved in lipid metabolism/lipid transport. Additionally, FABP1 was significantly downregulated in the OE cell line, possibly indicating a compensatory mechanism for the overaccumulation of lipids. Therefore, FABP1 is being downregulated where it normally plays an important role in intracellular lipid metabolism in the liver. Additionally, a study done by Mukai et al., showcased the silencing of FABP1 by adenovirus, which decreased liver weight and TG accumulation in mice that were fed an HFD. Indicating a potential approach to treating NAFLD by a decrease in FABP1 [59].

In the human liver cancer array indicated EGFR and ADAM17 upregulation in both KO and OE cell lines. Additionally, with the help of Dr. Karla Frietze, our data suggested EGFR can directly phosphorylate Arv1 on potentially tyrosine 68 residue or possibly more sites. Lastly, by lipid stain and imaging, our data showcases OE cells to be unhealthy in even DMSO and displaying massive cell death with the addition of palmitic acid. Interestingly, we were able to “rescue” the OE cells in palmitic acid with the addition of either EGFR inhibitor. Additional work will be needed to be done to map the structure of Arv1 and to see which phosphorylation

site(s) EGFR interacts with on Arv1 and to further investigate the reason why Arv1 OE cells are extremely lipotoxic.

References

1. Tinkelenberg, A.H., et al., *Mutations in yeast ARV1 alter intracellular sterol distribution and are complemented by human ARV1.* J Biol Chem, 2000. **275**(52): p. 40667-70.

2. Swain, E., et al., *Yeast cells lacking the ARV1 gene harbor defects in sphingolipid metabolism. Complementation by human ARV1.* J Biol Chem, 2002. **277**(39): p. 36152-60.

3. Kajiwara, K., et al., *Yeast ARV1 is required for efficient delivery of an early GPI intermediate to the first mannosyltransferase during GPI assembly and controls lipid flow from the endoplasmic reticulum.* Mol Biol Cell, 2008. **19**(5): p. 2069-82.

4. Shechtman, C.F., et al., *Loss of subcellular lipid transport due to ARV1 deficiency disrupts organelle homeostasis and activates the unfolded protein response.* J Biol Chem, 2011. **286**(14): p. 11951-9.

5. Ruggles, K.V., et al., *A functional, genome-wide evaluation of liposensitive yeast identifies the "ARE2 required for viability" (ARV1) gene product as a major component of eukaryotic fatty acid resistance.* J Biol Chem, 2014. **289**(7): p. 4417-31.

6. Gallo-Ebert, C., et al., *Mice lackingARV1have reduced signs of metabolic syndrome and non-alcoholic fatty liver disease.* J Biol Chem, 2018. **293**(16): p. 5956-5974.

7. Palmer, E.E., et al., *Neuronal deficiency of ARV1 causes an autosomal recessive epileptic encephalopathy.* Hum Mol Genet, 2016. **25**(14): p. 3042-3054.

8. Danford, C.J., Z.M. Yao, and Z.G. Jiang, *Non-alcoholic fatty liver disease: a narrative review of genetics.* J Biomed Res, 2018. **32**(5): p. 389-400.

9. Kanwar, P. and K.V. Kowdley, *The Metabolic Syndrome and Its Influence on Nonalcoholic Steatohepatitis.* Clin Liver Dis, 2016. **20**(2): p. 225-43.

10. Benedict, M. and X. Zhang, *Non-alcoholic fatty liver disease: An expanded review.* World J Hepatol, 2017. **9**(16): p. 715-732.

11. Lonardo, A., et al., *Epidemiological modifiers of non-alcoholic fatty liver disease: Focus on high-risk groups.* Dig Liver Dis, 2015. **47**(12): p. 997-1006.

12. Sung, K.C., S.H. Wild, and C.D. Byrne, *Development of new fatty liver, or resolution of existing fatty liver, over five years of follow-up, and risk of incident hypertension.* J Hepatol, 2014. **60**(5): p. 1040-5.

13. Mohanty, S.R., et al., *Influence of ethnicity on histological differences in non-alcoholic fatty liver disease.* J Hepatol, 2009. **50**(4): p. 797-804.

14. Satapathy, S.K. and A.J. Sanyal, *Epidemiology and Natural History of Nonalcoholic Fatty Liver Disease.* Semin Liver Dis, 2015. **35**(3): p. 221-35.

15. Brea, A. and J. Puzo, *Non-alcoholic fatty liver disease and cardiovascular risk.* Int J Cardiol, 2013. **167**(4): p. 1109-17.

16. Schwimmer, J.B., *Clinical advances in pediatric nonalcoholic fatty liver disease.* Hepatology, 2016. **63**(5): p. 1718-25.

17. Nobili, V., et al., *Non-alcoholic fatty liver disease and hepatocellular carcinoma in a 7-year-old obese boy: coincidence or comorbidity?* Pediatr Obes, 2014. **9**(5): p. e99-e102.

18. Godos, J., et al., *Mediterranean diet and nonalcoholic fatty liver disease: molecular mechanisms of protection.* Int J Food Sci Nutr, 2017. **68**(1): p. 18-27.

19. Zelber-Sagi, S., J. Godos, and F. Salomone, *Lifestyle changes for the treatment of nonalcoholic fatty liver disease: a review of observational studies and intervention trials.* Therap Adv Gastroenterol, 2016. **9**(3): p. 392-407.

20. Ravi Kanth, V.V., et al., *Genetics of non-alcoholic fatty liver disease: From susceptibility and nutrient interactions to management.* World J Hepatol, 2016. **8**(20): p. 827-37.

21. Romeo, S., et al., *Genetic variation in PNPLA3 confers susceptibility to nonalcoholic fatty liver disease.* Nat Genet, 2008. **40**(12): p. 1461-5.

22. Singal, A.G., et al., *The effect of PNPLA3 on fibrosis progression and development of hepatocellular carcinoma: a meta-analysis.* Am J Gastroenterol, 2014. **109**(3): p. 325-34.

23. Mahdessian, H., et al., *TM6SF2 is a regulator of liver fat metabolism influencing triglyceride secretion and hepatic lipid droplet content.* Proc Natl Acad Sci U S A, 2014. **111**(24): p. 8913-8.

24. Townsend, S.A. and P.N. Newsome, *Non-alcoholic fatty liver disease in 2016.* Br Med Bull, 2016. **119**(1): p. 143-56.

25. Buzzetti, E., M. Pinzani, and E.A. Tsochatzis, *The multiple-hit pathogenesis of non-alcoholic fatty liver disease (NAFLD).* Metabolism, 2016. **65**(8): p. 1038-48.

26. Bugianesi, E., et al., *Insulin resistance in nonalcoholic fatty liver disease.* Curr Pharm Des, 2010. **16**(17): p. 1941-51.

27. Cusi, K., *Role of insulin resistance and lipotoxicity in non-alcoholic steatohepatitis.* Clin Liver Dis, 2009. **13**(4): p. 545-63.

28. Brunt, E.M., et al., *Nonalcoholic steatohepatitis: a proposal for grading and staging the histological lesions.* Am J Gastroenterol, 1999. **94**(9): p. 2467-74.

29. Younossi, Z., et al., *Global burden of NAFLD and NASH: trends, predictions, risk factors and prevention.* Nat Rev Gastroenterol Hepatol, 2018. **15**(1): p. 11-20.

30. Rinella, M.E., *Nonalcoholic fatty liver disease: a systematic review.* JAMA, 2015. **313**(22): p. 2263-73.

31. Sutti, S. and E. Albano, *Adaptive immunity: an emerging player in the progression of NAFLD.* Nat Rev Gastroenterol Hepatol, 2020. **17**(2): p. 81-92.

32. Baffy, G., E.M. Brunt, and S.H. Caldwell, *Hepatocellular carcinoma in non-alcoholic fatty liver disease: an emerging menace.* J Hepatol, 2012. **56**(6): p. 1384-91.

33. Younes, R. and E. Bugianesi, *Should we undertake surveillance for HCC in patients with NAFLD?* J Hepatol, 2018. **68**(2): p. 326-334.

34. Patel, V., A.J. Sanyal, and R. Sterling, *Clinical Presentation and Patient Evaluation in Nonalcoholic Fatty Liver Disease.* Clin Liver Dis, 2016. **20**(2): p. 277-92.

35. Rotman, Y. and A.J. Sanyal, *Current and upcoming pharmacotherapy for non-alcoholic fatty liver disease.* Gut, 2017. **66**(1): p. 180-190.

36. Mintziori, G. and S.A. Polyzos, *Emerging and future therapies for nonalcoholic steatohepatitis in adults.* Expert Opin Pharmacother, 2016. **17**(14): p. 1937-46.

37. Tunissiolli, N.M., et al., *Hepatocellular Carcinoma: a Comprehensive Review ofBiomarkers, Clinical Aspects, and Therapy.* Asian Pac J Cancer Prev, 2017. **18**(4): p. 863-872.

38. Zou, R.C., et al., *Identification of metabolism-associated pathways and genes involved in male and female liver cancer patients.* J Theor Biol, 2019. **480**: p. 218-228.

39. Zheng, J., et al., *Actual 10-Year Survivors After Resection of Hepatocellular Carcinoma.* Ann Surg Oncol, 2017. **24**(5): p. 1358-1366.

40. Nakagawa, H., et al., *Lipid Metabolic Reprogramming in Hepatocellular Carcinoma.* Cancers (Basel), 2018. **10**(11).

41. Reeves, H.L., M.Y. Zaki, and C.P. Day, *Hepatocellular Carcinoma in Obesity, Type 2 Diabetes, and NAFLD.* Dig Dis Sci, 2016. **61**(5): p. 1234-45.

42. Park, E.J., et al., *Dietary and genetic obesity promote liver inflammation and tumorigenesis by enhancing IL-6 and TNF expression.* Cell, 2010. **140**(2): p. 197-208.

43. Tong, F., et al., *Decreased expression of ARV1 results in cholesterol retention in the endoplasmic reticulum and abnormal bile acid metabolism.* J Biol Chem, 2010. **285**(44): p. 33632-41.

44. Lagor, W.R., et al., *Deletion of murine Arv1 results in a lean phenotype with increased energy expenditure.* Nutr Diabetes, 2015. **5**: p. e181.

45. Lorenzen, I., et al., *Control of ADAM17 activity by regulation of its cellular localisation.* Sci Rep, 2016. **6**: p. 35067.

46. Schlessinger, J., *Ligand-induced, receptor-mediated dimerization and activation of EGF receptor.* Cell, 2002. **110**(6): p. 669-72.

47. Schneider, M.R. and E. Wolf, *The epidermal growth factor receptor ligands at a glance.* J Cell Physiol, 2009. **218**(3): p. 460-6.

48. Komposch, K. and M. Sibilia, *EGFR Signaling in Liver Diseases.* Int J Mol Sci, 2015. **17**(1).

49. Soto-Gamez, A., et al., *A Bispecific Inhibitor of the EGFR/ADAM17 Axis Decreases Cell Proliferation and Migration of EGFR-Dependent Cancer Cells.* Cancers (Basel), 2020. **12**(2).

50. Ohtsu, H., P.J. Dempsey, and S. Eguchi, *ADAMs as mediators of EGF receptor transactivation by G protein-coupled receptors.* Am J Physiol Cell Physiol, 2006. **291**(1): p. C1-10.

51. Murthy, A., et al., *Ectodomain shedding of EGFR ligands and TNFR1 dictates hepatocyte apoptosis during fulminant hepatitis in mice.* J Clin Invest, 2010. **120**(8): p. 2731-44.

52. Fujii, T., et al., *Mouse model of carbon tetrachloride induced liver fibrosis: Histopathological changes and expression of CD133 and epidermal growth factor.* BMC Gastroenterol, 2010. **10**: p. 79.

53. Berasain, C., et al., *Novel role for amphiregulin in protection from liver injury.* J Biol Chem, 2005. **280**(19): p. 19012-20.

54. McKee, C., et al., *Amphiregulin activates human hepatic stellate cells and is upregulated in non alcoholic steatohepatitis.* Sci Rep, 2015. **5**: p. 8812.

55. Ohyama, T., et al., *Transforming growth factor-α attenuates hepatic fibrosis: possible involvement of matrix metalloproteinase-1.* Liver Int, 2011. **31**(4): p. 572-84.

56. Qiao, Q., et al., *Over expression of transforming growth factor-alpha and epidermal growth factor receptor in human hepatic cirrhosis tissues.* Hepatogastroenterology, 2008. **55**(81): p. 169-72.

57. Tanabe, K.K., et al., *Epidermal growth factor gene functional polymorphism and the risk of hepatocellular carcinoma in patients with cirrhosis.* JAMA, 2008. **299**(1): p. 53-60.

58. Choung, S., et al., *Epidermal growth factor receptor inhibition attenuates non-alcoholic fatty liver disease in diet-induced obese mice.* PLoS One, 2019. **14**(2): p. e0210828.

59. Mukai, T., et al., *Silencing of FABP1 ameliorates hepatic steatosis, inflammation, and oxidative stress in mice with nonalcoholic fatty liver disease.* FEBS Open Bio, 2017. **7**(7): p. 1009-1016.

Appendix

ABCC2	ATP binding cassette subfamily C member 2
ACAT	Acetyl-CoA Acetyltransferase
ADAM	a disintegrin and metalloproteinase
AGTR1	Angiotensin II Receptor Type 1
AHD	ARV1 Homology Domain
APOC3	Apolipoprotein C3
AR	Amphiregulin
ARV1	Acyl-CoA cholesterol acyl transferase related enzyme-2 required for viability 1
ATF4	Activating Transcription Factor 4
ATF6	Activating Transcription Factor 6
BMI	Body Mass Index
BSA	Bovine Serum Albumin
BTC	Betacellulin
CHOP	C/EBP-Homologous Protein
DMEM	Dulbecco's Modified Eagle Medium
ECM	Extracellular Matrix

EGF	Epidermal Growth Factor
EGFR	Epidermal Growth Factor Receptor
ENPP1	Ectonucleotide Pyrophosphatase/Phosphodiesterase 1
EPGN	Epigen
ER	Endoplasmic Reticulum
ERAD	Endoplasmic-reticulum-associated protein degradation
EREG	Epiregulin
FA	Fatty Acid
FABP1	Fatty Acid Binding Protein 1
FADS1	Fatty Acid Desaturase 1
FGF21	Fibroblast Growth Factor 21
FXR	Farnesoid X Receptor
GAPDH	Glyceraldehyde 3-phosphate dehydrogenase
GCKR	Glucokinase Regulator
GCLC	Glutamate-Cysteine Ligase Catalytic Subunit
GDC	Genomic DNA Contamination
GOI	Gene of Interest
GPI	Glycophosphatidylinositol

HB-EGF	Heparin-Epidermal Growth Factor
HCC	Hepatocellular Carcinoma
HDL	High Density Lipoprotein
HDR	Homology Directed Repair
HPRT1	Hypoxanthine Phosphoribosyl transferase 1
IL6	Interleukin 6
IRE1α	Inositol-requiring enzyme 1 alpha
KLF6	Kruppel Like Factor 6
KO	Knock Out
LDL	Low Density Lipoprotein
LPIN1	Lipin 1
MCD	Methionine Choline-Deficient
MTTP	Microsomal Triglyceride Transfer Protein
NAFL	Non-Alcoholic Fatty Liver
NAFLD	Non-Alcoholic Fatty Liver Disease
NASH	Non-Alcoholic Steatohepatitis
NR1I2	Nuclear Receptor Subfamily 1 Group I Member 2
OE	Over Expression

PBS	Phosphate Buffered Saline
PDGF	Platelet-derived Growth Factor
PEMT	Phosphatidylethanolamine N-Methyltransferase
PERK	Protein Kinase R (PKR)-like Endoplasmic Reticulum Kinase
PNPLA3	Patatin Like Phospholipase Domain Containing 3
PPAR	Peroxisome Proliferator-Activated Receptor
ROS	Reactive Oxygen Species
RTC	Reverse Transcription Control
SLC	Solute Carrier
SOD2	Superoxide Dismutase 2
STAT	Signal Transducer and Activator of Transcription
T2DM	Type 2 Diabetes Mellitus
TGFα	Transforming Growth Factor alpha
TLR4	Toll Like Receptor 4
TM6SF2	Transmembrane 6 Superfamily Member 2
TNF	Tumor Necrosis Factor
UPR	Unfolded Protein Response

VLDL	Very-Low Density Lipoprotein
WAT	White Adipose Tissue
WPD	Western Pattern Diet
WT	Wild Type

Attributes

Table # 1 was modified from Benedict et al., Non-Alcoholic Fatty Liver Disease: An Expanded Review

Figure # 1 was modified from

Figure # 2 was modified from Benedict et al., Non-Alcoholic Fatty Liver Disease: An Expanded Review

Figure # 3 was from Santa Cruz Biotechnology website product sheet

Figure # 4 was generated on ApE plasmid editor

Figure # 5 was created by Nicholas Wachowski

Table # 2 was created by Nicholas Wachowski

Table # 3 was from Qiagen's website product sheet

Table # 4 was from Qiagen's website product sheet

Table # 5 was from Qiagen's website product sheet

Table # 6 was from Qiagen's website product sheet

Table # 7 was created by Nicholas Wachowski

Figure # 6 was created by Nicholas Wachowski

Figure # 7 data was generated by Nicholas Wachowski, Statistics and Graph was performed on Qiagen's Analysis Portal

Figure # 8 data was generated by Nicholas Wachowski, Statistics and Graph was performed on Qiagen's Analysis Portal

Figure # 9 data was generated by Nicholas Wachowski, Statistics and Graph was performed on Qiagen's Analysis Portal

Figure # 10 data was generated by Nicholas Wachowski, Statistics and Graph was performed on Qiagen's Analysis Portal

Figure # 11 data was generated by Nicholas Wachowski. Statistics and Chart was created by HeatMapper

Figure # 12 data was generated by Nicholas Wachowski. Chart was generated on ENRICHR

Figure # 13 data was generated by Nicholas Wachowski. Chart was generated on ENRICHR

Figure # 14 data was generated by Nicholas Wachowski

Figure # 15 data was generated by Dr. Karla Frietze

Figure # 16 data was generated by Dr. Karla Frietze

Figure # 17 was created by Nicholas Wachowski

Figure # 18 was created by Nicholas Wachowski

Figure # 19 was created by Nicholas Wachowski

Figure # 20 was created by Nicholas Wachowski

Figure # 21 was created by Nicholas Wachowski

Figure # 22 was created by Nicholas Wachowski

Figure # 23 was created by Nicholas Wachowski